CRANFIELD UNIVERSITY

Lingang Zhu

Damage Resistance of Aircraft Wing Structure Using Low Cost Carbon Fibre Composite Materials

School of Applied Science
MSc thesis

MSc by Research
Academic Year: 2010 - 2011

Supervisor: Mr Andrew Mills
12 2010

CRANFIELD UNIVERSITY

School of Applied Science
MSc thesis

MSc by Research

Academic Year 2010 - 2011

Lingang Zhu

Damage Resistance of Aircraft Wing Structure Using Low Cost Carbon Fibre Composite Materials

Supervisor: Mr Andrew Mills

12 2010

This thesis is submitted in partial fulfillment of the requirements for the degree of MSc by Research

ABSTRACT

This thesis investigated the damage resistance of aircraft wing structure using low cost carbon fibre composites. Experiments had been carried out to investigate their impact behaviour, damage characteristics and residual compression strength.

Current aircraft pre-impregnated materials processed by autoclave moulding and also some low-cost fibre preforms using vacuum infusion moulding were compared in this research. Novel tufting technology and veils were taken into consideration to find a cost-efficient method of improving the damage resistance of carbon fibre panels.

Initial damage was induced using a falling weight (2.38Kg) apparatus mounting a 16mm hemispherical tip. Various energy levels were applied for different panels, but the energy to thickness ratio was constant.

Visual inspection and ultrasonic C-scans were carried out to investigate both exterior and interior damage (fibre fracture, delamination, etc.). Micrographs of the cross-section through the impact point were employed to characterise the fracture mechanisms.

The detailed Compression After Impact (CAI) procedure was recorded and presented in this thesis. In order to investigate how much ultimate compression strength was reduced by impact, plain compression strength was also measured.

The behaviour of different materials, including damage size, damage shape and construction and residual compression strength were utilised in comparing the different effects on impact of different components such as fibre, fabric, interleaving of toughening layers and through thickness reinforcement. The results show that unidirectional fibre was more sensitive than woven fibre and that tufting and veils were the most affordable and efficient methods to improve the damage resistance of the laminates studied. Over 30% increase in residual compression strength was achieved via these methods.

Keywords:

Carbon Fibre, Composite, Aircraft, Impact, Damage, Tufting, Interleaving, Veil, Toughened resin, CAI, Fibre fracture, C-scan, delamination, Mechanism

ACKNOWLEDGEMENTS

I would like to take this opportunity to express my sincere thanks to COMAC and the Chinese Scholarship Council for funding the project.

I am very grateful to my wife Ling Cai for her love, understanding, support and being always by my side. Thanks to my family for consistently encouraging me in my aspirations.

I would like to acknowledge my supervisor Mr. Andrew Mills for being so patient and for his approachable support and professional direction. Throughout my 13 months at Cranfield, his encouragement and guidance have proved invaluable.

I would also like to express my gratitude to Mr. Jim Hurley, Dr David Ayre, Dr Giuseppe Dell'Anno, Dr Johannes Treiber, Dr Isidro Durazo-Cardenas, Miss Elisabete Costa, Mr. Ben Hopper, Dr Andrew Dyer, Dr Adam Joesbury, Mr. Tamas Nagy and everyone else who has helped me at Cranfield. Their guidance, constructive criticism and support have been fundamental to the progress in my individual research, and will continue to of use to me throughout my life.

I am also grateful to Dr Bowen Zhong and Dr Xiang Zhang for their help, friendship and fatherly understanding.

I am also deeply appreciative of the support of Dr. Al Savvaris, Dr Dimitris Drikakis, Dr Nicholas Lawson and all the people who were involved in this project for their kind assistance. The cooperation between Cranfield and COMAC could not be such effective without their hard work.

Finally, I am ever grateful for all the friends I have made at Cranfield. Being with them has provided one of the most precious experiences of my life.

Lingang Zhu

08.12.2010

Page left intentionally blank

Table of Contents

LIST OF FIGURES

LIST OF TABLES

1 INTRODUCTION

The emergence of the A380, Boeing-787 and the impending arrival of the A350, indicate that the proportion of composite materials application in aircraft has continually increased in recent years, indicating that it constitutes a key tendency in transport aircraft design. The Composite material utilisation of some mainstream commercial airliners is shown below (Figure 1).

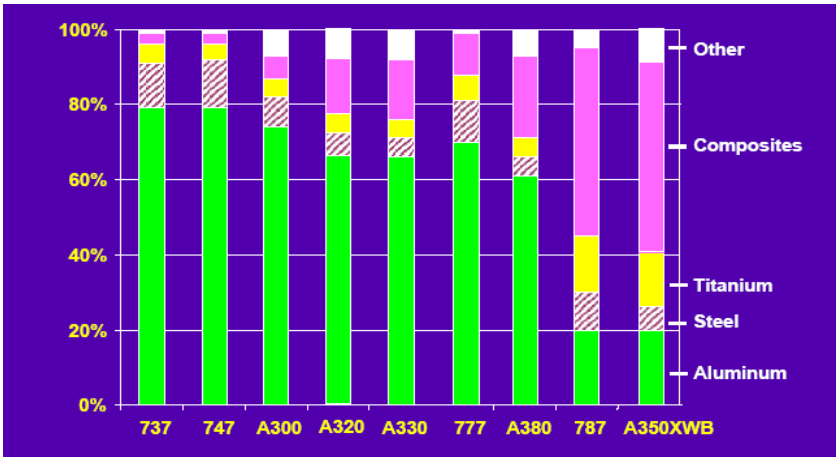

Figure 1 Composite material utilization of some significant vehicles

Composites reinforcements such as carbon fibre have many different fabric styles and can be moulded, formed and bonded with thermoset or thermoplastic matrices. Compared to conventional metallic aircraft structures, carbon fibre composites display excellent qualities, including high strength to weight ratio, low thermal expansion, outstanding stiffness, excellent fatigue behaviour, high levels of corrosion resistance and the possibility of tailored design. Fatigue itself is not an issue since the design maximum strains are below crack growth thresholds. Hence, there is no crack growth under the fatigue stress threshold when the composite structure is designed based on a "no-growth" requirement for damage, which is more stringent than in metal structures [1][2]. Nevertheless, they are more sensitive to impact damage and defects. The strength of composites structure drops significantly after impact because the loaded fibres are fractured and/or are no longer adequately supported by the matrix (e.g. a

carbon fibre bar is extremely stiff, but will crack easily if hit with a hammer or struck by stone fragments during take-off or landing) [4]. However, it is very hard to predict the residual compression strength of the faulty or damaged structure due to the difficulty of detecting both the damage area and the extent of damage. A significant body of academic and industrial research has been focused on the improvement of damage resistance through new materials development and processing technology.

This thesis investigates the key aircraft structure design issue -- the reduction in compression strength due to impact damage. It focuses on the relative performance of a wide range of established and emerging materials for improved damage resistance. Firstly, a series of panels using different carbon fibres and different epoxy matrices were manufactured and machined into standard sized specimens. Secondly, internal damage was induced utilising a dropping-weight device and investigated employing an ultrasonic C-scan system. The construction of internal damage was detected via the micrograph of a cross-section through the impact point. Subsequently, post-damage compression tests were carried out to obtain the residual compression strength. Finally, all the results were analysed in order to understand how and to what extent the individual components of the composite materials affected the damage resistance.

2 LITERATURE REVIEW

2.1 Basic composites knowledge and features

The concept of "Composite material = raw materials + manufacturing process + component design" depicts the feature of composites which is considerably different from metals. If any of these three things are modified, the final quality of the part is affected. This is why, within carbon fibre reinforced plastic (CFRP) world, any "little" modification can have strong consequences on the aircraft component.

The anisotropy in all directions of carbon fibre reinforced composite (CFRP) is very large. Recently, attention to off-axial behaviour has become important to ensure a good balance of composite performance [22]. Off-axial properties can be optimised by carbon fibre surface status and carbon fibre-resin compatibility [22].

As with metal structures, the integrity requirements of composite structures consist of several aspects, i.e. static strength, stiffness, durability, damage resistance and damage tolerance. For static strength, the design tensile allowance should be determined using the result of testing specimens with a 6.35mm diameter hole. On the other hand, the design compressive allowance should be determined using the results of Compression After Impact (CAI) [39]. As mentioned above, fatigue could not be an issue when the design maximum strains are below crack growth thresholds. The Barely Visible Impact Damage (BVID) inside structure should not extend within twice fatigue life and the structure containing VID should have enough residual strength after two inspiration intervals [38][39].

2.2 The main type of defects and damage

Based on published research, the types of defects and damage for a composite structure include wrinkles, water ingress (especially in honeycomb design),

de-bonding between structural parts, delamination between the layers, chemical degradation, perforation, scratches, dents and erosion (Figure 2) [36]. In the case of failure mechanisms, defects could be divided into physical damage to the fibres, resin matrix, and fibre/matrix interface, and also flaws in the fabric manufacturing process [18]. This review chapter focuses on delamination, de-bonding and particularly the mechanism of damage after impact and how to improve it.

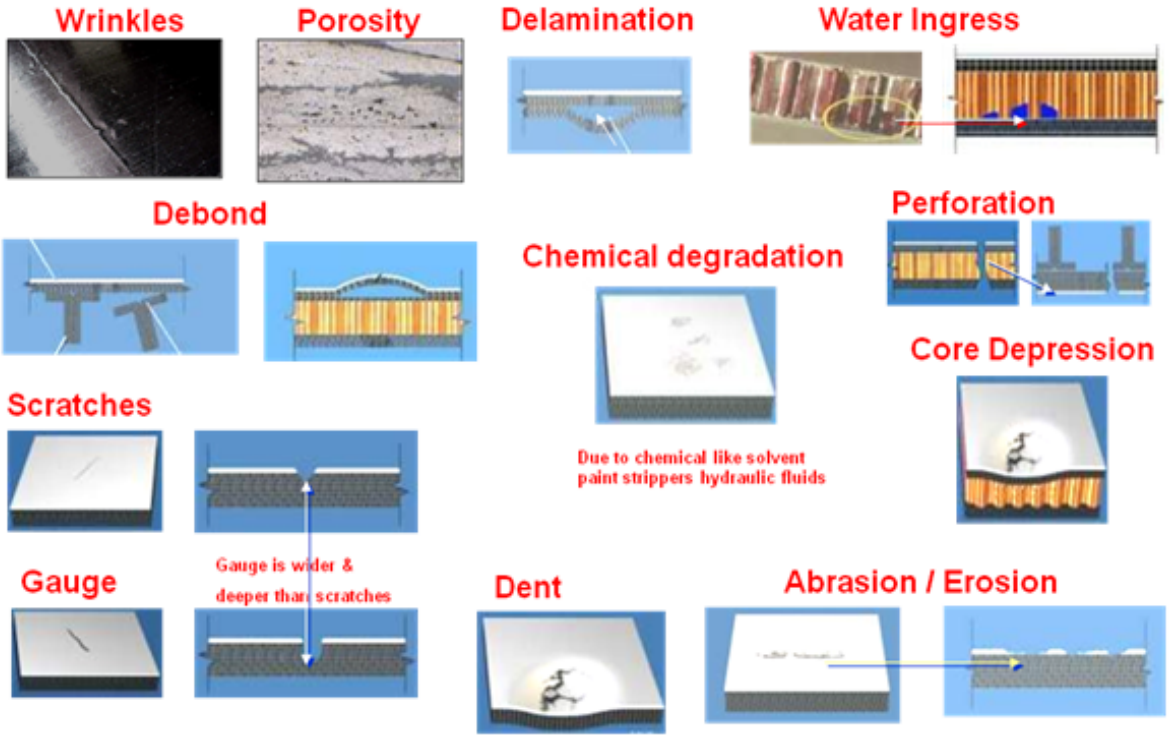

Figure 2 Main types of defects and damage

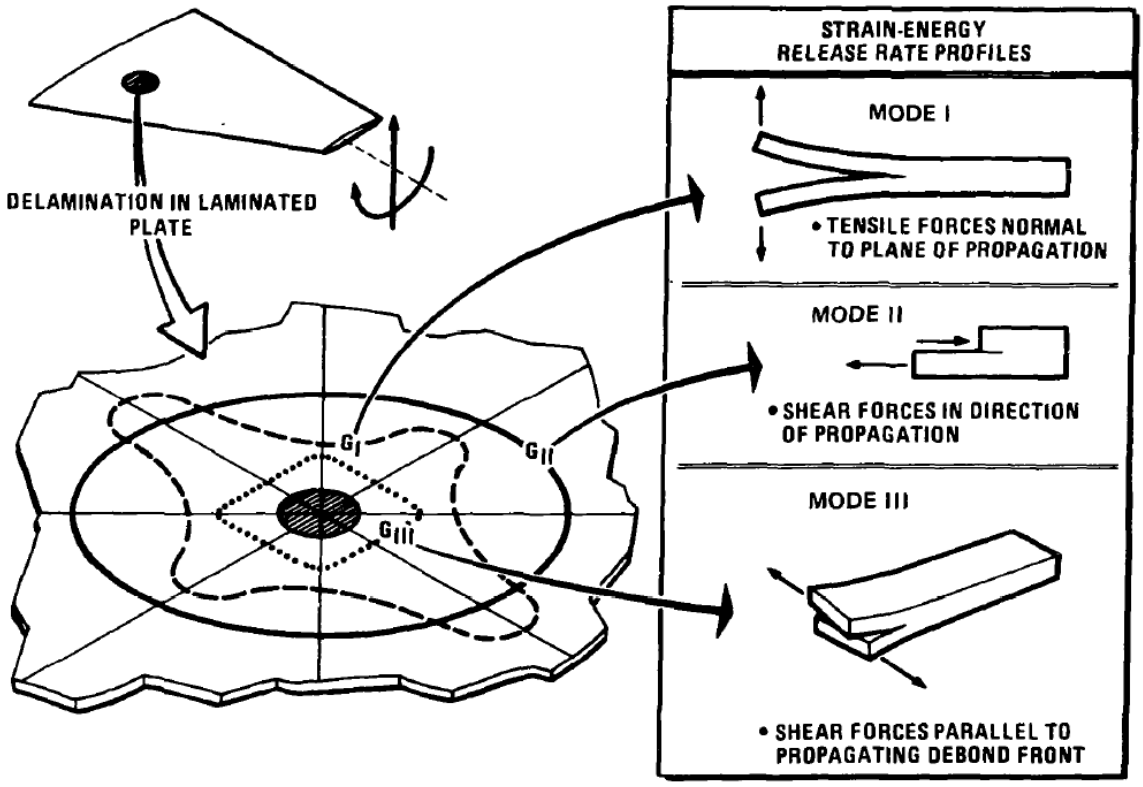

Figure 3 Three modes of delamination

According to adhesive fracture technology, when a laminated plate reacts to general loads, the profiles of strain-energy release rate around delamination can be broken into three modes [5]. Mode I (depicted in Figure 3) schematically shows the delamination under tensile load normal to the plane of propagation. Similarly, Mode II describes shear load in the direction of propagation and Mode III illustrates the case of shear load parallel to the propagating de-bond front. [5]

To a large extent, for a non-3D-reinforced composite, the inter-laminar and out-of-plane performance depends on the resin's capability, even for the intra-laminar property (Figure 4). Also for a 3D-reinforced composite, the combination of Z-fibres and matrix enhanced out-of-plane performance significantly. Therefore, much effort has been focused on how to improve resin's capability and enhance the effectiveness of inter-laminar mechanisms.

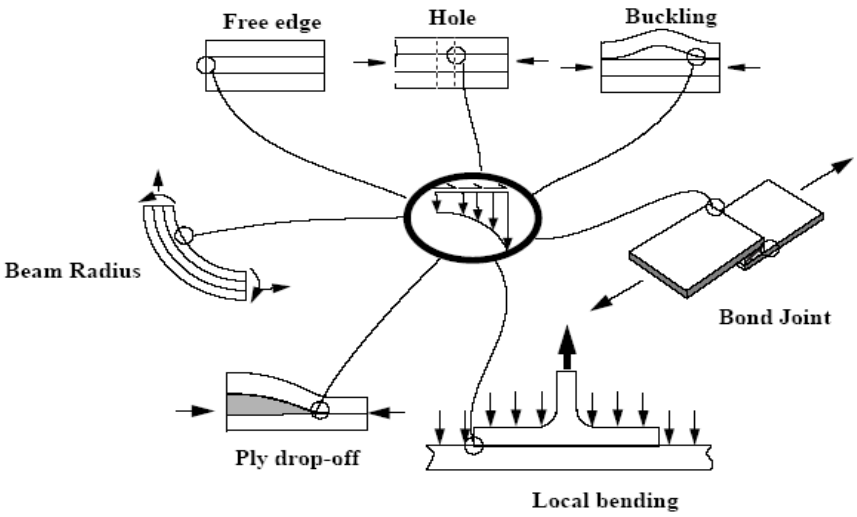

Figure 4 Weakness of composites

2.3 The issue of improving damage resistance for CFC aircraft

In recent years, there has been an increasing amount of research published on damage resistance. It has been demonstrated that the composite structure strength drops significantly after impact or when exposed to high shock because the highly loaded fibres are fractured and/or are no longer adequately supported by the matrix [2]. The aim of damage resistance improvement against impact is to reduce the susceptibility to and even eliminate delamination of the parts themselves or disbanding between structural parts.

Generally, damage resistance improvement is achieved by increasing composite laminates toughness, such as through using tougher resins, utilising toughening mechanisms and taking advantage of interleaving and veils, as described below. This review gives special attention to tufting because of its many unique properties. Much concern has been expressed about the innovation of these above-mentioned aspects rather than the fibre layer's fabric styles.

2.3.1 Tougher resins

Epoxy resins constitute one of the most broadly used thermoset materials due to the special chemical characteristics compared to other thermosetting resins: no co-products or volatiles are generated during curing procedures, thereby shrinkage is quite low. The range of temperatures required by epoxy resins curing is wide, and the degree of cross-linking can be controlled[11].

Drawing on the chemical structure of the curing agents and on curing conditions, the properties of cured epoxy resins are versatile, including commendable adhesive strength, low shrinkage, outstanding chemical and heat resistance, excellent strength and hardness, pre-eminent electrical insulation and good impact resistance [11].

Recently, many investigations have been carried out into improving the thermal and mechanical properties of epoxy resins, especially concerned with making them tough.

One important and efficient ways to achieve this is to merge a second phase component with the continuous matrix of epoxy resins through chemical reactions or physical blending.

Torayca 3900 provided by Toray is a toughened resin which has been used successfully in the Boeing 777 empennage and floor beams. [24]

Fracture toughness is a property that represents the capability of a material containing a crack to resist fracture, and is one of the most critical properties of any material, actually pertinent to all design applications. It is indicated by K_{IC} and has the unit of $KSI\sqrt{IN}$. The subscript '$_{IC}$' indicates mode I crack expanding vertically under a normal tensile stress. [4]

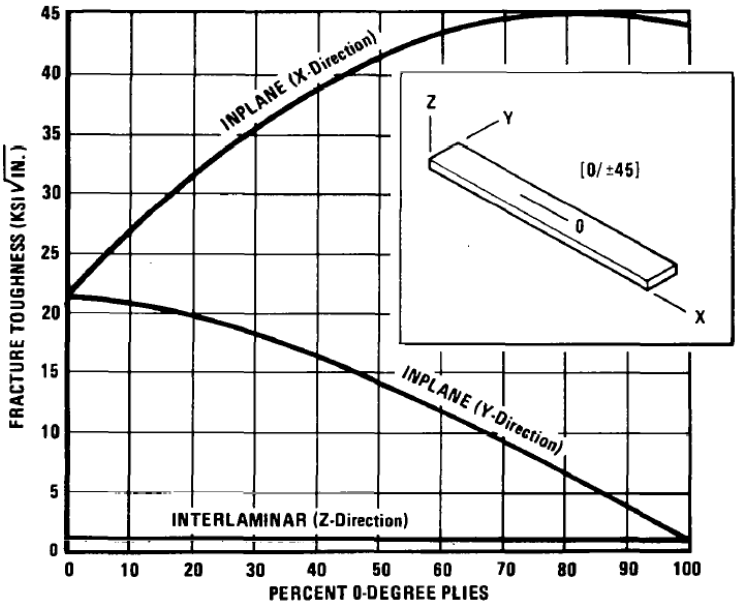

Figure 5 Graphite-epoxy fracture toughness

Figure 5, extracted from the conclusions of Reference 5, indicates the relationship between fracture toughness and the percentage of 0^0 plies in a symmetric, balanced laminate which consists of only 0^0 and $\pm 45^0$ plies of unidirectional fibre. The fracture toughness of an all-45^0 laminates is roughly $21ksi/\sqrt{in}$. The toughness would be doubled in x direction when 45^0 plies are substituted by the plies in x direction.

Meanwhile, the toughness drops significantly in the perpendicular direction (Y). The interlaminate fracture toughness always keeps steady and at a minimum, which means that the resin dominates the interlaminate capability of fracture toughness, and the fibre direction in each laminate has no effect on it. [5]

2.3.2 Toughening mechanisms

To date various methods have been developed and introduced to improve the damage resistance of Carbon Fibre Composites (CFC) structure. In composite materials science, structural toughness mechanisms are processes that increase energy absorption during impact.

To improve the interlaminar strength of composite structure, much concern has been expressed about the 3D (along the z-direction) reinforcement due to the dramatic improvement of the out-of-plane properties. Generally, 3D woven, stitching, tufting and Z-pinning are used in composite engineering as toughening mechanisms [1][7][9][10][12][13][17][30]. However, interlaminar reinforcing is usually accompanied by a reduction in in-plane properties caused by the damage to the X and Y direction fibres during 3D reinforced processing. Depending on textile styles and processing conditions, the least fibre failure should be expected with 3D woven and the most by Z-pinning [18]. The advantages and drawbacks of z-direction reinforcements have been thoroughly investigated in recent years.

2.3.2.1 3D woven

3D weaving is a novel fabric technique, in which through-thickness fibres in bundles or tows are introduced. There are interlaced with the intra-laminate warp and weft tows and hence can penetrate the thickness of the laminates without breaking in-plane fibres.

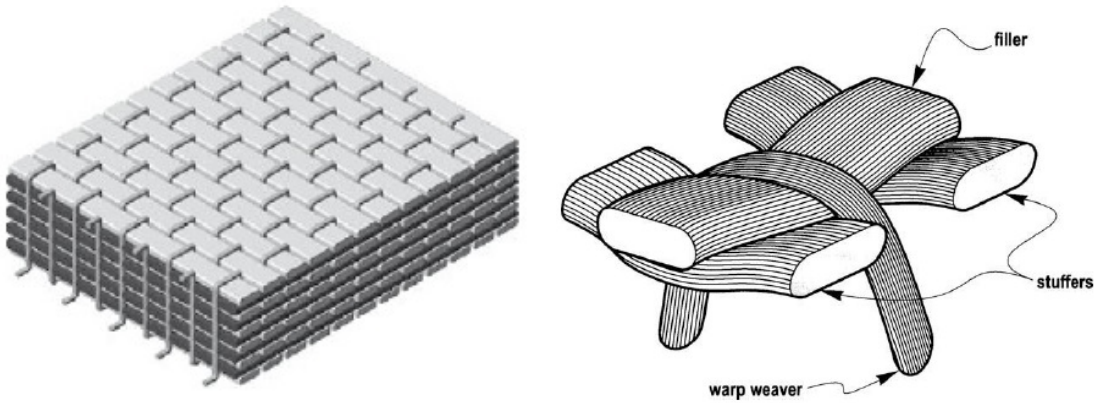

(a) (b)

Figure 6 (a) Ideal schematic of 3D woven fabric (b) Microscopic schematic of crimping of an in-plane tow by a tensioned z-binder in an angle interlock weave. [18]

Figure 6 (a) shows an ideal schematic of conventional 3D woven fabric in which the through-thickness fibres, warp fibres and weft fibres are mutually perpendicular. In addition to the widely known defects of 3D woven fabric such as machine complexity, low yarn deposition speed, no 45^{o} plies and very restricted shapes, other disadvantages include very difficult and complex tapering and regions of local fibre waviness due to the penetration of Z-binder yarns and the tensional load in Z-binder yarns. **Figure 6**(b) shows this effect microscopically, i.e. is a typical case of local crimping on a 3D woven composite [18].

According to A.P. Mouritz's investigation [18], reductions in the in-plane modulus, strength, fatigue and tolerance performance of 3D woven composites are tested, summarised, and compared to changes to the in-plane properties of composite materials (Figure 7, Figure **8**, Figure **9**).

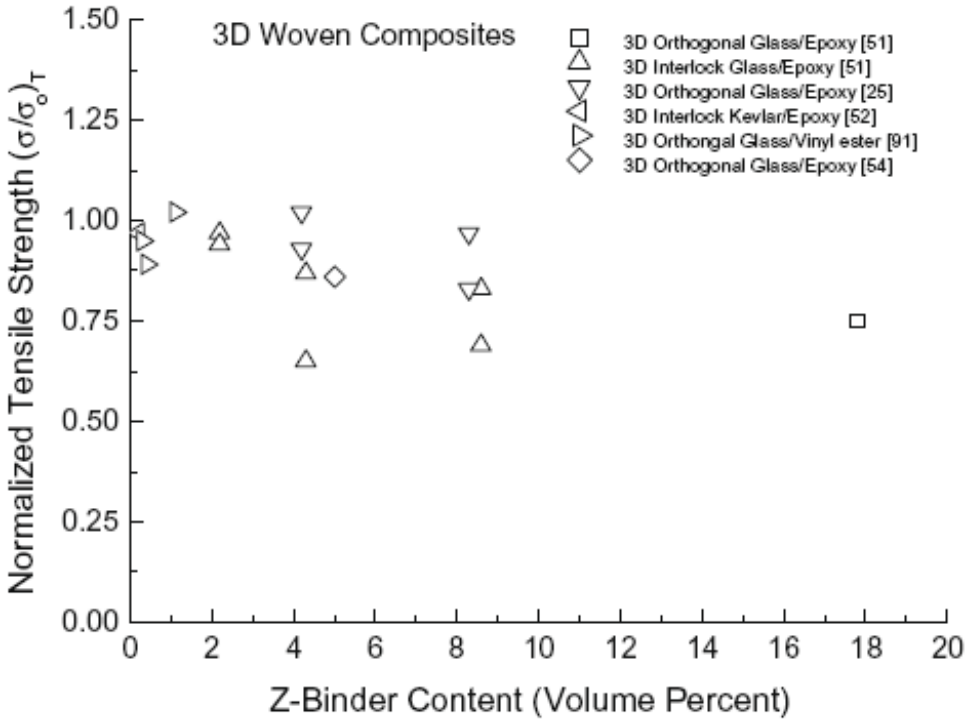

Figure 7 Influence of 3D woven on normalised Tensile strength [18]

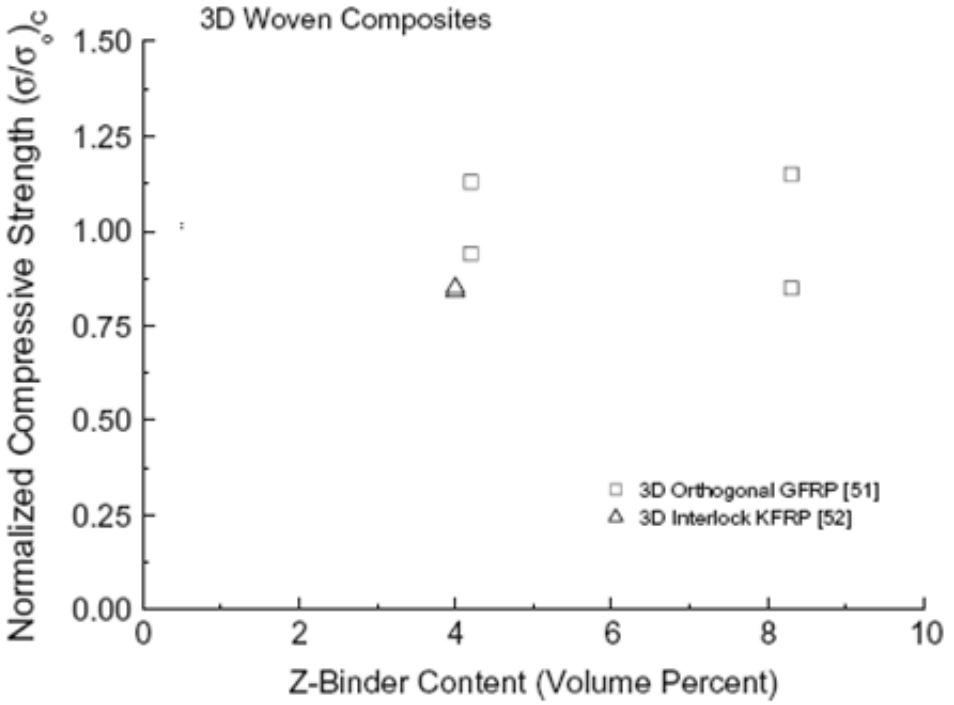

Figure 8 Influence of 3D woven on normalised compressive strength [18]

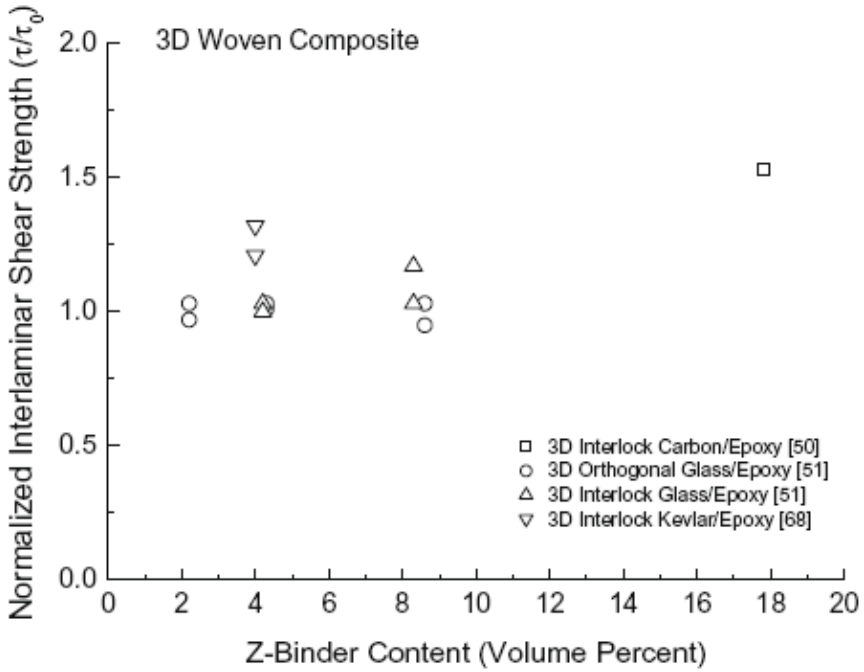

Figure 9 Influence of 3D woven on normalised interlaminar shear strength [18]

The 3 illustrations above indicate that, for 3D woven laminates, almost all the normalized tensile strengths are decreased slightly or significantly due to the fibre locally crimping, the normalised compressive strength in contrast keeps steady because the resin dominates the compression. Several normalised interlaminate shear strengths of 3D woven laminates are increased significantly because the shear load is supported by combinations of Z-fibres and resin. [18]

2.3.2.2 Stitching

It is believed that stitching is the simplest and cheapest way to reinforce interlaminar strength, using textile manufacturing techniques to raise the damage resistance and tolerance of laminar structures and for adding strength to composite joints [19].

Fundamentally, the stitching process, employing an appropriate sewing machine, consists of penetrating a needle, carrying the stitch thread through a pile of fabric laminates to achieve out-of-plane reinforcement, locking the thread and needle or needles return. Figure 10 shows three types of stitches. The first one is known as lock stitch which is predominantly used in the garment industry. It must be accessed from

both the bottom and the top of the laminates with two-thread loops between the needle thread and the bobbin thread. The intersection of the needle and bobbin threads is located in the fabric structure which is likely to generate a high stress concentration point and a resin rich zone. The second is known as modified lock stitch and is achieved by forcing the needle thread to travel on the surface of the laminate so that the bobbin thread must travel through the thickness of the structure and the intersection is at the top of the laminates. It mostly reduces the stress concentration and is outstanding in damage tolerance. The last one is known as the chain stitch, but is not available with advanced fibre threads [1] [3].

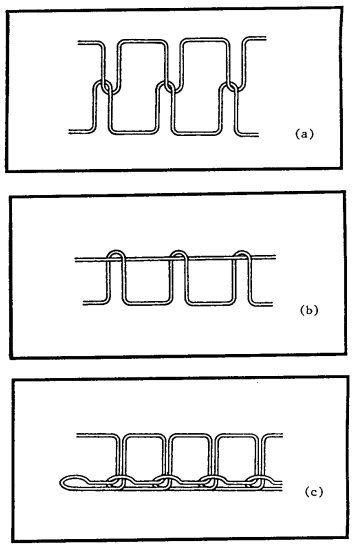

Figure 10 (a) Lock stitch, (b) Modified lock stitch, and (c) Chain stitch

One of the major advantages of stitching is that it can be utilised in both prepreg and preform, although the former may result in more induced fibre damage, thereby reducing the benefits of stitching. For stitched prepreg no further step is required before curing. It is, however, essential to infuse resin into stitched preform before curing [3]. Another benefit is that stitching has a significant effect on the initiation and propagation of delamination. In addition, stitching is more flexible and tailored to design because stitching parameters such as stitching density, pattern and span and the material properties of the fibre thread can be varied to influence the ability of the composite to resist delamination.

Most investigations indicate that 3D stitching reduces the in-plane properties to some degree as the penalty of increasing the inter-laminar strength. This is believed to be caused mainly by fibre misalignment due to the space occupied by the through-the-thickness thread [14, 18] and to a lesser extent by the damage induced during stitching especially for the prepreg as considerable dense fibres are inevitably broken due to forced through-thickness stitching (Figure 11) [18].

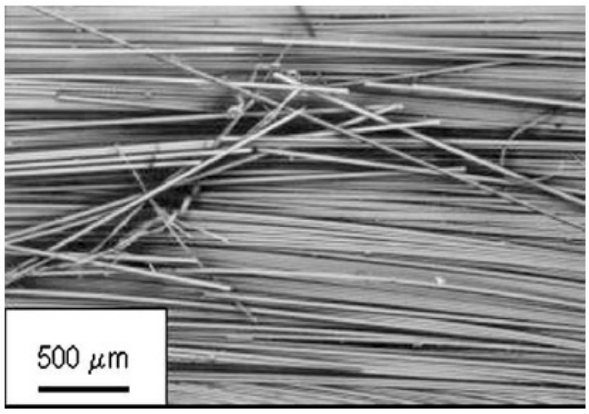

Figure 11 An example of fibre breakage caused by stitching [18]

For stitched preforms, as mentioned above, the likelihood exists that the reduction in intra-laminar strength is mainly caused by a mass of fibre misalignment and crimping and some fibre breakage due to the involvement and/or space invasion by the through-the-thickness thread. However, for stitched prepreg, it is believed that the situation is probably the opposite from preform (less misalignment and more fracture).

Regarding stitching, it is necessary to mention a thesis produced by Mouritz [19]. Based on statistics derived from an assessment of the effect of stitching, Mouritz demonstrates that it is common for stitching to reduce in-plane properties by up to 20%. Meanwhile, Young's modulus and strength can be unaffected or improved slightly (less than 10%) by stitching in some cases. Moreover, he declares that the fibre distortions are not dependent on the diameter, material and areal density of threads but on the degree of tightness of threads [19]. Unfortunately to date, few

studies provide adequate information and a definitive standpoint regarding the degree of tightness of threads has yet to be developed. It is suggested that further validatory experiments are carried out.

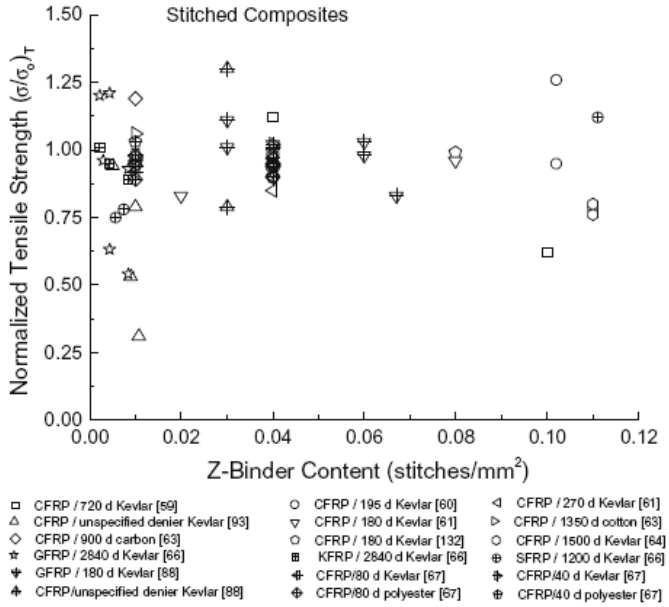

Figure 12 Influence of stitching on normalised tensile strength [18]

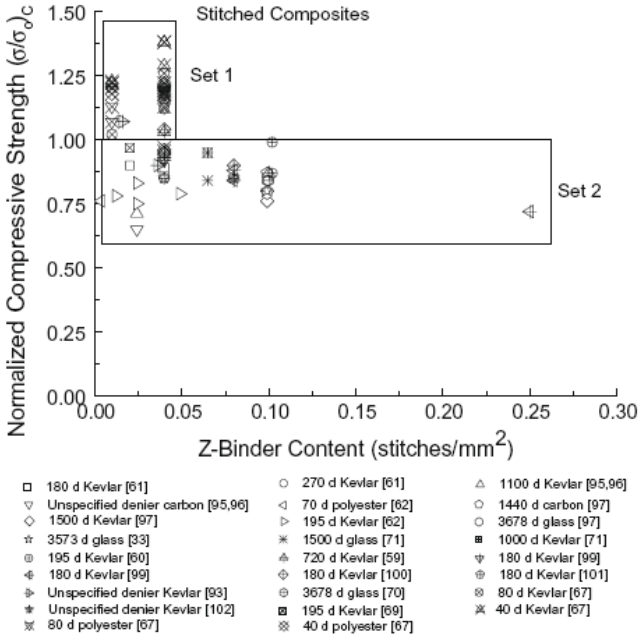

Figure 13 Influence of stitching on normalised compressive strength [18]

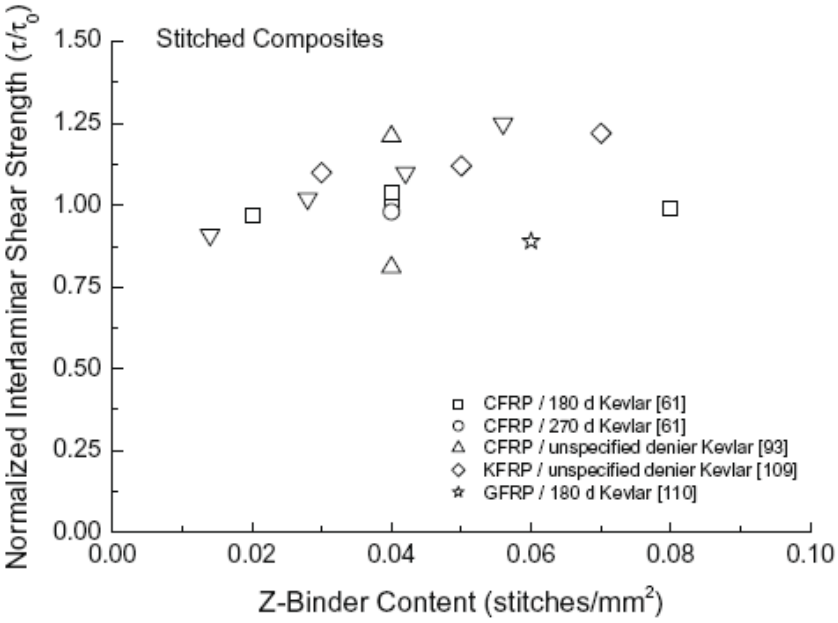

Figure 14 Influence of stitching on normalised interlaminar shear strength [18]

The three illustrations above (Figure 12, Figure 13,Figure 14) all show the normalized strength that defined as the tensile strength of the 3-direction composite divided by that of the equivalent 2-direction laminate; all of the illustrations reveal the effects of stitching on the composite laminates. Unfortunately, the author, Mouritz, didn't differentiate between tufting and stitching, so the corresponding numbers cannot be used directly, but they do however, allow a brief impression of effect of all types of stitching.

Akinori Yoshimura [10] compared the out-of-plane impact resistant performance of stitched CFRP laminates with those of unstitched laminates. His analysis indicated that stitching could effectively prevent the extension of cracks and that this effect becomes greater as the impact energy increases. [10]

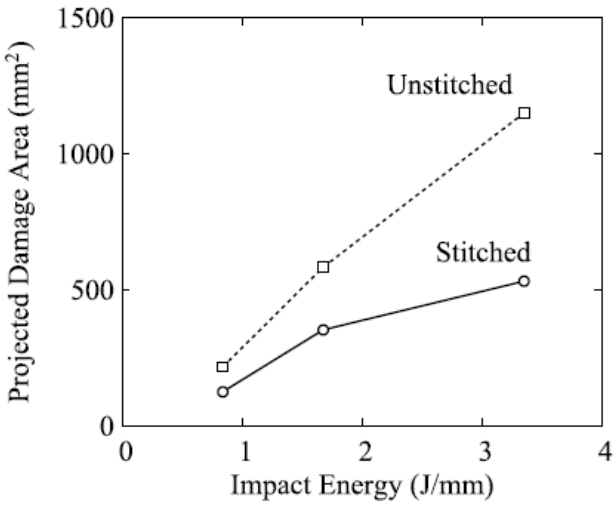

[10]

Figure 15 Projected area of measured impact damage as a function of impact energy

Hiroshi Saito [25] investigated the impact fracture mechanism of stitched laminates moulded by vacuum infusion (VI). In his study, both non-destructive evaluation (C-scan) and destructive evaluation (cross-section observations) were applied to detect damage. Several images obtained by C-scan device with x-y plane information accumulated in z-direction. In addition, several y-z plane cross-section observations were integrated in an x-direction. As a result, comprehensive 3D damage distribution was characerised, as seen in Figure 16. Based on this CAI testing experience, no damage was detected in the top layers, and the delamination initiated with two instances of symmetrical fan-shaped damage extended in a 0^{o}-direction. Furthermore, the delamination deteriorated in the z-direction because of the extension in the 90^{o}-direction, but the pattern of 0^{o}-direction damage was repeated in the bottom layers. [25]

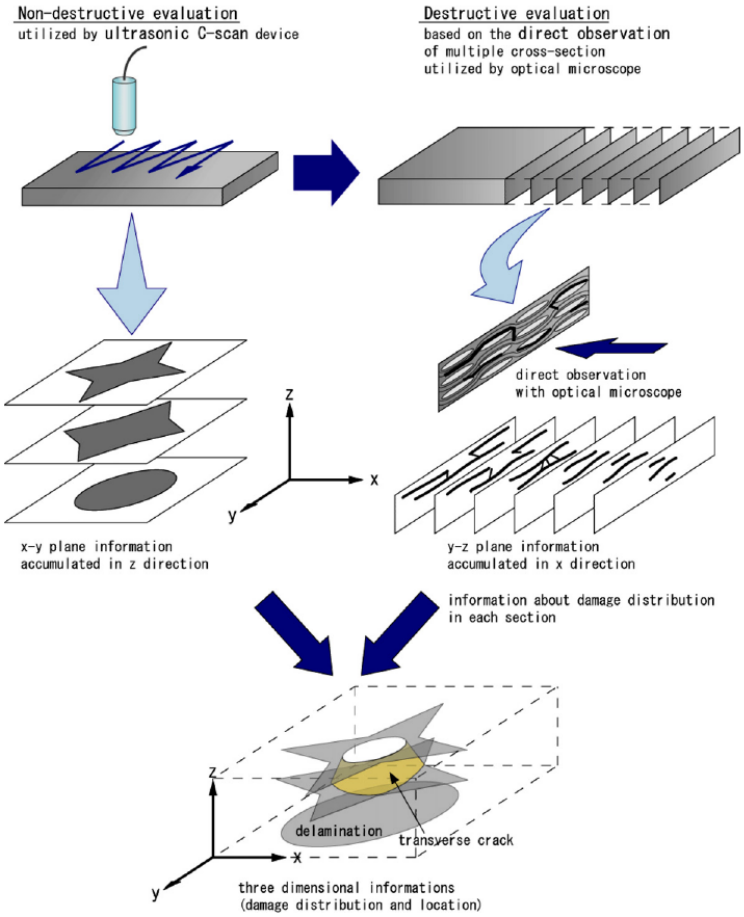

Figure 16 Methodology of the 3D characterisation of impact damage with laminate

An observation of mechanisms in stitched polymer laminates, in which a majority of fibres were aligned with the load direction, was conducted by Mouritz. His conclusions indicate that laminates usually fail in compression by one of three mechanisms (18(b)): delamination, kink band formation (Figure 17(a)) or fibre collapse [19].

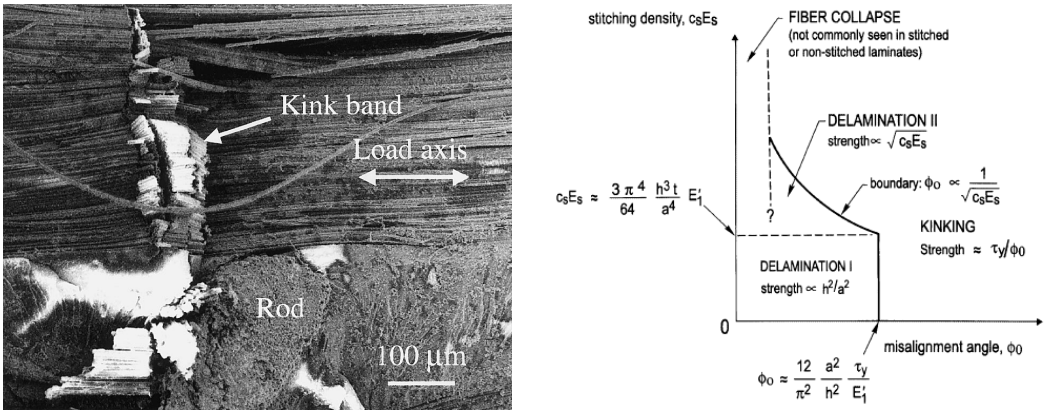

(a) (b)

Figure 17 (a) A kink band in a laminate reinforced through the thickness imaged by scanning electron microscopy (b) A failure map for stitched laminates under compressive loads aligned with the dominant in-plane fibre direction.

Among these mechanisms, stitching has a vital role to play in the transition between delamination and kink band formation [19]. As shown in Figure 18, the distortions are perhaps the most harmful for kink formation due to the misalignments of fibres and these are affected by the tension in the stitching threads. Therefore to minimize the reduction of stitching a low-yarn-tension stitching (tufting) is utilized. This will be discussed in chapter 2.3.2.3. When fibre misalignment is very small, the critical load for kinking is very high. In cases of failure due to fibre collapse, compressive failure within individual fibres occurs instead of kinking [19b].

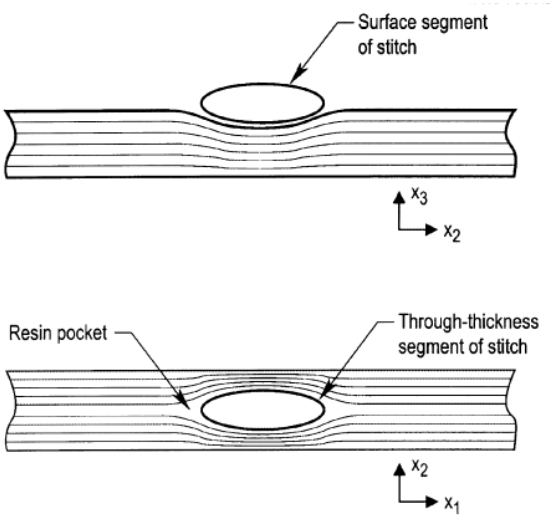

Figure 18 Diagram of distortions caused by stitching

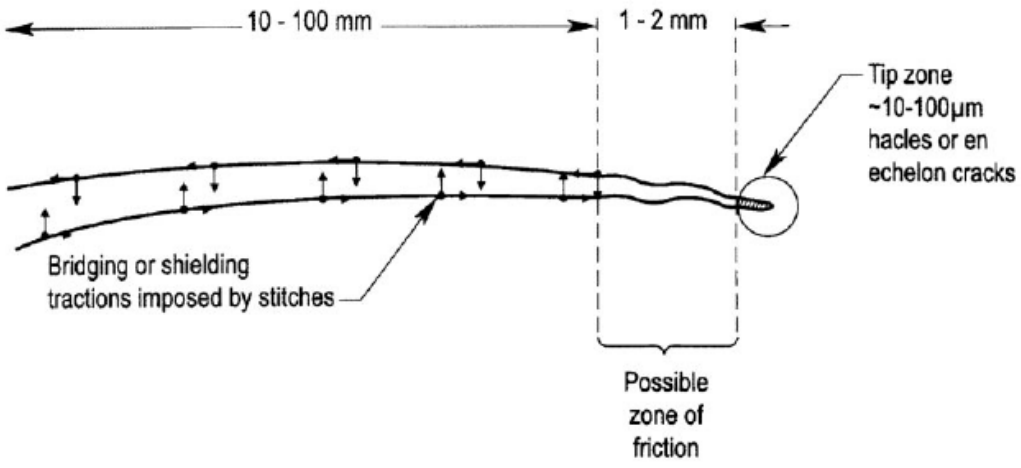

Figure 19 Schematic of a delamination crack in a stitched laminate, showing the different mechanism in different zones [19]

Distinguishing mechanisms, during delamination propagates in stitched laminates at different length scales, were summarised and illustrated by Mouritz (Figure 19) [19]. From his study it can be seen that the furthest point of a delamination crack possesses a relatively small tip zone, which consists of micro-cracking, resin splits and plastic yielding of the resin. With the help of high-resolution photographs, a relatively short friction zone of the order of 1-2mm is revealed following the tip zone. Within this field, the opening displacement of the delamination is negligible and rubble between the surfaces is created by micro-cracks. Even in the wake of the delamination crack, there is a relatively long zone of the order of several tens of mm; the unbroken but distorted stitches act as a bridge between the surfaces to restrain the delamination from expanding. [19]

It is particularly worth noting from Joon-Hyung Byun's investigation [7], that the effect of stitching on the impact performance is greatly reduced in relation to the increase of impact energy, and is negligible above the impact energy level of 8.67J/mm. Possibly the main reason of this, suggested by Guinard, is that delamination is restricted to a similar size zone and more fibre cracks are induced within this zone under such a high energy impact. [26]

2.3.2.3 Tufting

Tufting is an novel experimental technology in the field of composite materials, which enhances the out-of-plane properties of continuous fibre-reinforced composites in the Z-direction, with the purpose of improving the bearing capacity for the shear and interlaminar loads of the structure[8]. Initially, it was developed by DLR at Braunschweig and KSL GmBH in order to overcome the disadvantages of traditional stitching processes such as the requirement of accessing both sides of preform and the reduction in laminate mechanical properties.[1]

The process of tufting is described as follows (Figure 20): Penetrating a thread through a layered dry fabric using a hollow needle. After insertion, a loop of the thread is left on the bottom of the object as the needle moves back along the same trajectory to start a new tuft.

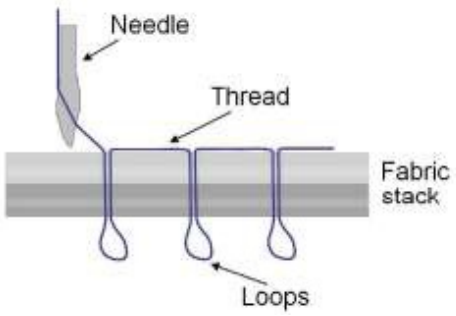

Figure 20 Diagrammatic representation for tufting

It is argued that tufting is a low cost and flexible method compared to 3D weaving in order to provide Z-fibres in laminated composite structures.[9] Firstly, tufting differs from common stitching in three aspects: one is that tufting only requires access from one side of preform rather than the two sides demanded by stitching; secondly, only one thread is used in tufting instead of two threads for stitching; finally, the thread with loops is much looser than items in stitched preform with a lock.

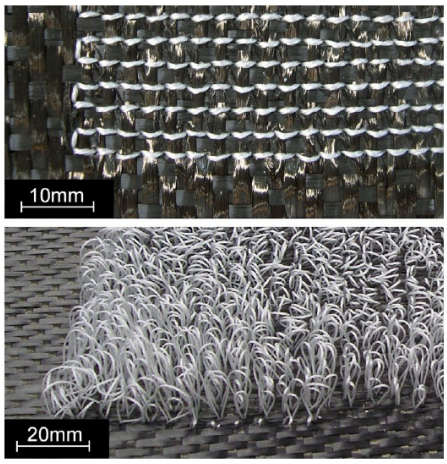

Figure 21 Top-side and underside view of typical tufting

Almost all shapes and forms are likely to be enhanced by tufting, using the appropriate equipment. Furthermore, the density of Z-fibres penetrated can be tailored in relation to the expected loading distribution. On the other hand, tufting is not perfect as tufted preforms are more difficult to handle than unreinforced ones before curing due to the loose loops. The other potential disadvantage of the loops is that items can affect the impregnation of the laminates during the resin infusion process. [8]

In reality, tufting is a technology developed for and used within preforms following resin infusion. Nevertheless, the possibility of whether or not prepregs can be perfectly tufted is currently being investigated. [8]

2.3.2.4 Z-Pinning

Z-pinning (also called Z-pins or Z-fibres) is an innovative technique in which reinforcing fibres are inserted along the Z-direction of continuous laminates or joints or the selective areas requiring local reinforcement, to improve the through-thickness properties such as delamination toughness, Z-direction modulus, impact damage resistance, damage tolerance and fatigue performance of composite joints[12]. Z-pins can be made of metal or pre-cured unidirectional composite fibres. They are designed for use only within prepreg technology since the pins are difficult to control and maintain in position in a dry preform. Much experimental evidence shows that Z-pinning dramatically improves the resistance of the composite structure to delamination.[13]

Several methods of inserting Z-pins have been developed to date. The most common is the Ultrasonically Assisted Z-Fibre process (UAZ, developed by Aztex Inc during the 1980s [15]), which involves the use of an ultrasonic hammer to force the Z-pins through the prepreg. The vibrating chamfered tip of the Z-pins and the locally heated and softened resin allows the Z-pins to penetrate the prepreg with minimal disruption to the long fibres. This differs from stitching and tufting since there is no needle to repeatedly penetrate the fabric. [14]

Z-pins act as fine nails that lock the laminate plies together with a combination of friction and adhesion [14]. Only a relatively small volume fraction of z-pins is needed to significantly enhance the through-thickness properties of laminates and the performance of joints.

Although the use of Z-pinned composites in aircraft is limited at present, an inspiring attempt in the F/A-18E/F provides a large cost saving (US$83,000) and a modest weight reduction (17 kg per aircraft) [17].

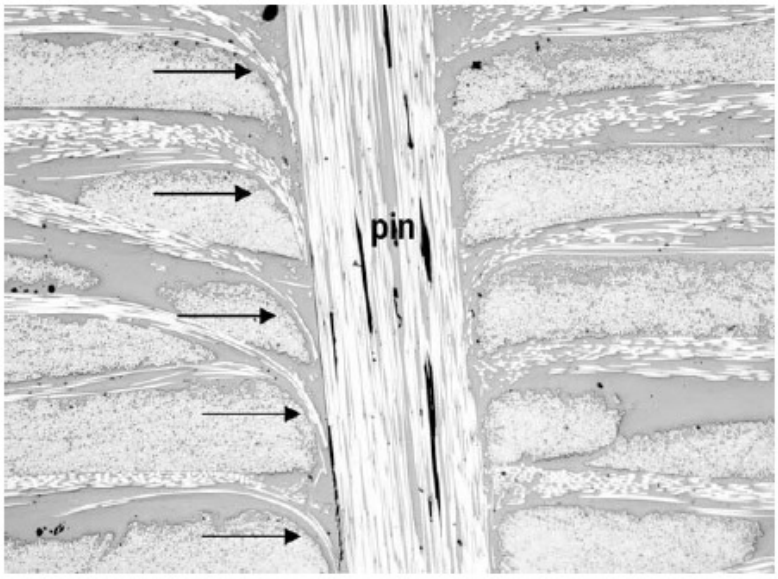

Figure 22 Crimping of in-plane fibres (indicated by the arrows) at a z-binder within a pinned composite (viewed parallel to the laminate plane) [18]

On the other hand, it is believed that fibre fracture is more serious in pinned composites made of prepreg than in 3D woven materials, and is similar to stitched, tufted composites using dry preforms, though the specific percentage of fibres broken due to pinning has never actually been reported [18]. However, the disadvantage of Z-pinning has been investigated recently. Figure 22 shows the crimping of in-plane fibres due to the penetration of Z-pins. Reductions of the in-plane modulus, strength, fatigue and tolerance performance attributed to z-pinning were tested, summarized, and compared with changes to the in-plane properties of composite materials (Figure 23,Figure **24**). [18]

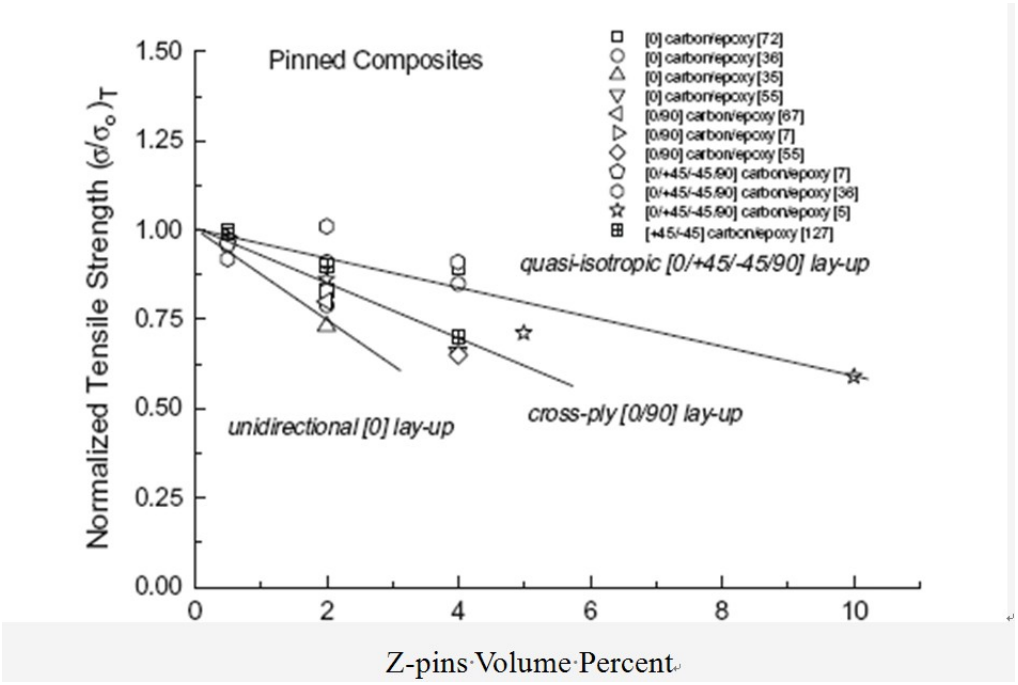

Figure 23 Influence of Z-pinning on Normalised Tensile Strength [18]

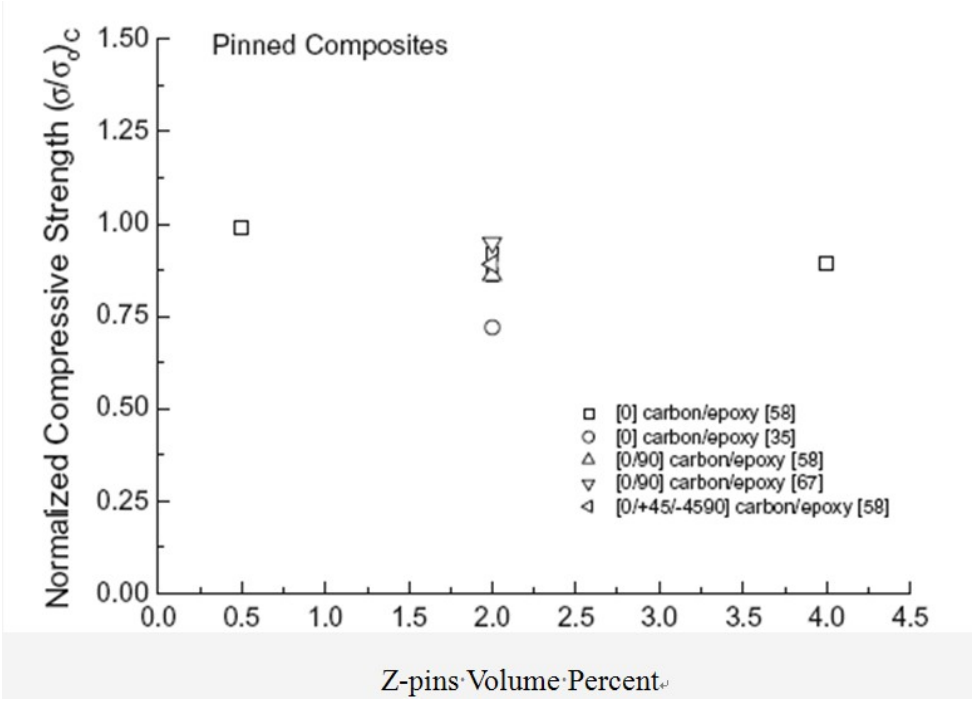

Figure 24 Influence of Z-pinning on Normalised Compressive Strength [18]

The two illustrations above indicate gradual decreases in the in-plane performance includes tensile and compressive as the Z-pins volume percent increases. However, for the common quasi-isotropic carbon/epoxy (0/+45/-45/90)n, the reduction is less than 10%.

2.3.3 Interleaving

Apart from applying tougher resins and structural toughness mechanisms, other techniques may be used to increase structure toughness such as interleaving using particles or veils.

Zhang Man (2003) reviewed the literature from the period and found a huge development in theoretical understanding regarding toughening mechanisms of both rubber and thermoplastic toughened epoxy resins [11]. The effect on fracture behaviour due to microstructure altering was illustrated quantitatively. Several reviews (Garg and Mai, 1988; Huang et al, 1993; Pearson, 1993) respectively summarised descriptions of the existing toughening mechanisms with the purpose of clarifying the principle of improved toughness for rubber and thermoplastic toughened epoxy resins. The mechanisms of particles are summarized below. [11]

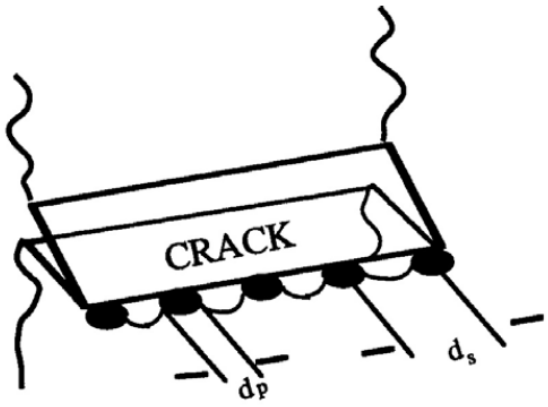

Figure 25 Schematic diagram of crack-pinning mechanism (Pearson, 1993)

1. Crack-Pinning Mechanism (Lange et al., 1971). This theory stated that the crack front bows out between the filler particles but remains pinned at the particles during the propagation of cracks through the resin. Figure 25 shows a schematic diagram of the crack-pinning mechanism (Pearson, 1993). This mechanism is based on small inorganic particles working as toughening agents to resist delamination during fracturing of the epoxy matrix resin (Evans, 1972; Rose, 1987). [11]

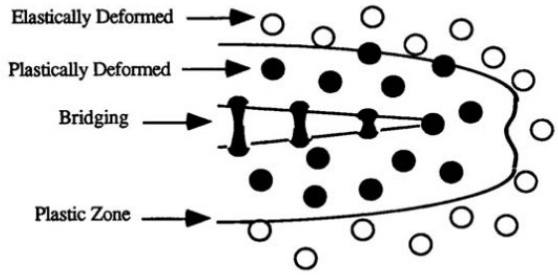

Figure 26 Schematic diagram of the particle-bridging mechanism (Pearson, 1993)

2. Particle Bridging (Rigid Particles) Mechanism (Sigl, et. al 1988). Figure 26 shows a schematic diagram of the particle-bridging mechanism. In this toughening mechanism, the rigid or ductile particle acts as a bridging particle that provides tightening traction in the crack front that dominates the improvement in toughness. While the ductile particle deforms plastically in the material surrounding the crack tip the particle-bridging has an auxiliary function. Compared with the crack-pinning mechanism, the particle in bridging mechanism is larger and emphasises the energy absorption during the rupture of the ductile phase. [11]

An investigation by Hillermeier indicates that a 30% improvement in Mode II interlaminar fracture toughness and a slight increase in the interlaminar shear strength are achieved by modifying spray tackifiers with polyamide particles. [28]

2.4 Resin Infusion moulding

Resin transfer or infusion moulding for dry preforms includes vacuum bag moulding, pressure bag moulding, resin transfer moulding, liquid resin infusion and resin film infusion, to name a few. Four typical resin transfer or infusion moulding methods are as follows:

A: Resin Transfer Moulding (RTM).

In order to form both surfaces of the panel, a mould cavity should be produced by a two-sided mould, which utilises a rigid mould as a base and a rigid or flexible mould

as a cover. A vacuum is usually applied to the mould cavity so that the transfer process can be accelerated and a low void of matrix facilitated. An advantage of this process is that it can be performed at either ambient or elevated temperatures (Figure 27). High Fibre Volume Fraction (FVF) could be achieved due to elevated pressure. Particular attention should be paid to the mechanics of how the resin is introduced to the preforms, which includes numerous varieties. [21]

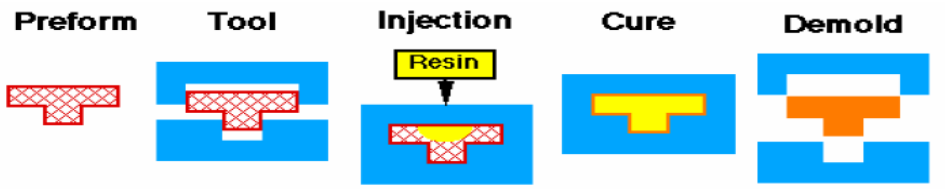

Figure 27 Flow chart of RTM

Nowadays in the aerospace industry, much interest has been expressed about the RTM process, focusing on the possibility of complex shapes and cost-effective production. At the same time, prepregs provide researchers and scientists with many advantages in terms of their familiarity, ease of handling, property reliability, low voids, and high fibre volume fraction. [21]

B: Vacuum Infusion (VI)

The main difference between VI and RTM is that the resin is injected under the atmosphere pressure rather than the elevated pressure in RTM. As a result, the FVF of VI panels should be much lower than that of RTM panels due to the lower preform compaction. But VI is selected in this research as the cost of this process is much lower than RTM due to the lower mold and equipment cost and thickness variations are simply accommodated.

C: Resin Film Infusion (RFI)

In RFI, a resin film is placed between dry reinforcements and the lower mould. A vacuum is applied to the mould cavity after the upper mould is installed. The whole

assembly is heated in an autoclave or an oven (Figure 28). Generally, this process is performed at both elevated pressure and elevated temperature so that a high fibre volume fraction and low void content for maximum structural efficiency is facilitated. [21] [7]

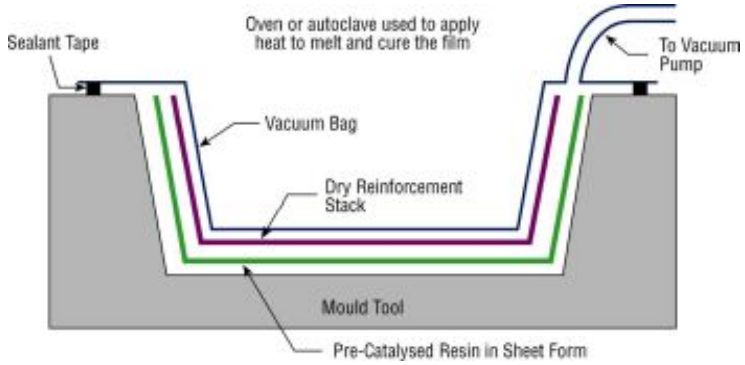

Figure 28 Schematic diagram of RFI

D: Single Line Injection (SLI)

A novel manufacturing process called Single Line Injection (SLI) has been developed by DLR in recent years. Excellent and void-free laminate quality and class-A surface statuses have been achieved by the Autoclave Process in which the resin is injected under pressure, allowing the laminate to be compacted by autoclave pressure. More intriguing is that the injection and evacuation of resin is carried out with the same resin transfer line and also the autoclave pressure can be selectively adjusted in order to reach the desired fibre volume content (typically 60%) (Figure 29).

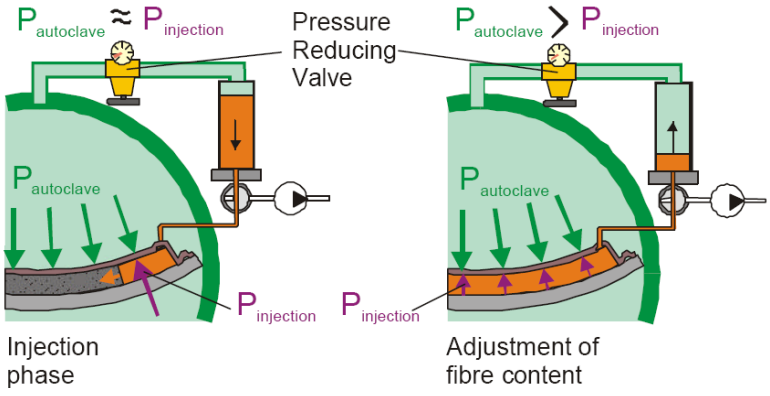

Figure 29 Pressure distribution during injection and adjustment phase

3 Materials

Every component of the composite laminates (such as; fibre, fabric, resin, interleaving and through thickness reinforcement (TTR)) influences the CAI performance. Therefore, the focus of this project is to quantify all the effects and behaviors of each material variable through thorough impact and CAI testing. A range of qualified, well-established materials and innovative materials offering potential damage resistance improvement was selected. These included through thickness strengthening and toughening materials, including powder binders, veils and tufting fibres.

3.1 Material List

Taking aviation applications into consideration, at the start of this research a materials list consisting of nineteen different composite panels was arrived at. A well-established aerospace high strength (HS) fibre and two kinds of representative resins (LY564 & RTM6) were chosen as the base line. In the same way, 19 different panels with one or more different components were designed for comparison so that the effect of every specific factor on CAI performance could be quantified and evaluated. The materials are as follows.

Table 1 Material List

NO.			Fibre	Fabric	Resin	TTR	Price	Comment
1		Prepreg	IM	UD tape	M21	-	£140/KG	
2		Prepreg	HS	Woven	M21	-	£150/KG	
3		Prepreg	HS	UD tape	M21	-	£80/KG	
4	A	Preform	HS	Woven	LY564	-	£79/KG	Baseline
	B	Preform	HS	Woven	RTM6	-	£79/KG	
5		Preform	HS	Woven	3508	-	£79/KG	
6		Preform	HS	Woven	LY564	Veil 1900	£79/KG £2/m^2	
7		Preform	HS	Woven	LY564	Veil 8014	£79/KG £2/m^2	
8		Preform	HS	Woven	LY564	Binder	£80/KG	

NO.			Fibre	Fabric	Resin	TTR	Price	Comment
9		Preform	HS	NCF	LY564	Binder	£35/KG	
10		Preform	HS	UD tape	LY564	Veil	£57/KG	
11		Preform	HS	Uniweave	LY564	Binder	£79/KG	
13	A_C	Preform	HS	Woven	LY564	Tufting	£79KG	Carbon thread
	A_G	Preform	HS	Woven	LY564	Tufting	£79/KG	Glass thread
	B_C	Preform	HS	Woven	RTM6	Tufting	£79/KG	Carbon thread
	B_G	Preform	HS	Woven	RTM6	Tufting	£79/KG	Glass thread
14		Prepreg	HS	Wove	913	-	£85/KG	
15		Preform	HS	UD tape	LY564	Veil & Binder	£50/KG	
17		Preform	HS	Woven	LY564	Veil 4605	£79/KG £2/m^2	

The price of veils is £2/m^2 which is equivalent to £6 per kilogram preform.

The tufting machine used in this research cost £50000, the normal tufting speed is 1 meter per three minutes and the labour cost for a professional technician is £30 per hour including overhead. The layup for the veils is simply stacking between each layer.

The materials list could be classified into four main sub-groups (Table 2): (A) 5HS preform, (B) unidirectional preform, (C) woven prepreg, and (D) UD tape prepreg.

Table 2 Material groups

Group	Member	Comments
A	No.4A, No.4B, No.5, No.6, No.7, No.8, No.13AC, No.13AG, No.13BC, No.13BG, No.17	Woven Preform, with or without TTR
B	No.9, No.10, No.11, No.15	Unidirectional Fibre Preform, with or without TTR
C	No.2, No.14	Woven Prepreg, without TTR
D	No.1, No.3	UD Tape Prepreg, without TTR

Group A: The control panel used HS fibre in a five-harness woven fabric. This type of material is currently used in the aerospace industry and in the novel unmanned aircraft vehicles in UK. The resin selected for the base line was the LY564, which is a low cost, brittle type. Another resin is a high temperature resin, RTM6, which is a

pre-degassed mono-component resin. A toughened medium temperature curing 3508 epoxy system was also selected for this research (No.5). In order to investigate the effects of TTR and interleaving, tufting was applied in No.13, three kinds of veil were selected for No.6, No.7 and No.17, and DX69 binder was employed in No.8. It is worth noting that all of these panels were the same, apart from their interlaminar reinforcements.

Among Group B, in an attempt to compare the straight and undulating fibre architectures, three types of common unidirectional fibre fabrics were also selected for the research (NCF (No.9), uniweave (No.11) and UD tape (No.10 and No.15)).

As any comparison data between prepreg and dry fabrics has yet to be found, Group C, which consists of two kinds of woven fabrics using high strength fibre was appropriate.

Finally, Group D, representing carbon fibre usage in existing commercial aircraft, including the HS (T700G) and IM fibres (T800H), was taken into consideration.

The material samples are shown in Table 5 and all the properties are summarised in **Table 3** and **Table 4**

Table 3 The properties of carbon fibre

Fibre	Young's Modulus GPa	Tensile Strength mPa	Density g/cm^3
T800H	294	5490	1.81
T700GC	240	4900	1.80
T300J	230	3200	1.77
AS7	241	4830	1.79
HTA	238	3950	1.77

Table 4 The properties of resin

Resin	Young's Modulus mPa	Tensile Strength mPa	Flexural Strength mPa	Density g/cm^3	G_{1c} J/m^2
LY564	3100~3200	75	140~150	1.22	100~125
3508	--	--	140~150	1.22	210~240
RTM6	2890	75	132	1.14	168
M21	3500	--	147	1.28	--
913	3390	65.5	--	1.23	--

Table 5 Thumbnails of different materials

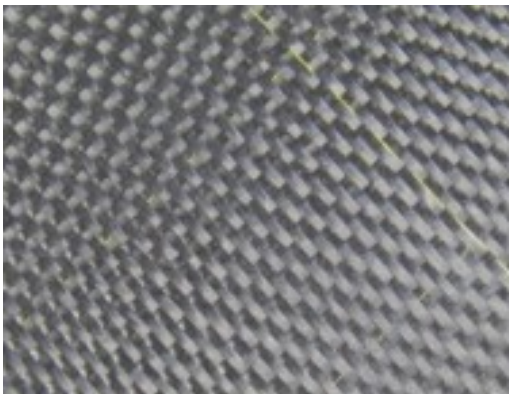 5HS	 5HS+Binder
 5HS+Veil	 5HS+Tufting

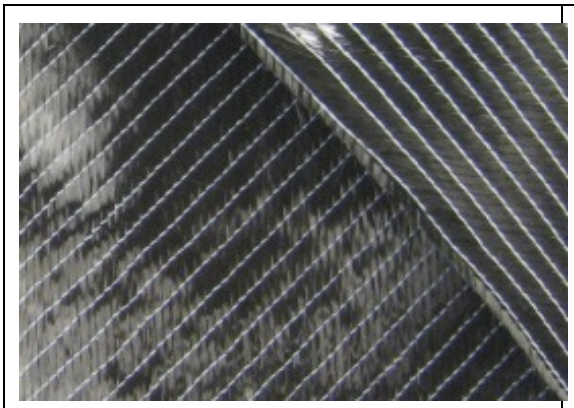 NCF	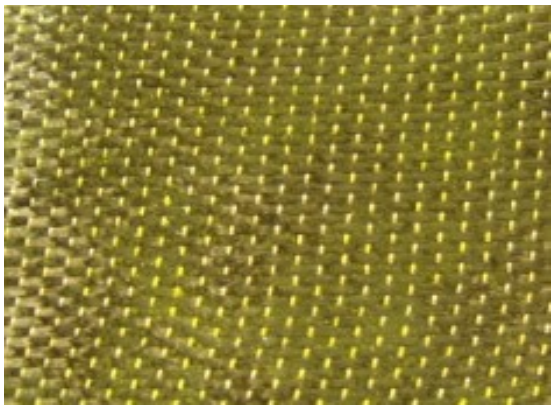 Uniweave+Binder
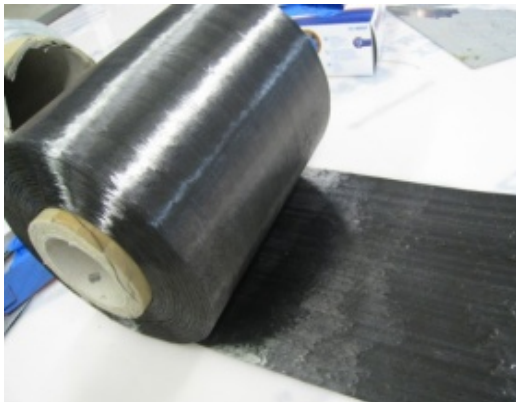 UD Tape+Veil	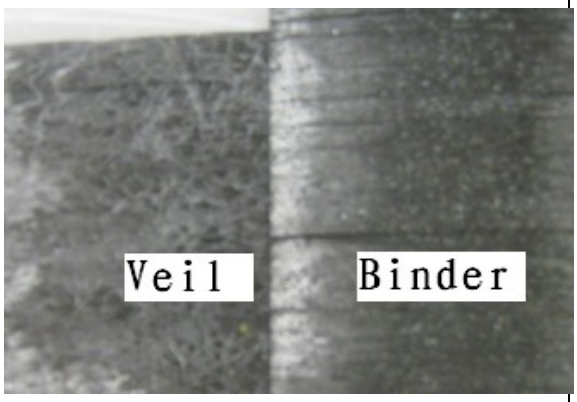 UD Tape+Veil+Binder
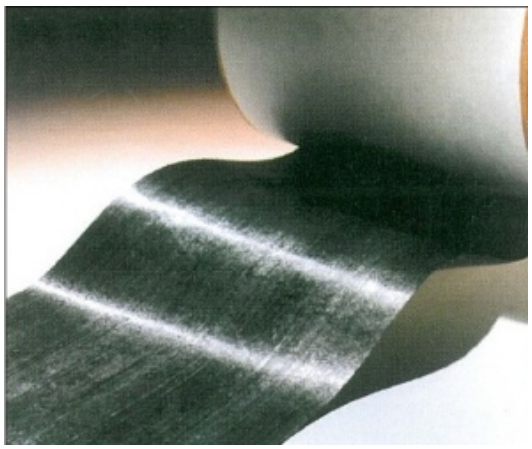 UD tape prepreg	 Woven Prepreg

3.2 Raw Material Characteristics

3.2.1 Carbon Fibre Prepreg

3.2.1.1 T800H UD Tape/M21-Hexcel Composites

T800H carbon fibre is an intermediate modulus type, which has approximately 35% greater strength and 20% higher stiffness than high strength fibre. It is supplied by TORAY industry and was developed to meet the high strength-weight ratio demanded by aircraft. It is the standard material for existing aircraft in highly loaded primary structures such as vertical fins and horizontal stabilizers.

Table 6 T800H fibre properties

	English	*Metric*	*Test Method*
Tensile Strength	796 ksi	5,490 MPa	TY-030B-01
Tensile Modulus	42.7 Msi	294 GPa	TY-030B-01
Strain	1.9 %	1.9 %	TY-030B-01
Density	0.065 lbs/in^3	1.81 g/cm^3	TY-030B-02
Filament Diameter	2.0E-04 in.	5 µm	

Resource: Toray Carbon Fibre Technical Data Sheet (T800H) Ref-No.CFA-007.

HexPly M21 is a high performance, very tough epoxy matrix, supplied with unidirectional or woven carbon or glass fibres, which is applied in primary aerospace structures. It exhibits excellent damage tolerance, especially at high-energy impacts. It has excellent toughness particularly at high-energy impact, outstanding residual compression strength after impact and effective translation of fibre properties especially with intermediate modulus carbon fibre.

Hexcel Composites M21 is a thermoplastic toughened 180C cure epoxy developed in conjunction with Airbus Industries. The particulate toughener acts as crack stopper inside of matrix.

Resource: Hexcel HexPly M21 Product Data. Combine the below.

3.2.1.2 T800 Woven/M21-Advanced Composites Group

The woven version of T800 /M21 prepreg provides lower stiffness and strength, as a result of the fibre undulations caused by the weaving. However, this provides a rough interface between layers which confers much higher interlaminar fracture toughness and hence should provide greater damage resistance.

3.2.1.3 T700GC/M21 UD Tape Prepreg-Hexcel Composites

T700GC is a carbon fibre with enhanced tensile modulus and adhesion properties compared to T700S. The applications of this include aircraft and high performance sporting goods. It is produced by TORAY industries.

The fibre properties are shown in Table 7 below.

Table 7 T700GC fibre properties

	English	*Metric*	*Test Method*
Tensile Strength	711 ksi	4,900 MPa	TY-030B-01
Tensile Modulus	34.8 Msi	240 GPa	TY-030B-01
Strain	2.0 %	2.0 %	TY-030B-01
Density	0.065 lbs/in^3	1.80 g/cm^3	TY-030B-02
Filament Diameter	2.8E-04 in.	7 µm	

Material label: HexPly® UD/M21/35%/268/T700GC/300
Resource: Toray Carbon Fibre Technical Data Sheet (T700G) Ref-No.CFA-006.

3.2.1.4 T300J/913 Woven Prepreg-Hexcel Composites

The prepreg material is 300gsm five-harness satin weave fabric pre-impregnated with low curing temperature 913 epoxy resin. Toray T300J fibre was developed as a higher strength grade of T300 for general purpose use. Hexcel Composites 913 was the first prepreg epoxy resin to be qualified by Airbus Industries in the 1970s. It is a 130°C cure resin with relatively low toughness.

The fibre and resin properties are shown in Table 6 and 7.

Table 8 Properties of T700J fibre and resin

	T300	913
Young's Modulus, E (GPa)	230	3.39
Shear Modulus, G (GPa)	8.96	1.21
Poisson's ratio, ν	0.2	0.41
Density, ρ (kg/m^3)	1770	1230
Tensile Strength, σ_{TS} (MPa)	3200	65.5
Compressive Strength, σ_{CS} (MPa)	2000	-

Table 9 Ultimate strains along fibres

Specimen	Orientation	Tension ε_T (%)	Compression ε_C (%)	Bending ε_B (%)
T300/913	[0,90]	1.00±0.09	0.95±0.12	2.71±0.05
	[±45]	-	-	2.29±0.02
	$[0,90]_2$	0.99±0.04	0.69±0.01	1.89±0.09
	$[\pm45]_2$	-	-	1.77±0.03

Resource: material data sheets.

3.2.2 Carbon Fibre Preform

3.2.2.1 UD Tape-Hexcel Composites

A 95mm wide carbon unidirectional tape, provided by Hexcel Composites, as shown in Table 5, is a newly developed high strength and standard modulus material AS7-12 dry fibre with DX69 binder powder on one side and two gsm veil on the other. The powder binder enables it to be rigidised by hot compaction to provide accurate dimension preforms and the veil allows it to be handled and cut during preform lay-up. This enables a fibre tape to be produced with no textile architecture and hence no inherent fibre undulation. The tensile strength is 4830mPa.

The second type of tape provided by Hexcel Composites, as shown in Table 5, is a more recent development. A 350mm wide carbon unidirectional tape, termed NAPPE. It is a combination of Hexcel 12k AS7GS dry fibre tow and SDV32 3 gsm veils on both sides.

Resource: material data sheets.

3.2.2.2 NCF- Devold AMT

Non-crimp fabric is a novel type of fibre reinforcement, where layers of fibre are assembled in a warp knitting machine into 0.2mm – 2mm thick multi-angular assemblies using a LIBA machine. The fabrics offer the advantages of low cost, low fibre crimp (undulations), high drape to allow easy conformance to double curvature surfaces and the tailoring ability of layer angles and thickness, allowing a fabric to be produced individually for a particular structure.

The NCF material used in this study is DB450 (biaxial, -450/+450, 410gsm, with polyester tricot style) provided by Devold AMT.

Resource: material data sheets.

3.2.2.3 Uniweave- Hexcel Composites

Uniweave is a woven fabric with the reinforcement applied along the warp axis and held together by a very light, in this case E glass fibre, woven weft yarn. The weft yarn is around 0.5% of the fabric weight and hence does not cause significant undulation of the carbon fibre warp tow.

This G1157 material is fabricated using 96% Tenax unidirectional 6k HTA 5131 carbon fibre and 4% EC9 34 E-glass thread, as shown in Table 5. The fabric is coated on one side with Hexcel E01 type epoxy powder binder at 3% by weight to allow hot preform compaction.

Resource: material data sheets.

3.2.2.4 Woven- Hexcel Composites

The base line, Hexcel G0926 carbon fabric, is a 5 harness satin (5HS) weave. Another 5HS fabric has the same basal body coating with the E01 binder applied as per the Uniweave material. Both of the samples are shown in Table 5.The carbon tow is of 6k filaments and the fabric areal weight is 370 gsm. This binder-coated fabric is consolidated in a heated press at 80°C to 140°C for around 20 minutes.

Resource: material data sheets.

3.2.3 Resin Characteristics

3.2.3.2 LY564 Epoxy Resin/ HY 917 Hardener/ DY 070 Accelerator-Huntsman Advanced Materials

This combination is provided by Huntsman for low cost production. The recommended cure schedule is four hours at 80℃ and four hours at 120℃ (post-curing). Its flexural strength is 140~150mPa and ultimate flexural elongation is 6.0~7.0%. Its fracture toughness G_{IC} is 100~125 J/m^2. The mix ratio by weight is 100:98:3 (resin: hardener: accelerator).

Resource: Huntsman Data sheet.

3.2.3.3 Araldite XU 3508 /Aradur 917/Accelerator DY 070-Huntsman Advanced Materials

This toughened hot curing epoxy system was developed by the Huntsman Corporation. The reactivity of this combination is regulable by variation of the accelerator ratio. It is easy to process and to achieve outstanding mechanical, dynamic and thermal performance.

The ratio of the combination is 100:90:0.5~2 (resin: hardener: accelerator). The flexural strength is 140-150mPa. Its fracture toughness G_{IC} is 210~240 J/m^2.

Resource: Huntsman Data sheet.

3.2.3.4 HexFlow RTM6- Hexcel Composites

HexFlow RTM6 was developed by Hexcel Composites for aircraft primary structures. It is a mono-component resin with a high glass transition temperature, excellent hot/wet properties and minimal moisture absorption.

The strength of the resin is 75mPa and the young's modulus is 2890mPa. Its fracture toughness G_{IC} is 168 J/m^2.

Resource: Hexcel HexFlow RTM6 Product Data.

3.2.4 Tufting Material Characteristics

Single sided stitching using the tufting technique was selected owing to its recent uptake by the aircraft composites industry. It has been shown to cause less in plane fibre damage and can be effectively applied at lower cost than other stitching techniques [30].

Both carbon thread and glass thread were selected for the study. The tufting material characteristics are presented below.

3.2.4.1 Glass Fibre Thread.

Glass fibre thread is preferred for stitching reliability since it is far tougher than carbon. The glass fibre used tufting was a 9.4μm diameter filament E glass fibre. The glass thread consists of three yarns (411 filaments in each) twisted into each other to provide higher breaking strength during stitching. The overall diameter of the thread was 0.47 mm; the tensile strength is 1319mPa. The glass fibre was supplied by Saint Gobain Vetrotex, reference EC9-68 × 3 S260.

3.2.4.2 Carbon Fibre Thread

The carbon thread was Tenax high flexibility textile behaviour yarn (HTA 40), developed by Toho Tenax. It is manufactured with two closely entwined yarns (1000 filaments in each). The overall diameter of the thread was 0.42 mm; the tensile strength is 1848mPa. The detailed properties of the two types of tufting threads are shown in Table 10 below.

Table 10 Tufting threads properties

Thread type		Carbon	Glass
Thread specification	-	Tenax® Carbon	EC9 68x3 S260
Fibre	-	HTA40	EC9 68 Z28
Manufacturer	-	Schappe Techniques®	Saint Gobain Vetrotex
Linear weight	g/km	140	204
Filament count	-	2 x 1000	3 x 411
Dry cross-section area	mm^2	0.077	0.078
Average property (St. dev)		Carbon	Glass
Filament diameter	µm	7.2 (0.4)	9.4 (0.9)
Filament count	-	1974 (10)	1194 (6)
Thread diameter (dry)	mm	0.42 (0.11)	0.47 (0.01)
Twist thread (S-/Z-direction)	m^{-1}	S 190 (11)	S 253 (3)
Twist yarns (S-/Z-direction)	m^{-1}	Z 237 (3)	Z 287 (1)
Linear weight (dry)	g/km	136 (0.5)	205 (0.3)
Tensile modulus (dry)	GPa	195 (9)	53 (4)
Tensile strength (dry)	mPa	1848 (81)	1319 (45)
Ultimate strain (dry)	%	0.9 (0.05)	2.1 (0.3)
Impregnated cross-section area	mm^2	0.121 (0.006)	0.130 (0.005)
Tensile modulus (impregnated)	GPa	199 (10)	70 (2)
Tensile strength (impregnated)	mPa	3544 (72)	2382 (39)
Ultimate strain (impregnated)	%	1.7 (0.1)	3.6 (0.1)
Resin weight content	%	0.31	0.3

3.2.5 Veil

Three types of separately applied veils were provided by Toho Tenax GMBH. These materials are applied during the laying up separate from the fabrics and are expected to locally toughen the laminates at the ply interfaces.

3.2.5.1 8014 System Veil

The areal weight of 8014 veil is 20gsm, and its melting point is 140°C.

3.2.5.2 4605 System Veil

The areal weight of 4605 veil is 6gsm, and its melting point is 140°C.

3.2.5.3 1900 System Veil

The areal weight of 1900 veil is 3gsm, and its melting point is 170°C.

4 Manufacturing

Once the preform or prepreg material layers for each panel have been precisely cut to the required dimensions from the material roll, it is possible to start the laying-up process. The lay-ups of all the panels were quasi-isotropic, as shown in Table 11. In order to compare the construction in different material panels, similar lay-ups were applied. Because the areal weights of different fabrics varied, the numbers of layers was varied in order to achieve a similar cured thickness. The laying-up procedures in each case differed slightly due to the different physical conditions of the raw materials.

Table 11 Lay-up illustration

Lay-up A	
Layer	Direction
1	45/-45
2	0/90
3	45/-45
4	0/90
5	90/0
6	-45/45
7	90/0
8	-45/45
9	45/-45
10	0/90
11	45/-45
12	0/90
13	90/0
14	-45/45
15	90/0
16	-45/45

Symmetric Plane

Lay-up B	
Layer	Direction
1	45
2	0
3	-45
4	90
5	90
6	-45
7	0
8	45
9	-45
10	0
11	45
12	90
13	90
14	45
15	0
16	-45

Symmetric Plane

Lay-up C	
Layer	Direction
1	45/-45
2	0/90
3	45/-45
4	0/90
5	45/-45
6	0/90
7	90/0
8	-45/45
9	90/0
10	-45/45
11	90/0
12	-45/45

The process of prepreg lay-up (No.1, 2, 3, 14) by hand was difficult because the pre-impregnated tapes were tacky. During the lay-up procedure it was necessary to pay significant attention to each layer in order to minimise the fibre orientation deviation away from the exact specified angle. All the layers were stacked carefully in

the desired directions according to the lay-up illustrations. The de-bulking and pre-compacting procedure for the laminates was applied every four layers so that that air and volatiles could be removed between plies and the probability of the formation of voids in the laminates could be minimised. The principle of this procedure is that the resin became thinner and less viscous and so would allow trapped air to be easily emitted when the laminates were pre-heated to a low temperature and under a low vacuum pressure.

The process of dry preform manual laying-up (No.4, 5, 6, 7, 9, 13, 17) was the simplest one. The relative movement between layers was much easier than with prepreg due to the smooth and non-tacky surface. Similarly, the accuracy of fibre direction was essential. For panels including veils, one layer of veil was simply laid up in every interface between each two adjacent layers, as shown in **Figure 30**.

The most complex lay-up process was for the No.8, 10, 11 and 15. An iron was used to thermally activate the epoxy binder powder and/or veils, and naturally pre-bond the layers together during the fibre laying-up. A release film was placed on the top of the ongoing laminate in order to avoid a direct contact between the iron and the veil or the powder binder on the material surface. Hand pressure was applied and the iron was switched to the lowest setting for synthetic fibres. A simple but beneficial metal sheet was utilised to follow the moving iron so that the preform could be cooled down and consolidated quickly.

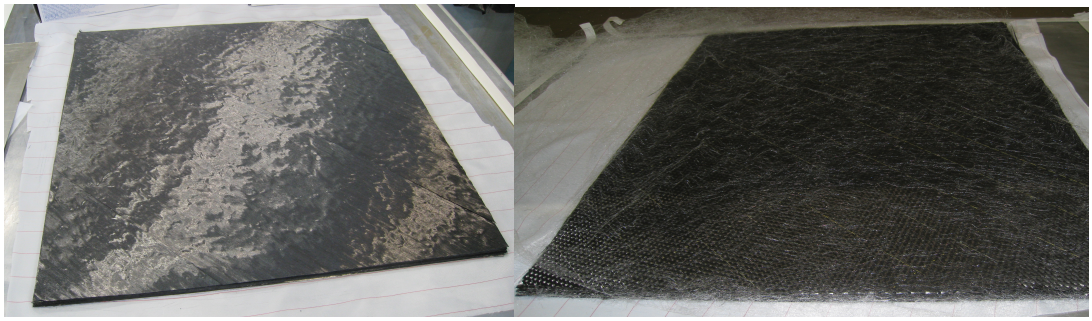

(a) (b)

Figure 30 (a) prepreg (b) preform with veils

4.1 Tufting

In order to investigate the effect on the CAI strength properties of tufting (Figure 31), this novel manufacturing technology was applied to two dry fibre preforms using two kinds of threads separately (No.13A, 13B) .

The plies were stacked up on a polystyrene foam plate, and a vacuum bagging film was sandwiched between them as shown in Figure 32. The polystyrene foam was necessary for the purpose of protecting the penetrating needle and the working plate during perforation. A further advantage of using polystyrene foam was to hold the processing thread loop firmly and continually so that all the loops were consistent. The vacuum bagging film was used to separate the preform from the foam.

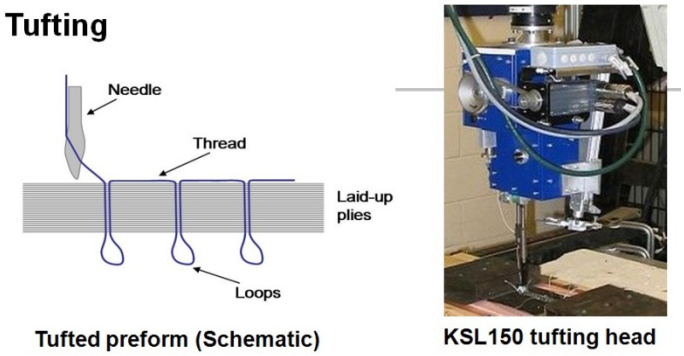

Figure 31 Tufting illustration

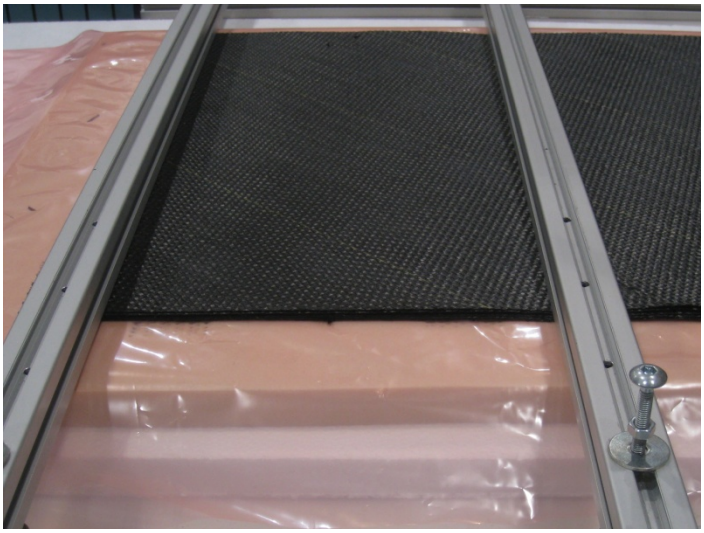

Figure 32 Tufting setting up

Two kinds of threads were selected, glass thread and carbon thread, as shown in Table 10. The tufting density was 2 threads per 16 mm^2, i.e. the spacing between each individual tuft in a row was 4 mm, and the pitch between each row was also 4mm.

Because the glass thread is very smooth and relatively tough, it could be easily tufted even though the preform was very tight because of the presence of hard binder particles in the fibre tows. The carbon thread is stiffer and the flexibility is lower than for glass thread; as a result the carbon thread was broken during several trials, even though two supplementary methods were used, i.e. preheating and lower tufting speed. A more effective technique used sprayed water as a lubricant. The water was sprayed on the top of the preform beforehand and sprinkled on the ongoing area during the tufting process. Disadvantageously however, the preform needed to be dried at 50°Cfor two days.

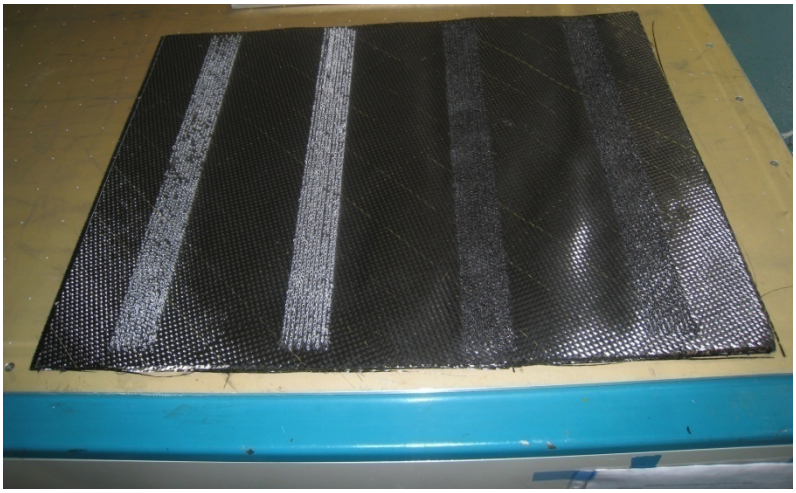

Figure 33 Picture of tufted preform (loop side), the white is glass and the black is carbon

As observed in Figure 33, in order to reduce the tufting cost and save time, only four separate tufting zones, which consisted of 11 rows with 4mm pitching, 4mm spacing and 3~4mm deep loops, were processed in the preform. This dimension of tufted zone was determined by the projected impact-induced damage area (40 mm round) of the baseline (No.4A), which was the same preform without any TTR. This specific decision made it possible to ensure that the damage area due to impact did not extend

beyond the tufted region. The tufted position was accurately calculated in order to make sure it would be in the middle of the testing specimens after cutting.

4.2 Vacuum Infusion Moulding

With a view to lower the cost of manufacturing, Vacuum Infusion (VI) was selected rather than Resin Transfer Moulding (RTM) even though the latter usually provides a lower void content, higher fibre volume, excellent thickness tolerance and class-A quality surface on both sides. The use of VI is sufficient for the purposes of this research and provides a uniform compaction pressure for the various preforms.

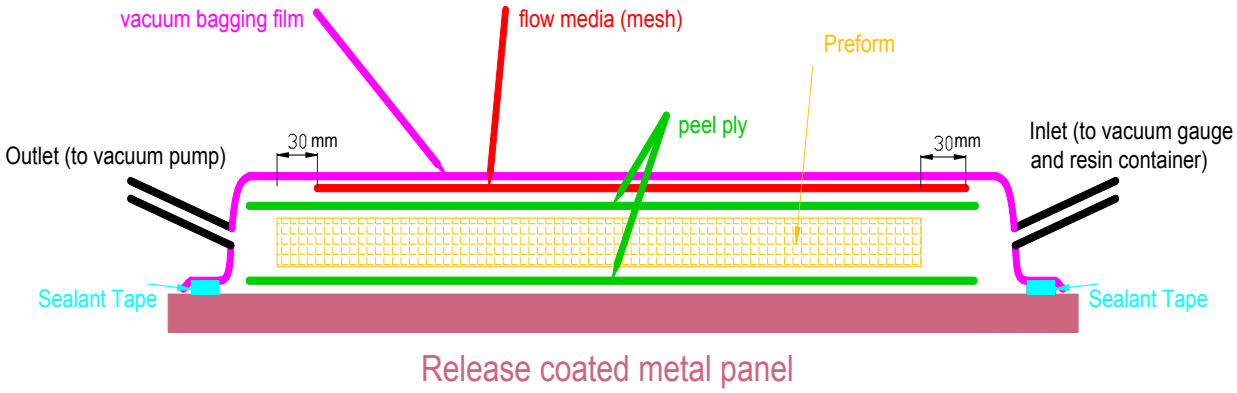

Figure 34 Vacuum bag setting up for VI moulding

As shown in the vacuum bagging illustration (Figure 34), the metal panel was coated by a mould release agent before stacking the peel ply, preform, flow media and vacuum bagging film on top of it specified by the illustration. The vacuum bag with inlet and exit was set up and sealed with circuitous and occlusive mastic tape and vacuum bagging film.

Degassing was required before injecting the resin into the vacuum bag. The most important factor was to keep a 30mm wide gate at the inlet end and a 30mm wide gap at the outlet end. The function of the gate at the inlet was to let the resin flow quickly across the full width of the laminate. The purpose of the gap at the exit end was to provide sufficient time for the resin to fully penetrate the preform thickness direction

after moving rapidly through the flow media. The vacuum level was around 3.0 mBar.

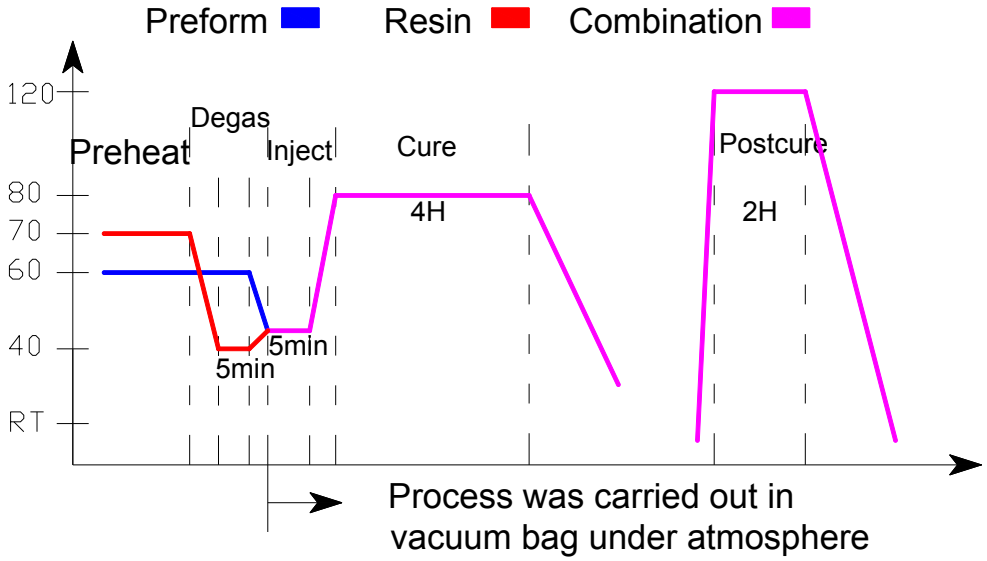

Figure 35 Manufacturing flowchart for normal panel

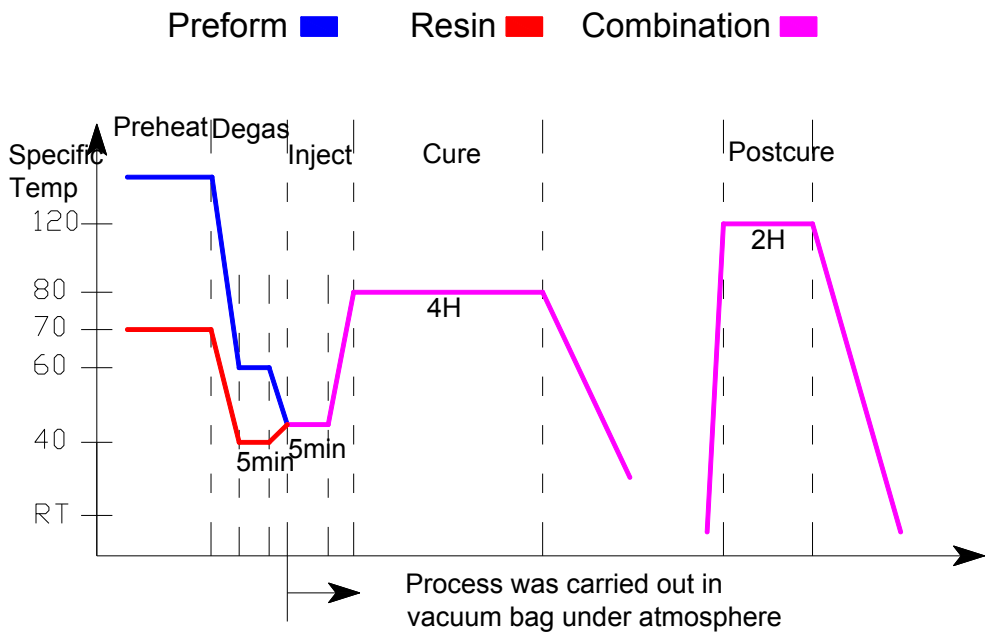

Figure 36 Manufacturing flowchart for veiled panel

The VI procedure for the 13 preform panels in the manufacture list can be categorised into 3 types as shown in Figure 35, Figure **36** and Figure **37**. As shown in Figure 35, in normal VI, the resin (LY564) was preheated to 70℃ before being mixed with hardener (HY917) and accelerator (DY070) according to the ratio of 300:294:1. The

combination was degassed for 5 minutes inside the vacuum pump and kept at a temperature of around 40℃ before being injected into the vacuum bag which was heated to 60°C. The injection duration was around 5 minutes. Once filled, the inlet was closed and the whole set up was heated to 80°C. The vacuum pump and the heating were working constantly during the whole 2 hours of the curing phase. After curing, the panel was cooled naturally. 2 hours post-curing procedure at 80℃ was carried out after the panel was cut into 100mm×150mm specimens.

The VI procedure for veiled or/and bindered preform differs from normal VI procedure in one simple but critical way, i.e. the veils or/and binder needs to be activated at a specific high temperature before infusion (Figure 36).

The VI for 3508 resin combination was exactly the same as for the LY564 system.

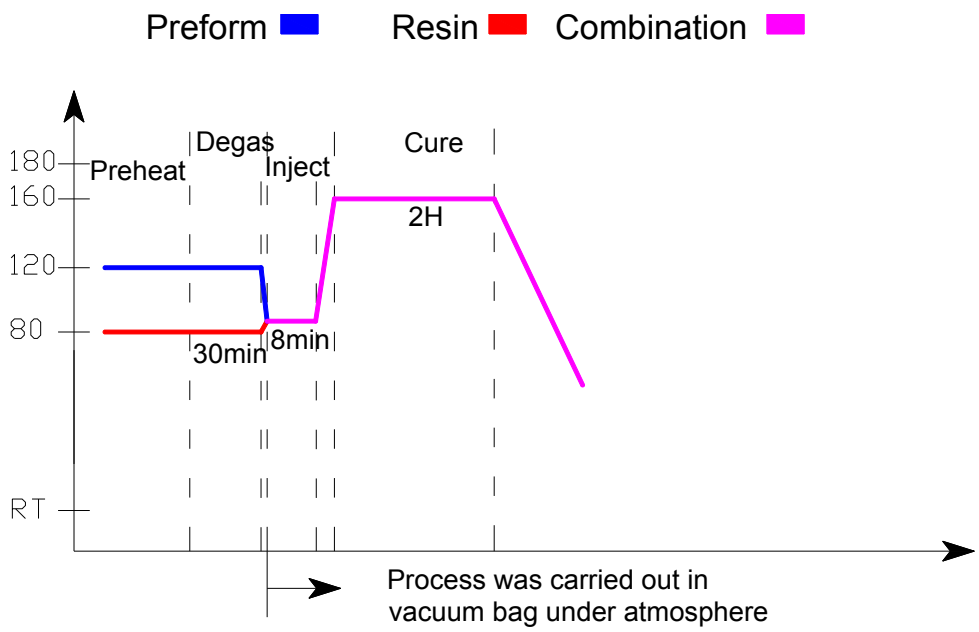

Figure 37 Manufacturing flowchart for RTM6 panel

The RTM6 infusion proved highly complex, requiring a long degassing time and careful temperature control (Figure 37). Six kinds of cure cycle possibilities are provided in the HexFlow RTM 6 product data sheet. Cycle No.2 was selected, in which the resin was cured at 160℃ for 2 hours and post-curing not required. The

RTM6 infusion duration was around 8 minutes. Copper pipes rather than plastic one were used in RTM6 infusion due to the high injection and curing temperature.

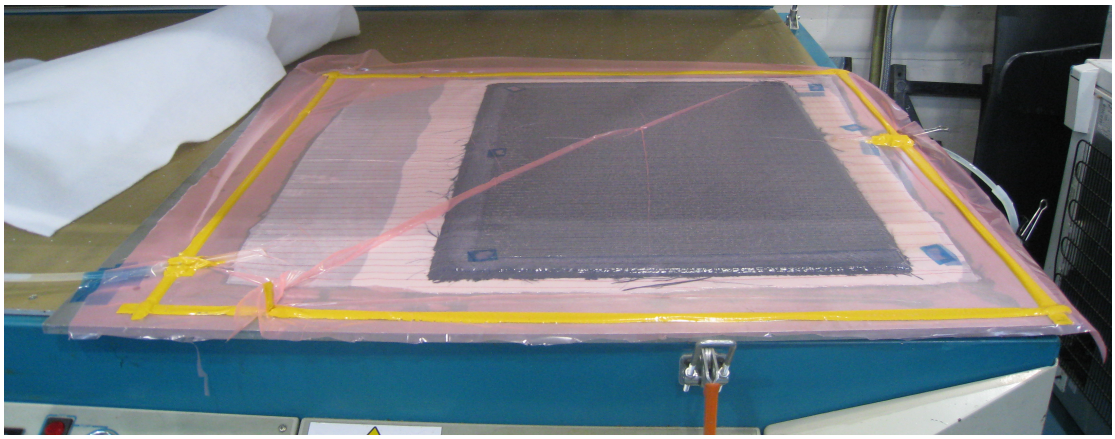

Figure 38 Typical set up for vacuum infusion

4.3 Autoclave Moulding

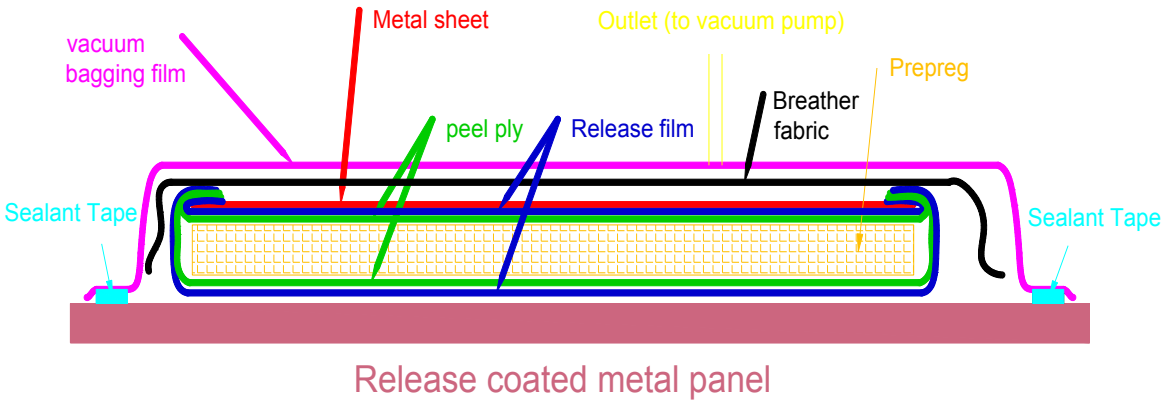

Figure 39 Vacuum bag setting up for prepreg moulding

The curing routine for the prepreg panels' autoclave moulding, was much easier than for VI. The prepreg was laid up manually and de-bulked for 15 minutes in advance. The prepreg panel was bagged by peel ply and release film on both sides and with a metal caul sheet on the top, as shown in Figure 39. A breather fabric was placed on the top of this package in order to provide venting for gas in the vacuum bag. A full vacuum was applied before placement in the autoclave. After this, the prepreg panel was cured at 180℃ for 2 hours under 4Bar gauge autoclave pressure. Such an

elevated pressure and elevated temperature provides high fibre volume fraction and low void content for maximum structural efficiency.

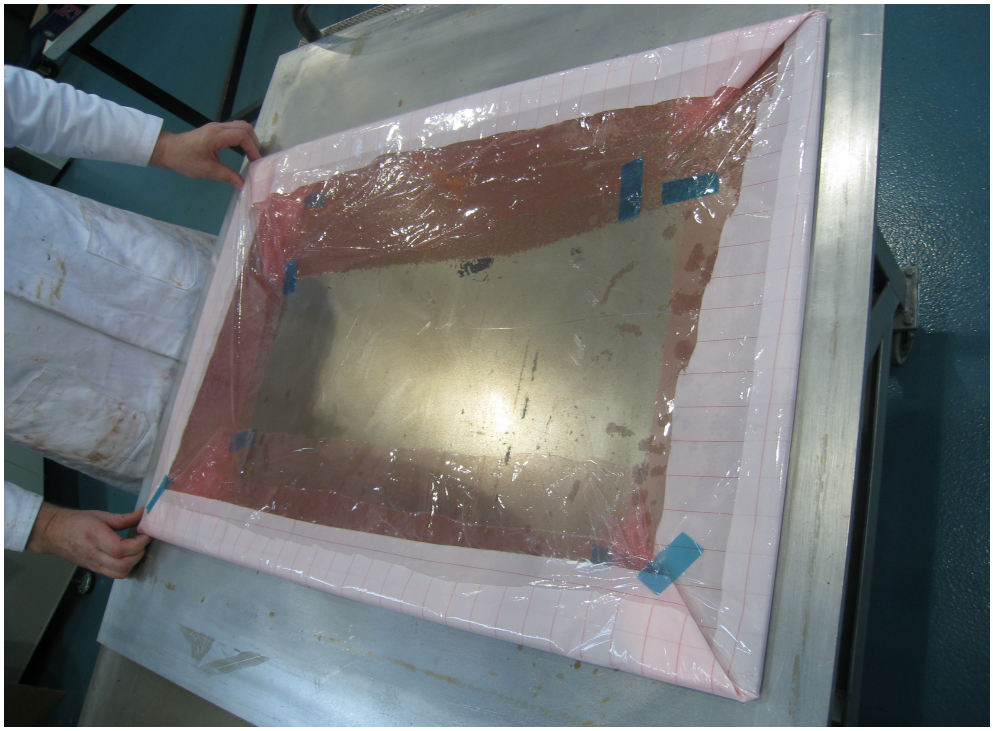

Figure 40 Typical bagging for prepreg panel

5 Testing

This chapter describes the procedure of Compression-After-Impact (CAI) testing in the following order: Impact Test, C-scanning, post-impact compression test. In addition, compression failure tests were carried out in order to evaluate how much compression strength was reduced due to impact. All the CAI tests were carried out according to the Boeing standard, which is the virtual standard used world-wide [Ref: BS ISO 18352:2009]. Considering the comparability with the CAI test, some significant treatment for the specimen was utilised from the ASTM D 695 (Standard Test Method for Compressive Properties of Rigid Plastics) in the compression failure test.

Table 12 Various industrial protocols for the measurement of residual compression strength [29]

Protocol	Material thickness and layup (mm)	Impactor tup and support conditions (mm)	Compression after impact		
			Specimen dimensions (mm)	Loading arrangement	Loading rate
CRAG	3 $(45/-45/0/90)_{nS}$	Tup: 10 dia Mass: open Height: 1 m Energy: open Support: 100 ring/clamped	180 by 50 (cut to size post-impact) Damage width not to exceed 40	End-tabs are recommended but other end grips accepted	Adjust to give failure in 30–90 s
NASA	6.35 $(45/0/-45/90)_{nS}$	Tup: 12.7 dia Mass: 4.5 kg Height: 0.61 m Energy: 27 J Support: 127 square/clamped	(254–318) × 178 (cut to 127 post-impact)	End loaded	1.27 mm min^{-1}
Boeing	4 to 5 $(-45/0/45/90)_{nS}$	Tup: 15.75 dia Mass: 4.5/6.8 kg Energy: open Support: 127 × 76 clamped	152 × 102 (cut to size before impact)	End loaded	0.5 mm min^{-1}
SACMA	4 to 5 $(-45/0/45/90)_{nS}$	Tup: 15.88 dia Mass: 5 kg Energy: open Support: 127 × 76 clamped	152 × 102 (cut to size before impact)	End loaded	1.27 mm min^{-1}
Airbus	4 $(45/0/-45/90)_{nS}$	Tup: 16 dia Mass: 1–6 kg Energy: 9–40 J Support: 125 × 75 clamped	150 × 100 (cut to size before impact)	End loaded	0.5 mm min^{-1}
British	4 to 5 $(-45/0/45/90)_{nS}$	Tup: 16 dia Mass: 1–6 kg Energy: 9–40 J Support: 125 × 75 clamped	150 × 100 (cut to size before impact)	End loaded	0.5 mm min^{-1}

5.1 Testing Preparation

As mentioned in chapter 3, 15 panels were infused via VI moulding (preform) and 4 panels were cured in the autoclave (prepreg). All the panels were machined into 150mm×100mm specimens. Six specimens were selected from each set for impact testing, but only five of them were compression tested. The remaining one destructively was used for investigation of the internal damage.

5.2 Impact

Visual detection was used for all specimens, both sides and cross sections, in order to check for manufacturing defects prior to testing. The surfaces of all the specimens' used were flat and without any visible void or un-impregnated regions. However, sporadic, discontinuous, small voids [Appendix C] were observed in cross sections of the unidirectional fibre preform panels.

The thickness of each specimen was the average of the thicknesses of each edge of the specimen, which were measured using digital vernier caliper. Similarly, the average of the specimens' thicknesses was adopted as the thickness of each panel. The thicknesses of all the panels were varied due to the different areal weight of the fabrics. Three ideas regarding how to decide the impact energy were considered, i.e. constant energy to fibre weight ratios, constant energy to FVF ratios and constant energy to thickness ratios. Because the maximum thickness was 4.84mm but he minimum one was only 3.49mm, it is unfair to impact such different panels with same energy. On the other hand, because the fibre weight of the veiled or tufted panel was the same as the un-veiled or tufted one, and the FVF of the former was lower than the latter due to interleaving and through thickness threads. It was unreasonable to choose the constant energy to FVF ratio, in respect that it means that the toughened panel would be impacted with low energy. Therefore, the general approach that constant energy to thickness ratio was the best choice which could obtain an effective

comparison between different materials and different reinforcements (Table 13).

An instrumented drop-weight machine (Rosand Type 5 falling weight impact tester, Figure 41 left) was used to create impact damage on the specimens with a typical 16mm hemispherical impact tip. During impact testing, the specimen was simply supported on the steel base, having a 127mm×76mm square opening, held at four corners by rubber clamps (Figure 42) and struck by a 16mm diameter hemi-spherical impactor weighing 2.28 kg. The range of impact energies was achieved by releasing the impactor from different heights. Multiple impacts were eliminated by a pneumatic device (Figure 41 right) in the impact machine, which could be ejected and held the impactor automatically after the first rebound.

Table 13 Impact energy of all sets

ID	Fibre	Fabric	Resin	TTR	Thickness (mm)	Energy(J)
1	IM	UD	M21	---	4.00	22.47
2	HS	Woven	M21	---	3.49	19.61
3	HS	UD	M21	---	4.19	23.54
4-A	HS	Woven	LY564	---	4.45	25.00
4-B	HS	Woven	RTM6	---	4.55	25.56
5	HS	Woven	3508	---	4.45	25.00
6	HS	Woven	LY564	Veil/3gsm	4.45	25.00
7	HS	Woven	LY564	Veil/20gsm	4.72	26.52
8	HS	Woven	LY564	Tough Binder	4.64	26.07
9	HS	NCF	LY564	---	5.00	28.09
10	HS	Woven	LY564	---	4.00	22.47
11	HS	Uniweave	LY564	Tough Binder	4.84	27.19
13-AC	HS	Woven	LY564	Tufting	4.45	25.00
13-AG	HS	Woven	RTM6	Tufting	4.45	25.00
13-BC	HS	Woven	LY564	Tufting	4.55	25.56
13-BG	HS	Woven	RTM6	Tufting	4.55	25.56
14	HS	Woven	913	---	4.80	26.97
15	HS	UD tap	LY564	Veil/Binder	4.68	26.29
17	HS	Woven	LY564	Veil/6gsm	4.62	25.96

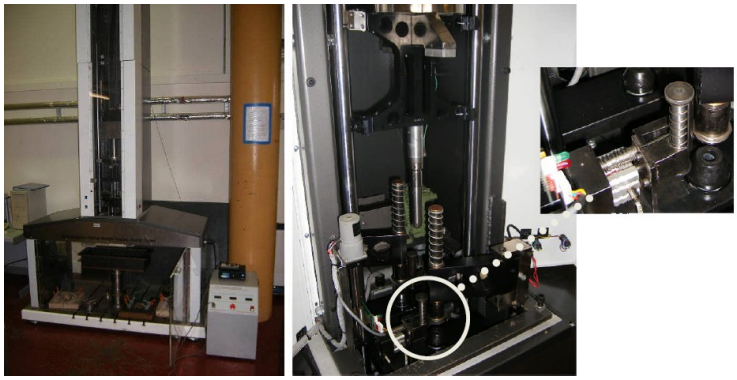

Figure 41 Rosand Type 5 falling weight impact tester (L), Second strike catcher (R)

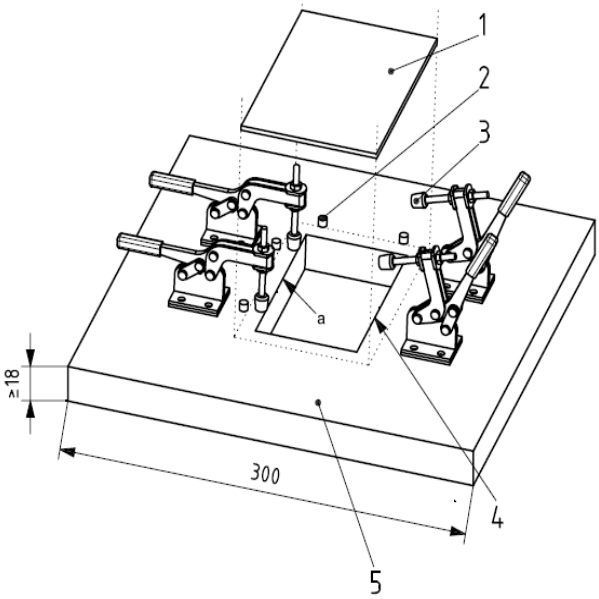

Key

1 specimen
2 guide pin
3 rubber bush
4 (76 ± 1) mm × (127 ± 1) mm window
5 base-plate
a 1 mm × 45° chamfer.

Figure 42 Illustration of a specimen support fixture

The thickness of each single panel was consistent except for the tufted one. As mentioned previously, tufting was only processed for a panel in several 40mm wide belts rather than for the whole panel. Hence, the thickness of the tufted zone was 1.2mm thicker than the un-tufted part. A ridge could be clearly observed in the middle of the tufted specimens. The key issue is that the impact energy for tufted panels was determined by the thickness of the un-tufted area of the specimen as the ridge was only formed of resin and flattened tuft loops.

5.3 Ultrasonic C-scan

After impact, visual inspection was carried out on the impacted and the opposite surfaces to determine the level of visible damage regarding the dent size and shape, fibre breakage, ply splitting, etc. As it is common knowledge that the inside damage size usually exceeds the visible size, therefore, the ultrasonic C-scan (Figure 43) was processed in order to investigate the projected cumulative damaged and delaminated area.

All the specimens were examined by ultrasonic C-scanning before post-impact compression. During the C-Scan process, the specimens were immersed in water, and a PC controlled ultrasonic pulser-receiver continuously scanned the ongoing specimen automatically after setting the beginning and ending point. A digital oscilloscope was used for adjusting the signal. The resolution of C-scanning was 0.4mm×0.4mm. Considering the scanning time and the accuracy, the resolution was sufficient to meet the demand of area measurement.

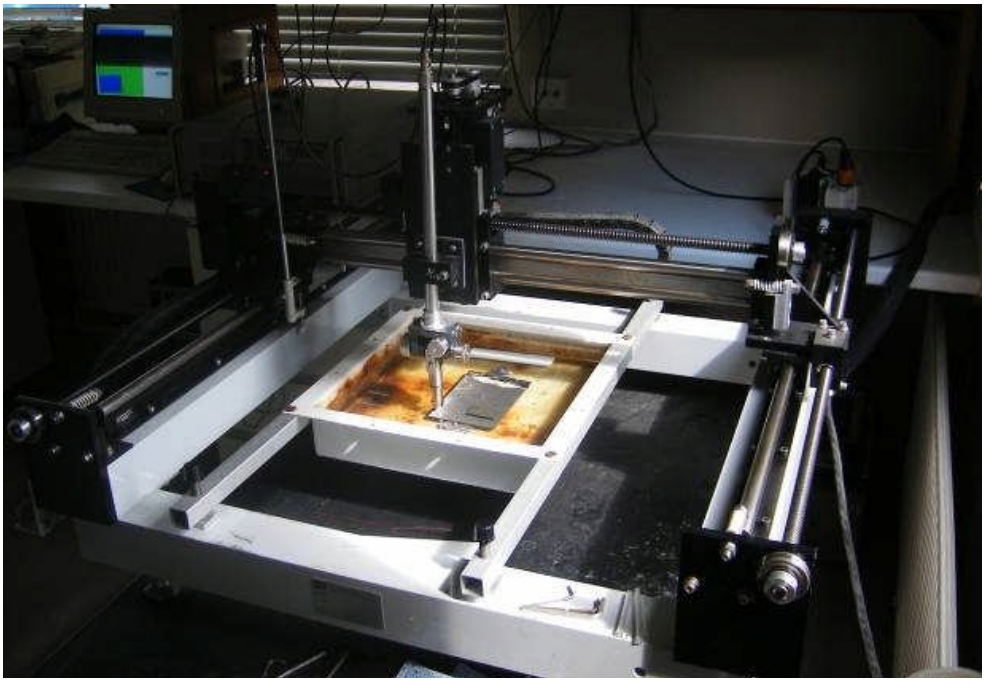

Figure 43 A specimen in C-scanning

The C-scanned pictures with cumulative damage and delamination projected area were saved for each ultrasonically C-scanning using the ANALYSIS software. The damage area could be measured using the pictures. The damage area used in the final analysis and comparison was the mean of a set of measurements.

5.5 Compression

Because all the specimens were immersed in water during C-scanning, they were dried in the oven at 80℃ for 8 hours immediately afterwards.

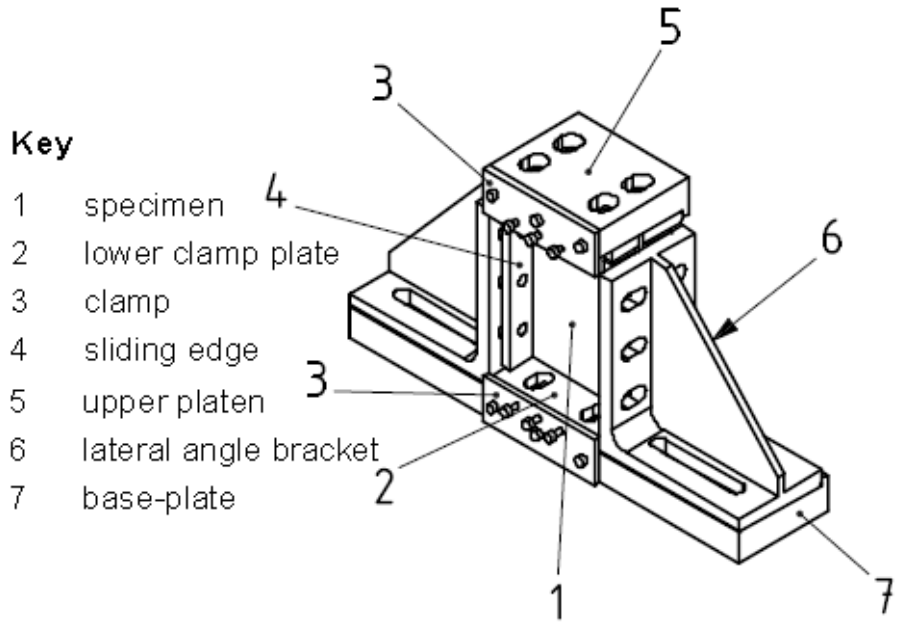

Figure 44 Illustration of compression-loading fixture

The machine used for compression testing was the ROUSAN 250 kN hydraulic testing system. The specimen was clamped in the jig, as illustrated in Figure 44. The machined ends of specimen were precisely parallel, which resulted in the lower clamp plate being essentially parallel to the upper platen. The sliding edges were held by sliding knife-edges which provided simple support for the longitudinal sides. This meant that translational motion of the specimen in the out-of-plane direction was prevented but rotation was allowed. In contrast, both ends of the specimen were clamped tightly in order to prevent both out-of-plane translational and rotational

motion as far as possible. The whole fixture was placed carefully between the loading-platens of the compression-testing machine, and the vertical axis of the fixture was aligned with the loading direction and the central axis of the machine.

Compressive loading procedure was controlled automatically using the displacement rate of 0.5mm per minute until the maximum load had been reached and the specimen failed. Both the loads and displacements were recorded at the rate of 10 times per second during the whole compression procedure. The loading procedure was terminated immediately after failure happened so that the initial distortion was retained.

All the specimens which sustained impact damage, without exception, were crushed through the damaged region of the specimen around the point of impact. The resulting data including loading time, displacement and compressive load data was saved for each compression test.

Alongside the actual CAI results, it was considered useful to understand the effect of the impact damage. To measure this, plain compression failure tests of undamaged specimens were also carried out. However, since the plain strengths were much higher and the majority of specimens failed due to end brooming during the first stage testing trail, the following methods were taken into consideration.

A: ASTM D 3410, Procedure B. This method is described indetail in the ASM HANDBOOK Vol. 21[31, P771]. The recommended dimensions of the testing samples are 140-155mm long and 10-25mm wide. All the samples should be typically tabbed with 10-25mm gauge length in the middle. A specific testing fixture is required. During the testing procedure, the compressive load applied in the fixture is transferred from the wedge grips to the specimen tabs through shear, and from the tabs to the test specimen, also through shear. Strain gauges or extensometers are required for modulus and strain at failure calculation.

B: SACMA SRM 1. This method is also elaborated in the ASM HANDBOOK Vol. 21[31, P771]. The recommended dimensions of the testing samples are 80mm long and 6.4mm wide. A specific testing fixture is required as ASTM D 3410. However, this method is not currently maintained since SACMA is no longer in existence.

C: Considering the comparability between the compression strength test and CAI test, it was important for all the specimens to be tested in a similar size. Hence, one ingenious treatment was copied from ASTM D 695 (Standard Test Method for Compressive Properties of Rigid Plastics). All the undamaged specimens were tailored in the middle of longitudinal edges. Two symmetrical strips (10mm wide) were cut off in order to create an artificial weak zone and induce a direct breakage in this zone. Such a long strip with a large circular transition could greatly reduce and even eliminate the stress concentration (Figure 45). To ensure continuity between the CAI test and the plain compression test, the same fixture was employed and same displacement rate applied during plain compression testing. However, during several testing trials, global buckling occurred as the failure mode because the roughly 80mm longitudinal edge in both sides could not be effectively supported (Figure 45). With the purpose of avoiding the risk of global buckling, two 1mm thick steel anti-buckling sheets were stuck back to back on both sides of the specimens. As shown in Figure 45, compared to the testing specimen, the anti-buckling sheet was 10mm shorter at each end, which gave enough clearance for compression deformation, and had a 40mm×60mm opening in the middle which avoided the unrequired reinforcement. The effects however, were not as effective as aspect since the steel sheet buckled in the middle.

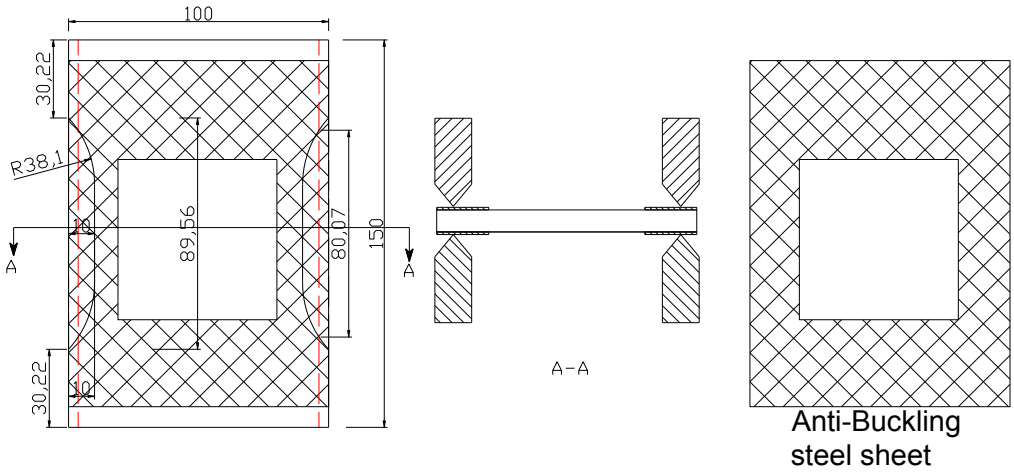

Figure 45 Dimension of the undamaged-specimen size for compression test

A technical refinement was applied to the fixture in order to solve the problem. A 10mm thick steel shim was added between the support knife and the frame so that the tailored specimen could be effectively supported and the weak region was approximately near to the middle as in CAI testing, as illustrated in Figure 46. No modification was applied to the holding device at the top or the bottom.

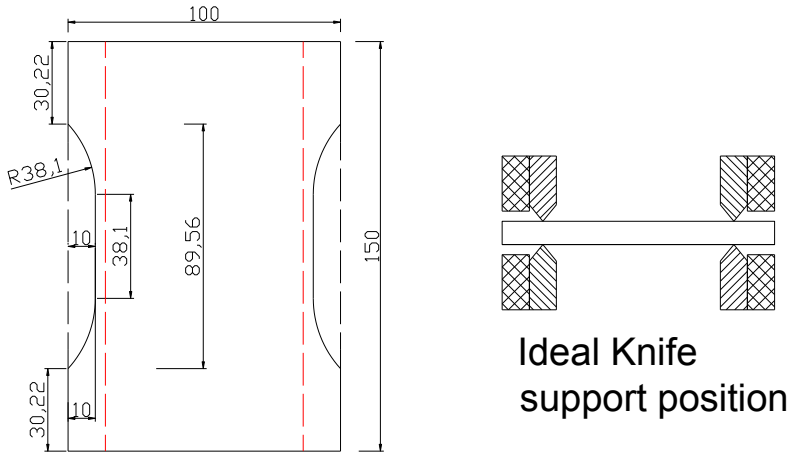

Figure 46 Ideal knife support position

All the failures happened in the tailored region as aspect after using the improved

fixture.

Three protective measures were strictly applied during the CAI tests: setting up the maximum and minimum load limits, setting up the minimum displacement limit and terminating the loading procedure as soon as the failure occurred.

6 Experimental Results and Findings

6.1 Fibre Volume Fraction (FVF)

The Fibre Volume Fraction (FVF) and Fibre Weight Fraction were calculated using the following formulae.

$$FVF = n \times \frac{W_f}{T \times \rho_f} \quad (1)$$

$$FWF = \frac{\rho_f \times FVF}{[\rho_m + ((\rho_f - \rho_m) \times FVF)]} \quad (2)$$

Where:

FVF	=	Fibre Volume Fraction
FWF	=	Fibre Weight Fraction
ρ_f	=	Density of Fibre (g/cm^3)
ρ_m	=	Density of Cured Resin/Hardener Matrix (g/cm^3)
n	=	Number of layers
W_f	=	Fibre Areal Weight of each ply (gsm)
T	=	Thickness of sample

The assumption for these formulae is the absence of internal voidage, but this is impossible for vacuum infused panels. It was inevitable that sporadic and small voids would be formed by air particles due to the lower vacuum level and artificially controlled degassing. Therefore, the calculated volume fraction was higher in varying degrees than that it should be. Another factor altering FVF was the thickness. The thickness of the vacuum infused panel varied over the surface because of lower flow-ability and vacuum level. Therefore the mean thickness at several different locations was used in the calculation.

Simply, the FVF was calculated using formula 1, in which W_f was obtained from either material data sheets or measurement in the laboratory. The FWF was calculated using formula 2.

Table 14 Fibre Volume Fraction Calculation

ID	ρ_f	W_f	ρ_m	FWF	Layers	T(mm)	FVF
1	1810	268	1280	67.2%	16	4.00	59.2%
2	1810	228	1280	66.0%	16	3.49	57.9%
3	1800	268	1280	64.9%	16	4.19	56.8%
4A	1760	370	1219	65.4%	12	4.45	56.7%
4B	1760	370	1140	65.7%	12	4.55	55.4%
5	1760	370	1223	65.3%	12	4.45	56.7%
6	1760	370	1219	65.4%	12	4.45	56.7%
7	1760	370	1219	65.2%	12	4.72	56.4%
8	1760	370	1219	63.2%	12	4.64	54.3%
9	1770	440	1219	68.2%	12	5.00	59.6%
10	1760	268	1219	69.2%	16	4.00	60.9%
11	1760	292	1219	63.7%	16	4.84	54.9%
13AC	1760	370	1219	65.4%	12	4.45	56.7%
13AG	1760	370	1219	65.4%	12	4.45	56.7%
13BC	1760	370	1140	65.7%	12	4.55	55.4%
13BG	1760	370	1140	65.7%	12	4.55	55.4%
14	1770	270.6	1230	59.9%	16	4.80	50.9%
15	1760	279	1219	63.1%	16	4.68	54.2%
17	1760	370	1219	63.5%	12	4.62	54.6%

** Values in yellow cells came from material data sheet; values in blue cells obtained by lab measurements and/or calculations.*

6.2 Impact Procedure Reappearance

Damage initiation was identified by the undulatory motion of the load and energy against time plots recorded during the drop-weight impact test. Two examples of load and energy against time histories are shown in Figure 47. It is clearly shown that the whole impact procedure only lasted for 0.003 seconds and the onset of damage occurred in the example at 6300N roughly. The impact load and energy reached the peak point at the moment that the velocity of the impactor was temporarily zero. Part of the impact energy was absorbed at damage initiation occurring as fibre fracture and delamination; the rest of impact energy was re-transferred to the impactor expressed as rebounding. Six specimens of each material set were impacted.

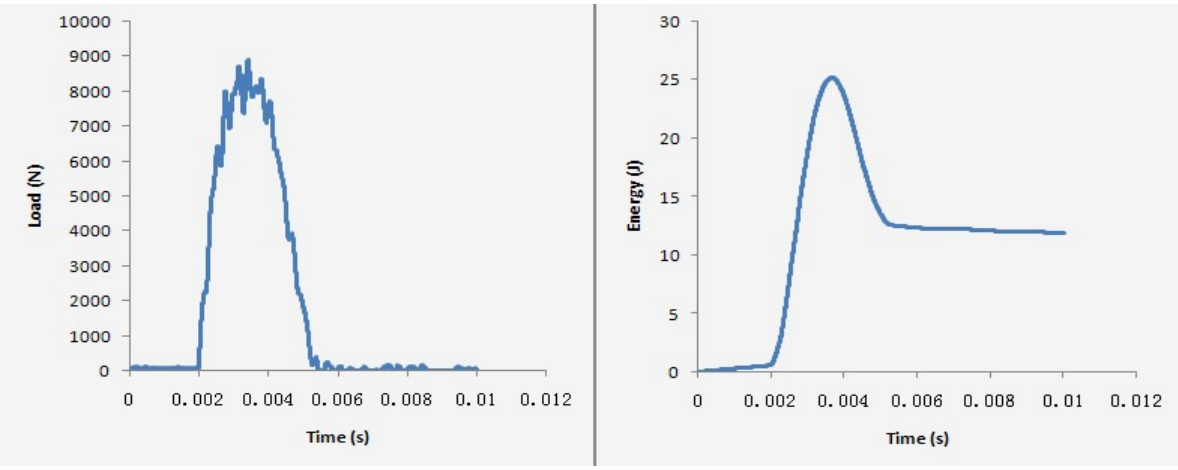

Figure 47 Two examples of load and energy against time histories during impact tests

6.3 Visual Investigation

After incident impact, all the specimens underwent visual inspection in order to provide an initial impression of surface flaw/spalling. All the dimensions of surface flaw were measured immediately after impact except the dent depth which was measured two weeks later. A digital vernier caliper with depth gauge was used in these measurements. The end of the caliper was simply stacked on the edge of the dent in the specimen and the reading number indicated the depth value when the depth-gauge contacted the bottom of the dent. Finally, the maximum value was selected as the dent depth after several measurements. All the pictures were taken during the damage dimension measurement. The severity of visible damage was divided into 3 degrees ranging from weak to strong: faintest, light and obvious.

The entire detailed surface situations are as follows.

Table 15 Visible surface flaw on both sides of damaged specimen in detail

ID	Two Sides	Picture Picture	Damage Description	Fibre Fracture Fracture	Delamination Delamination
1	Impacted	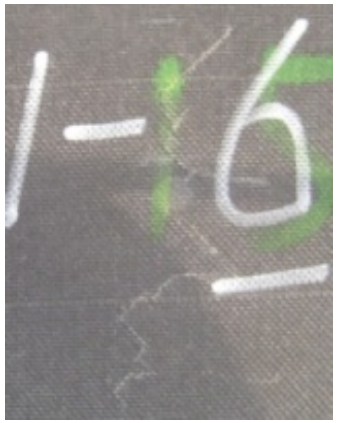	0.15 mm deep dent Rectangle shape	Obvious Fracture Longitudinal extension 51.9×17.54mm	Light visible
	Opposite		Crack	Not visible	Obvious delamination along 45°direction 41.6 mm

ID	Two Sides	Picture Picture	Damage Description	Fibre Fracture Fracture	Delamination Delamination
2	Impacted		0.1 mm deep dent Rectangle shape	Obvious Fracture Longitudinal extension 34.5×15.1mm	Not visible
	Opposite		Long Shatter	Obvious Fracture 22.1×10.3mm	Not visible

ID	Two Sides	Picture Picture	Damage Description	Fibre Fracture Fracture	Delamination Delamination
3	Impacted		0.15 mm deep dent	Not visible	Not visible
	Opposite		Crack	Not visible	Obvious delamination along 45°direction 58.2 mm
4A	Impacted		0.15 mm deep dent Rectangle shape	Light Fracture Longitudinal extension 27.2×14.7mm	Not visible

ID	Two Sides	Picture Picture	Damage Description	Fibre Fracture Fracture	Delamination Delamination
4A	Opposite		Small Shatter	Obvious Fracture 7.3×14.3mm	Not visible
4B	Impacted	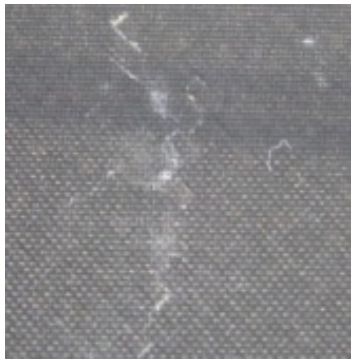	0.15 mm deep dent Rectangle shape	Light Fracture Longitudinal extension 33.0×9.4mm	Not visible
	Opposite		Small Shatter	Obvious Fracture 22.5×17.2mm	Not visible

ID	Two Sides	Picture Picture	Damage Description	Fibre Fracture Fracture	Delamination Delamination
5	Impacted		0.2 mm deep dent Rectangle shape	Obvious Fracture Longitudinal extension 40.2×14.4mm	Not visible
	Opposite		Small Shatter	Obvious Fracture 15.4×17.2mm	Not visible
6	Impacted		0.15 mm deep dent Rectangle shape	Light Fracture Longitudinal extension 20.9×7.7mm	Not visible

ID	Two Sides	Picture Picture	Damage Description	Fibre Fracture Fracture	Delamination Delamination
6	Opposite		Shatter	Obvious Fracture 22.7×16.4mm	Not visible
7	Impacted		0.1 mm deep dent	Faintest Fracture	Not visible
	Opposite		Small Shatter	Obvious Fracture 20.3×10.1mm	Not visible

ID	Two Sides	Picture Picture	Damage Description	Fibre Fracture Fracture	Delamination Delamination
8	Impacted		0.2 mm deep dent Rectangle shape	Light Longitudinal Fracture	Not visible
	Opposite		Small Shatter	Obvious Fracture 10.3×10.1mm	Not visible
9	Impacted		0.1 mm deep dent	Not visible	Not visible

ID	Two Sides	Picture Picture	Damage Description	Fibre Fracture Fracture	Delamination Delamination
9	Opposite	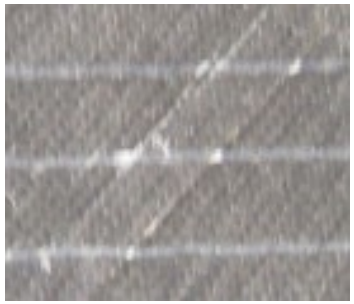	Crack	Not visible	Obvious delamination along 45°direction 63.2 mm
10	Impacted		0.1 mm deep dent	Not visible	Not visible
	Opposite		Crack	Not visible	Obvious delamination along 45°direction one side from impact point 40.9 mm

ID	Two Sides	Picture Picture	Damage Description	Fibre Fracture Fracture	Delamination Delamination
11	Impacted		0.1 mm deep dent	Not visible	Not visible
	Opposite		Light Shatter	Light Fracture	Not visible
13AC	Impacted		0.1 mm deep dent	Light Fracture	Light Fracture

ID	Two Sides	Picture Picture	Damage Description	Fibre Fracture Fracture	Delamination Delamination
13AC	Opposite	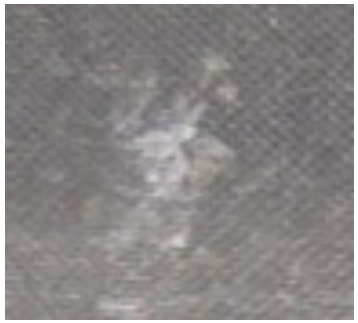	Light Shatter	Light Fracture	Light Fracture
13AG	Impacted	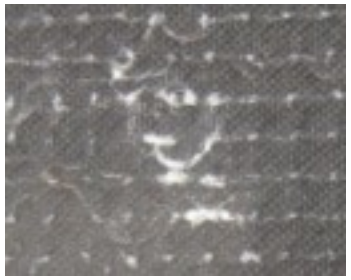	0.1 mm deep dent	Light Fracture	Light Fracture
	Opposite	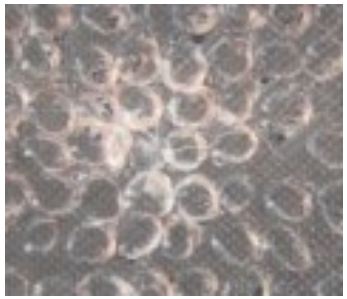	Light Shatter	Light Fracture	Light Fracture

ID	Two Sides	Picture Picture	Damage Description	Fibre Fracture Fracture	Delamination Delamination
13BC	Impacted		0.1 mm deep dent	Light Fracture	Light Fracture
	Opposite		Light Shatter	Light Fracture	Light Fracture
13BG	Impacted		0.1 mm deep dent	Light Fracture	Light Fracture

ID	Two Sides	Picture Picture	Damage Description	Fibre Fracture Fracture	Delamination Delamination
13BG	Opposite		Light Shatter	Light Fracture	Light Fracture
14	Impacted		0.5 mm deep dent Flower shape	Light Longitudinal 13.0×13.0	Not visible
	Opposite		Dome Shatter	Obvious Fracture Flower shape 23.6×21.0 mm	Not visible

ID	Two Sides	Picture Picture	Damage Description	Fibre Fracture Fracture	Delamination Delamination
15	Impacted		0.1 mm deep	Light Transverse Flaw 21.5 mm	Not visible
	Opposite		Crack	Not visible	Obvious delamination along 45°direction one side from impact point 53.4 mm
17	Impacted		0.1 mm deep Rectangle damage	Light Fracture 16.2×20.2	Not visible

ID	Two Sides	Picture Picture	Damage Description	Fibre Fracture Fracture	Delamination Delamination
17	Opposite		Long Shatter	Obvious Fracture 25.2×13.7 mm	Not visible

6.4 C-scanning Investigation

Ultrasonic C-scanning was selected in order to obtain the subsurface damage and delamination images. The equipment utilised for C-Scans was a water immersion ultrasonic C-scan system coupled with an ultrasonic flaw detector (2~10KHZ), controlled by a 386 industrial computer running Windows 3.11. Each specimen was C-Scanned after impact using the SDI SCAN-4 program with a scanning pitch of 0.4mm×0.4mm, thus achieving an acceptable C-scan resolution. One un-impacted specimen of each panel was C-scanned in order to check whether any birth defect was inside. The record of C-scan could be unscrambled via the ANALYSIS program. The final C-Scan bitmaps were screen-captured from the ANALYSIS program. PHOTOSHOP was chosen to measure the dimension of the projected subsurface damage including delamination. The ultrasonic C-scans showed that almost all damage was confined to an independent area centred at the impact point. All the areas were calculated using approximate oval area formula.

The detailed subsurface damage follows in Table 16.

Table 16 Subsurface damage projected images in detail

ID	Image	comment	Length / Width	1st mm	2nd mm	3rd mm	4th mm	5th mm	6th mm	Mean mm	Mean of Area cm^2
1	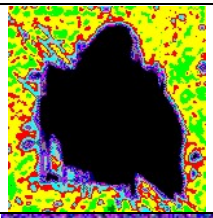	Irregular	Length	38.1	39.9	41.6	--	--	--	39.9	15.04
			Width	45.2	50.0	48.7	--	--	--	48.0	
2	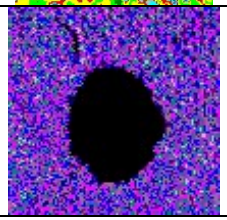	Oval	Length	18.0	18.0	18.3	18.0	17.6	16.2	17.7	2.96
			Width	20.8	21.2	19.8	20.1	24.7	21.5	21.4	
3	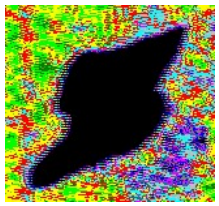	Lightning	Length	46.6	44.1	44.8				45.2	16.33
			Width	48.3	44.5	45.2				46.0	
4A	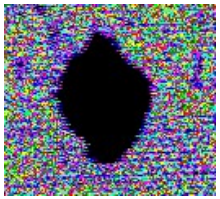	Oval	Length	27.2	22.6	23.3	26.8	26.8	28.2	25.8	6.38
			Width	35.6	28.6	27.5	31.8	32.8	31.4	31.3	

ID	Image	comment	Length Width	1st mm	2nd mm	3rd mm	4th mm	5th mm	6th mm	Mean mm	Mean of Area cm^2
4B	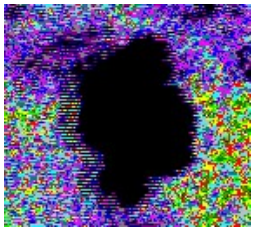	Parallelogram	Length	21.9	26.8	28.9	--	--	--	25.9	7.33
			Width	33.2	37.0	37.4	--	--	--	35.9	
5	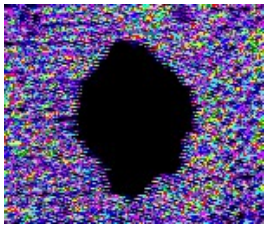	Oval	Length	26.8	29.3	26.5	26.8	27.5	27.2	27.4	7.26
			Width	33.5	33.2	35.0	32.5	31.8	36.8	33.8	
6	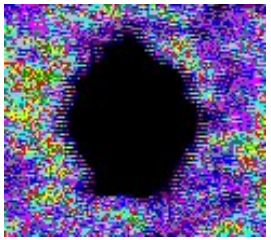	Oval	Length	26.8	24.0	24.7	--	--	--	25.2	5.66
			Width	30.0	26.8	28.9	--	--	--	28.6	
7	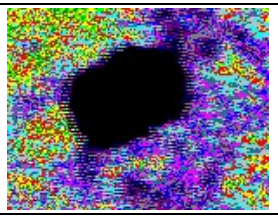	Parallelogram	Length	26.1	25.0	26.1	--	--	--	25.7	5.11
			Width	26.8	26.5	22.6	--	--	--	25.3	

ID	Image	comment	Length Width	1st mm	2nd mm	3rd mm	4th mm	5th mm	6th mm	Mean mm	Mean of Area cm^2
8	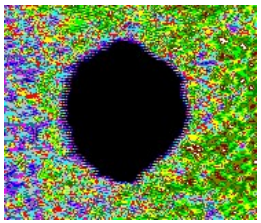	Oval	Length	33.9	32.1	31.8	32.8	39.5	32.1	33.7	10.51
			Width	39.9	38.1	41.3	36.7	43.0	38.5	39.6	
9	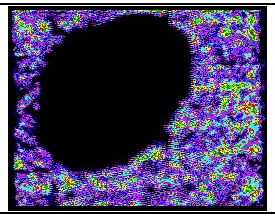	Oval	Length	55.0	49.7	60.3	57.2	48.7	53.6	54.1	21.41
			Width	47.6	49.7	48.7	56.4	47.3	52.2	50.3	
10	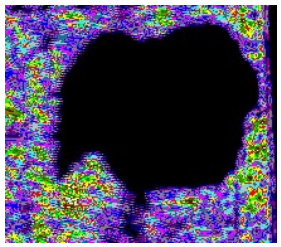	Irregular	Length	56.8	57.9	49.7	60.3	49.0	--	54.7	21.52
			Width	50.8	52.2	45.2	55.0	45.5	--	49.7	
11	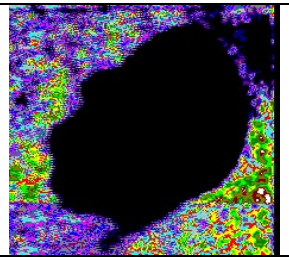	Irregular	Length	58.2	46.2	46.1	64.9	63.1	53.3	55.3	24.23
			Width	49.0	50.1	67.7	65.3	60.3	40.9	55.6	

ID	Image	comment	Length Width	1st mm	2nd mm	3rd mm	4th mm	5th mm	6th mm	Mean mm	Mean of Area cm^2
13AC	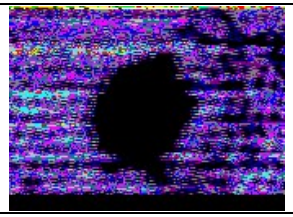	Oval	Length	24.5	24.3	24.7	--	--	--	24.5	5.33
			Width	27.7	29.3	26.1	--	--	--	27.7	
13AG	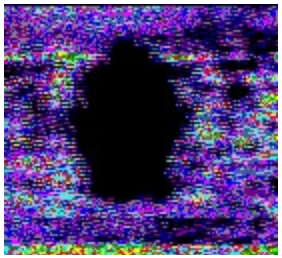	Oval	Length	22.2	22.2	20.5	--	--	--	21.6	5.13
			Width	30.0	29.6	31.0	--	--	--	30.2	
13BC	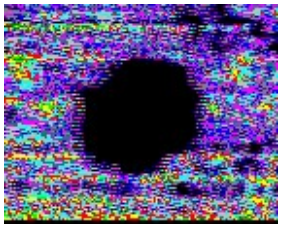	Oval	Length	22.9	23.3	22.2	--	--	--	22.8	4.36
			Width	21.5	25.8	25.8	--	--	--	24.4	
13BG	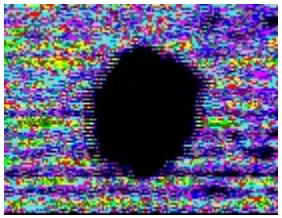	Oval	Length	21.2	19.4	20.8	--	--	--	20.5	3.65
			Width	21.2	23.3	23.6	--	--	--	22.7	

ID	Image	comment	Length Width	1st mm	2nd mm	3rd mm	4th mm	5th mm	6th mm	Mean mm	Mean of Area cm^2
14	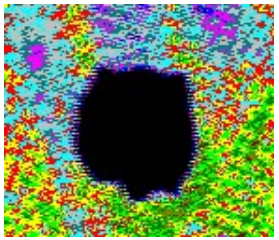	Square	Length	21.5	22.6	24.3	25.8	24.0		23.6	4.91
			Width	22.6	27.5	25.4	30.3	25.8		26.3	
15	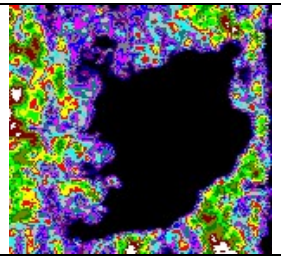	Irregular	Length	39.1	44.7	45.6	--	--	--	43.1	15.50
			Width	40.2	48.5	47.8	--	--	--	45.5	
17	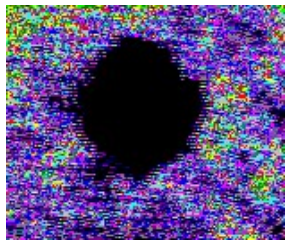	Oval	Length	26.5	24.3	26.2	--	--	--	25.7	5.40
			Width	24.7	27.5	28.2	--	--	--	26.8	

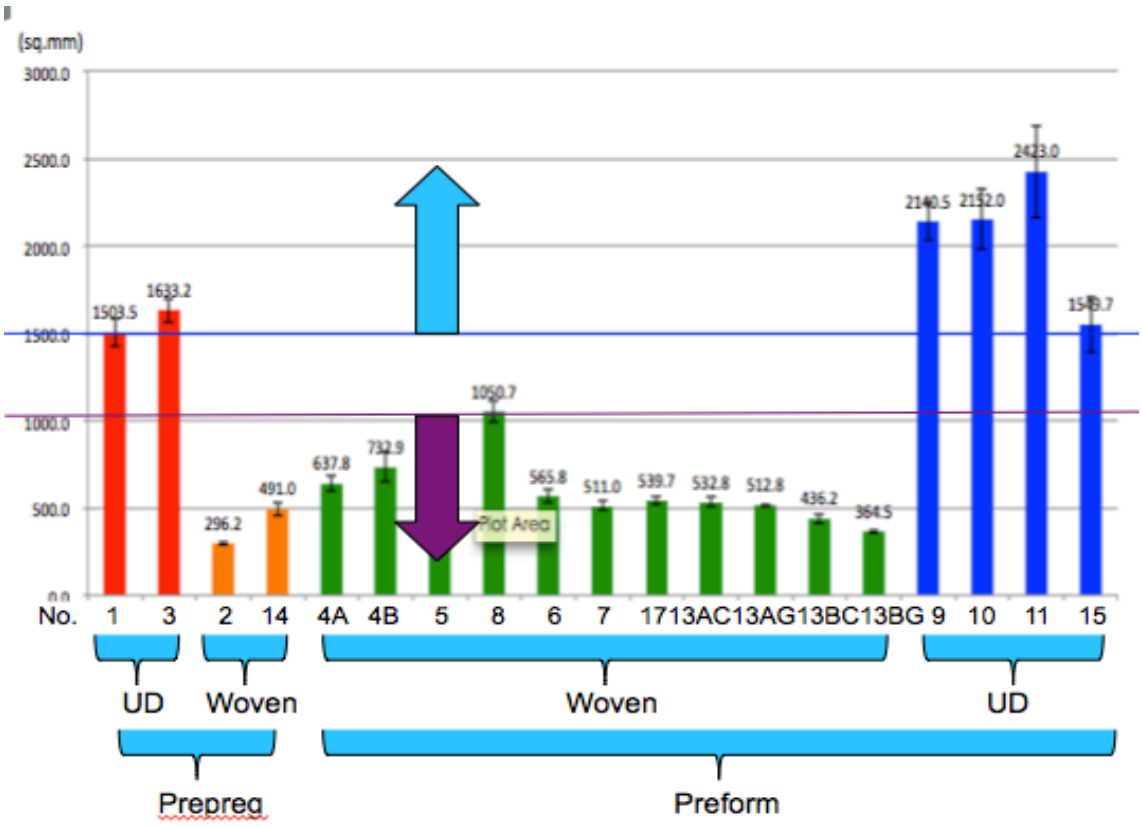

Figure 48 Damage area with standard deviation (mm^2)

It is clearly showed in **Figure 48** that the greatest damage was generated within the uniweave panel while the least damage was within the woven prepreg panel. Furthermore, the damage area inside the panels manufactured using unidirectional fibres (UD, NCF or uniweave fabrics) was significantly bigger than what contained in the panels made from woven fabric.

6.5 Micrograph Examination

In order to investigate the fracture mechanism and damage distribution, one impacted specimen from each set was sacrificed for a destructive investigation method. The specimens were cut 5mm off impact centre along the longitudinal direction. A 5mm clearance was reserved with a view to avoiding creating a new fracture. All the samples were polished back to the impact centre so that the through thickness damage and delamination distribution could be clearly detected via micrograph and high resolution photographs. In addition, delamination expanding routes, fibre fractures and resin matrix cracks could be directly observed. All the photographs in Appendix B display the cross-sections through the impact centre of all the specimens.

6.6 CAI Testing

Five specimens of each panel (in total 92+) were tested to measure the CAI strength.

The testing specimen was manually clamped in the fixture. The quality of assembly should account for the initial loading stage performance but made no or acceptable difference to the subsequent stages.

As mentioned earlier, the top platen was fixed and the loading procedure was controlled by the displacement rate of the bottom loading plate (0.5/minute) using hydraulic system. The results data including the displacements of the bottom platen and the compression loads were collected 10 times per second during the entire loading procedure.

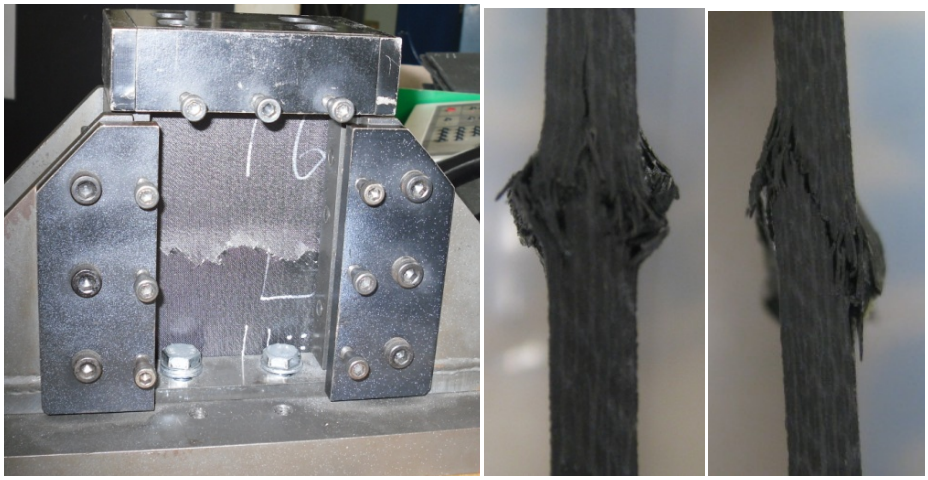

a (front view) b (brooming) c (shear)

Figure 49 Typical CAI failure

All the damaged specimens failed due to local buckling with kink bands through the damage region. There were only two distinguishable failure modes observed in the CAI tests, i.e. brooming failure (Figure 49 b) and overlapping shear failure (Figure 49 c). These also were identified by Odom [33]. The failure occurred suddenly but with accompanying erratic blips. Relaxation of the broken fibre and/or de-bonded plies was observed in varying degrees after unclamping.

The CAI testing histories of the control (No.4) are presented in Figure 50 by plotting the compressive load against the displacement. Load versus displacement plots for each compression test are included in Appendix A, which intuitively reappeared the histories recorded during loading procedure. The behaviour during the CAI history can be divided into 5 regions on the basis of loading and reaction.

Region A shows the bedding-in period of the fixture and the tested specimen. There were undoubtedly some small clearances between the specimen and the fixture, and also between the fixture and the loading plate, because the top of the specimen could not be cut extremely accurately by hand, hence the top could not be critically parallel to the bottom. Another reason is that the upper platen of the fixture was slightly slanted relative to the upper loading platen due to the hand-operated assembly.

Region B describes the smooth loading procedure. The slopes of the load-displacement curves are almost identical even if the durations of region A are varied. No noise was heard during this region.

Region C is the failure period which came suddenly with an abrupt rupture, fore-warned by erratic blips. The factor most worth mentioning is that compared to Region B the load increased at a slower pace and the blips were emitted more frequently and more loudly when the compressive load was near to the ultimate post-impacted compression strength.

Region D represents the sudden unloading period. The loading platen was controlled by a hydraulic pump, which could respond to the failure in a short time but not immediately. As a result of this, the loading platen had a precipitate motion due to the high hydraulic pressure and no counter-force from the testing-fixture at the moment of failure. In every record, region D only lasted for less than 1/5 second.

Region E reveals the self-adaption period of the testing machine. Because the loading rate was dominated by loading platen displacement, the loading platen would

automatically come to where it should be. This explains why there was a bulge at end of every curve.

Table 17 The individual data from all CAI tests

No	T(mm)	E(J)	1st	2nd	3rd	4th	5th	F-Mean	STD DEV
1	4.00	22.47	100.1	111.4	101.4	113.2	110.2	107.3	6.1
2	3.49	19.61	76.2	76.7	75.9	75.1	77.2	76.2	0.8
3	4.19	23.54	91.7	102.9	107.3	102.7	109.5	102.8	6.9
4-A	4.45	25.00	93.7	98.8	94.1	94.3	97.1	95.6	2.2
4-B	4.55	25.56	110.4	109.5	105.3	106.6	105.0	107.4	2.5
5	4.45	25.00	101.2	93.6	99.2	98.1	99.1	98.2	2.8
6	4.45	25.00	112.0	115.7	111.8	112.4	116.8	113.7	2.3
7	4.72	26.52	132.9	135.7	132.8	134.1	---	133.9	1.4
8	4.64	26.07	92.4	95.3	92.3	92.3	92.3	92.9	1.3
9	5.00	28.09	104.3	96.6	104.6	98.5	99.4	100.7	3.6
10	4.00	22.47	78.1	80.5	68.7	84.6	71.2	76.6	6.6
11	4.84	27.19	86.1	96.7	---	88.7	99.2	92.7	6.3
13-AC	4.45	25.00	141.7	142.1	149.5	---	---	144.4	4.4
13-AG	4.45	25.00	131.8	130.0	136.2	---	---	132.7	3.2
13-BC	4.55	25.56	138.6	138.7	146.1	---	---	141.1	4.3
13-BG	4.55	25.56	143.8	146.6	145.0	---	---	145.1	1.4
14	4.80	26.97	102.1	100.4	101.7	---	---	101.4	0.9
15	4.68	26.29	91.8	93.8	105.2	89.4	85.1	93.1	7.5
17	4.62	25.96	113.6	118.5	119.2	118.4	114	116.7	2.7

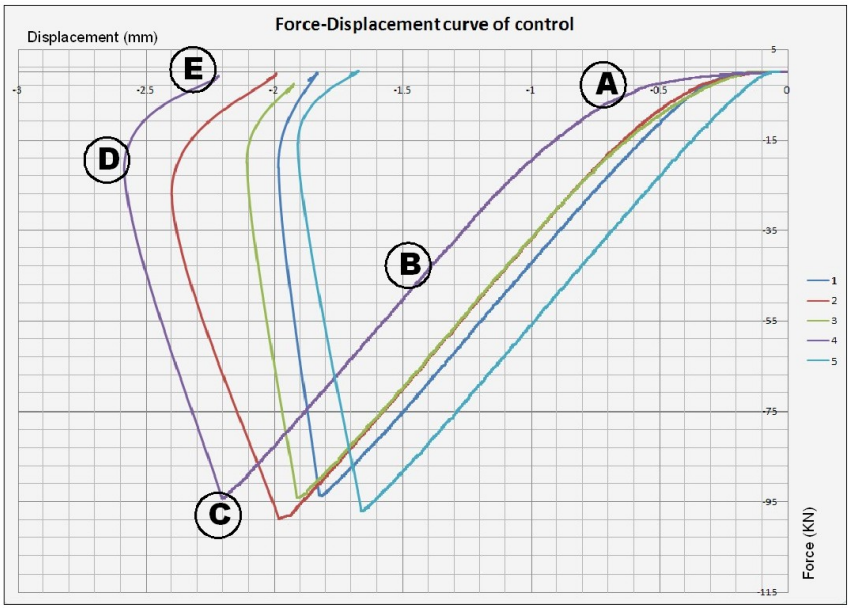

Figure 50 CAI load-displacement cuves of the control

Because no any strain gauge or extensometer were employed into these tests. Therefore, with the precondition that the stiffness of the whole specimen was consistent, the stiffness could be similarly calculated using the gradient of the load-displacement output recorded automatically by the sensor pre-installed in the loading platform. Only the linear elastic region was taken into consideration in order to eliminate the effect of the machine slackness. Some key mechanical features of each panel were listed in **Table 18** and the relativity was shown in **Figure 51**.

Table 18 Key mechanical features of each panel

F-Com (kN)	Thickness (mm)	Slope of Linear Load-Displacement (kN/mm)	E (mPa)	σ (mPa)	ξ
107.3	4.00	72.5	2.72E+04	268	0.0099
76.2	3.49	59.4	2.55E+04	218	0.0086
102.8	4.19	63.9	2.29E+04	245	0.0107
95.6	4.45	64.7	2.18E+04	215	0.0098
107.4	4.55	64.2	2.12E+04	236	0.0112
98.2	4.45	65.2	2.20E+04	221	0.0101
113.7	4.45	67.7	2.28E+04	256	0.0112
133.9	4.72	66.5	2.11E+04	284	0.0134
92.9	4.64	65.1	2.10E+04	200	0.0095
100.7	5.00	75.2	2.26E+04	201	0.0089
76.6	4.00	66.8	2.51E+04	192	0.0076
88.9	4.84	65.1	2.02E+04	184	0.0091
144.4	4.45	67.0	2.26E+04	325	0.0144
132.7	4.45	66.6	2.25E+04	298	0.0133
141.1	4.55	65.1	2.15E+04	310	0.0144
145.1	4.55	63.6	2.10E+04	319	0.0152
101.4	4.80	65.3	2.04E+04	211	0.0104
93.1	4.68	66.4	2.13E+04	199	0.0093
116.7	4.62	67.5	2.19E+04	253	0.0115

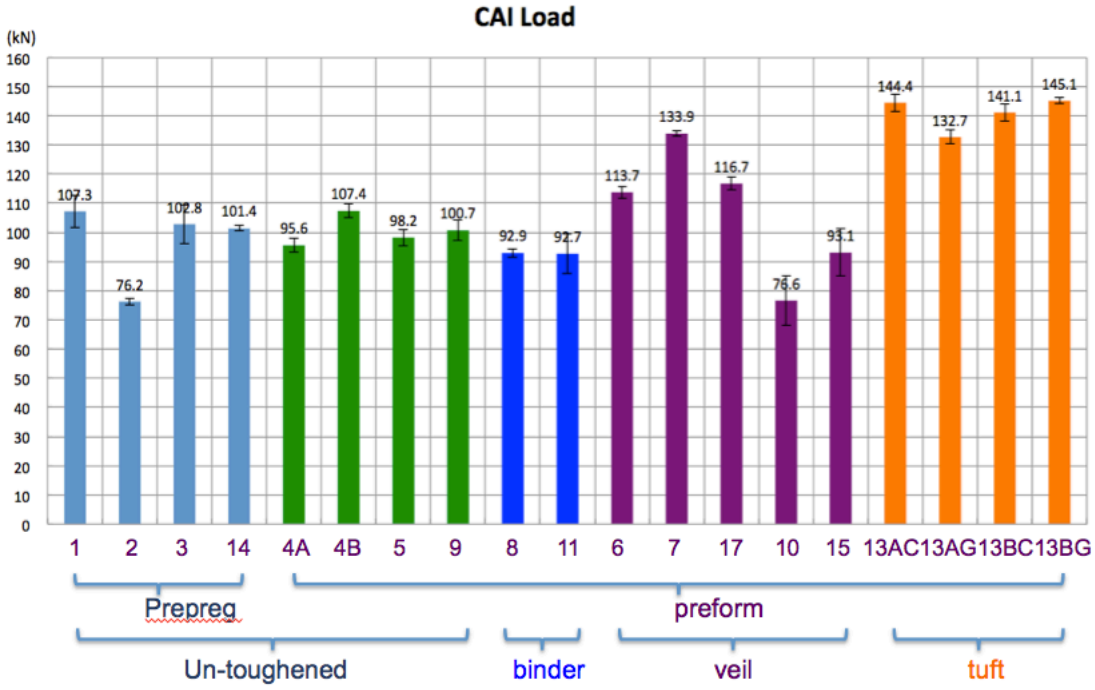

Figure 51 CAI load of all materials with standard deviation

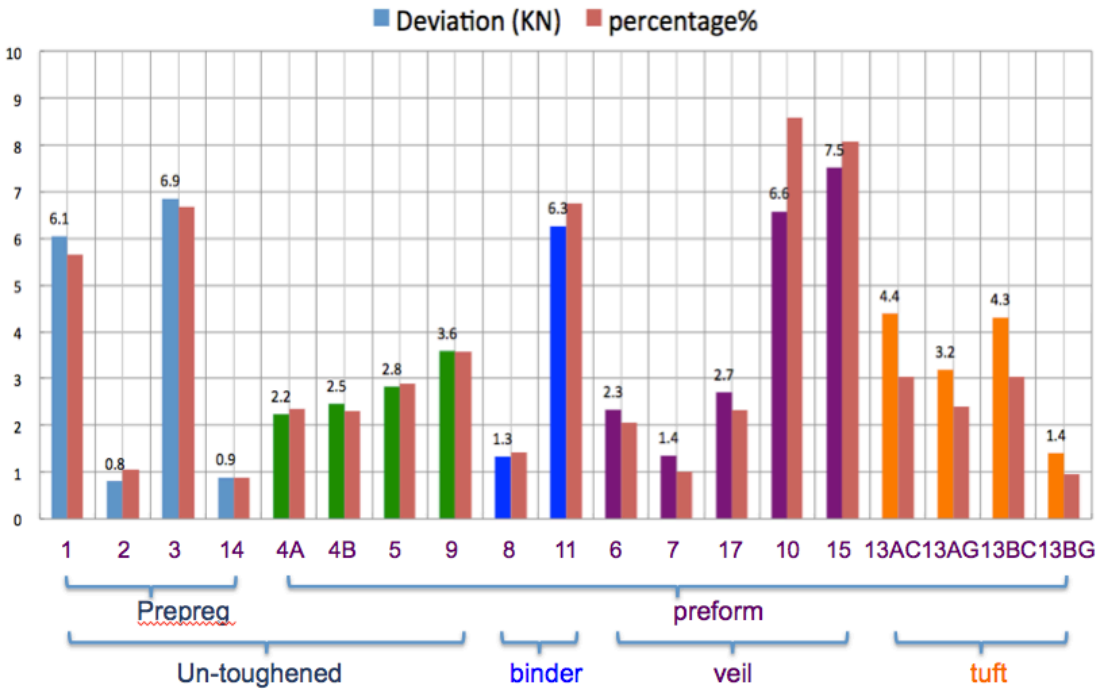

Figure 52 Standard deviation (right bar) and the scatter percentage (left bar) for CAI load

The individual data of all ultimate CAI strengths are listed in **Table 17**. Each value is the maximum compressive load during the whole testing procedure, but none of these

occurred at the moment of failure. Figure 51 displays the various CAI strengths resulting from the 19 sets with considerable scatter within each set. This histogram (Figure 52) has been constructed utilising the standard deviations (left) and the variation percentages of the CAI strength (right).

Figure 52 obviously reveals that the variations of CAI strength of unidirectional fibre panels were not more significant than 12% and of woven fibre panels were less than 4% level. The high scatter observed in CAI strength of unidirectional fibre panels was thought to result from the high scatter of damage areas described above.

Compared to the control, the glass-tufted panel (No.13BC) exhibited the highest CAI performance. The highest average CAI strength was 145.1 kN with a standard deviation of 1.4 kN, giving a coefficient variation of 1%.

6.7 Undamaged Compression Strength Test

Because of the quantitative restriction of specimens in each set, only 3 undamaged specimens were tested for each set. No specimens for laminate of No.2, No.8 and No.14 were available, hence the test for these 3 sets are suggested for future work (Chapter 10). The whole compression procedure records as shown in Figure 53 (the test history of No.1 T800 UD/M21 panel) were very similar to the CAI procedure but the failure appeared less complex, occurring very suddenly.

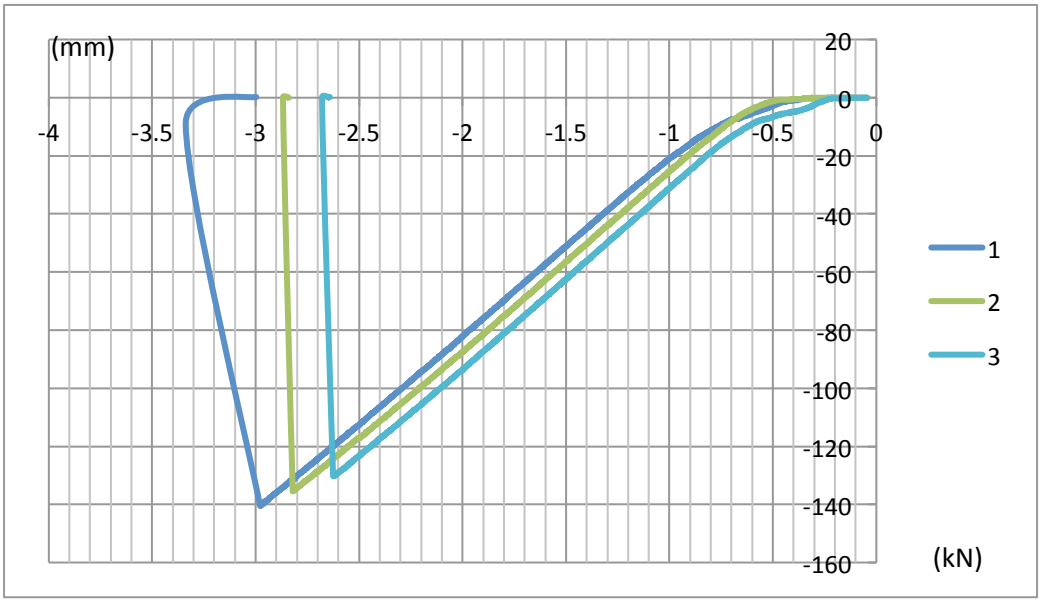

Figure 53 Compression loads to displacement plot of plain strength test

The individual data of all ultimate plain compression strengths (PCS) is listed in Table 19. All the values are the maximum compressive load during the whole testing procedure, but none of them emerged at the failure moment. Because the specimens for PCS tests were narrowed in the longitudinal middle, the ultimate compressive strength could be calculated using the compressive strength of the narrowed specimen simply divided by 80% (the specimen width is 100mm, with a 10 mm wide cut-off on both sides).

Figure 54 is a histogram revealing the various PCS means of the 19 material sets with standard deviation. Figure 55 has been constructed using the standard deviations (left)

and the variation percentages of the means of PCS strength (right).

Table 19 The individual data from all PCS tests (load)

No	T(mm)	Original test results (kN)				Correct for the narrowed (kN)	
		1st	2nd	3rd	F-Mean	F-Com	STDEV
1	4.00	134.8	141.4	---	138.1	172.6	5.8
2	3.49	---	---	---	---	---	---
3	4.19	130.9	142.7	145.4	139.7	174.6	9.6
4-A	4.45	145.4	138.4	---	141.9	177.4	6.2
4-B	4.55	149.2	155.7	145.7	150.2	187.8	6.3
5	4.45	153.4	140.6	130.6	141.5	176.9	14.3
6	4.45	140.5	135.5	130.2	135.4	169.3	6.4
7	4.72	155.9	153.0	148.4	152.4	190.5	4.7
8	4.64	---	---	---	---	---	---
9	5.00	141.5	162.0	155.0	152.8	191.0	13.0
10	4.00	116.1	106.2	102.5	108.3	135.3	8.8
11	4.84	116.7	117.7	112.7	115.7	144.6	3.3
13-AC	4.45	118.3	103.1	110.1	110.5	138.1	9.5
13-AG	4.45	114.6	121.4	123.8	119.9	149.9	6.0
13-BC	4.55	130.4	---	131.2	130.8	163.5	0.7
13-BG	4.55	117.4	111.7	126.9	118.7	148.3	9.6
14	4.80	---	---	---	---	---	---
15	4.68	117.6	117.8	---	117.7	147.1	0.2
17	4.62	130.4	148.8	133.9	137.7	172.1	12.2

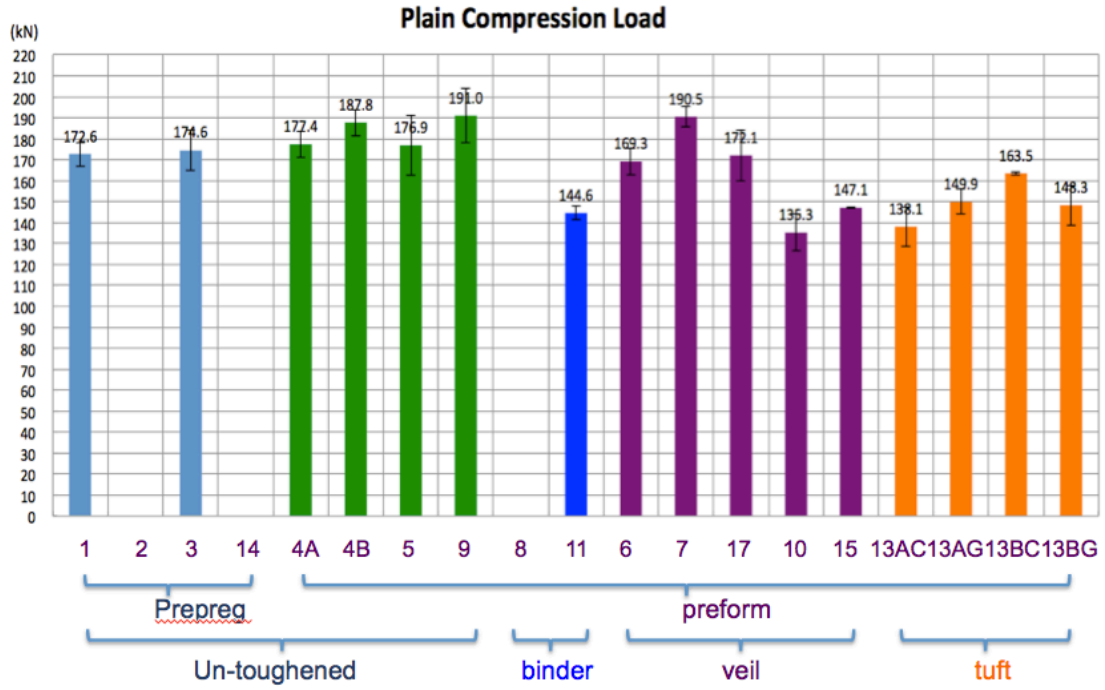

Figure 54 Means of PCS loads with standard deviation (kN)

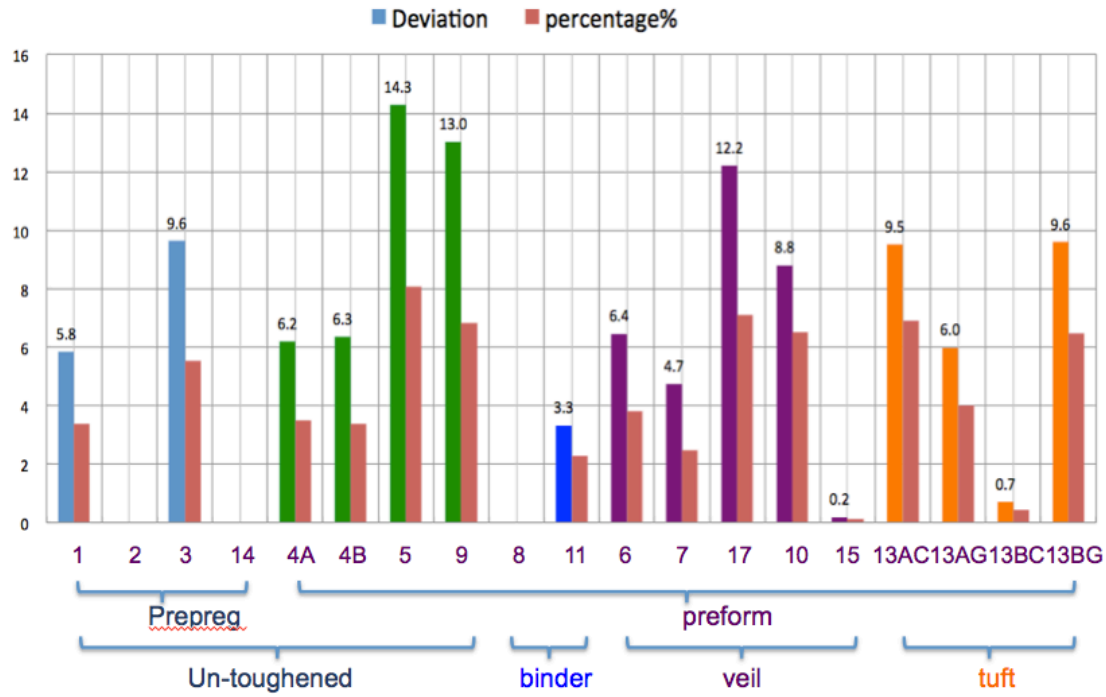

Figure 55 Standard deviation (right bar) and the scatter percentage (left bar)

The average PCS of the control (No.4A) was 177.4kN with a standard deviation of 6.2kN, giving a coefficient of variation of 3%.

7 Discussion

7.1 Impact Induced Damage

The damage revealed by un-destructive visual inspection and ultrasonic C-scanning is of great interest. Damage causes huge degradation in post-impact compression strength.

The following is easily perceived from the visible inspection and C-scanning:

1: Comparing the C-scanning images with standard photographs, it is easy to see that the visible surface flaw sizes shown in **Table 15** is smaller that the subsurface damage sizes shown in **Table 16**. It means that the subsurface damage (fibre fracture and/or delamination) caused by impact extends further than the visible surface flaw regions .

2: Delamination wasn't visible in the surfaces of laminates using woven fabric, but long and obvious delamination could be noted macroscopically in UD, NCF and uniweave ones. On the other hand, huge delamination was detected by C-scanning for impacted unidirectional specimens, compared to relatively small delamination in woven ones. One possibility is that delamination is more difficult to propagate between layers of woven specimens due to the irregular and uneven surface of each ply. Tufting technology was shown to be the most effective in preventing and even eliminating the delamination.

3: Under the same energy level (constant energy to thickness ratio) impact, the dent depth has no obvious relationship with damage size and delamination size, and has no close relevancy with specimen thickness and fibre fabric.

4: Most fibre fracture was constructed in a longitudinal direction on the impacted side. In other words, the longitudinal length of damage was far larger than the transverse width of damage, but this phenomenon did not appear on the opposite side. One

possibility is that the specimen was more efficiently supported in a transverse direction than in a length direction due to the rectangular opening in the supporting base.

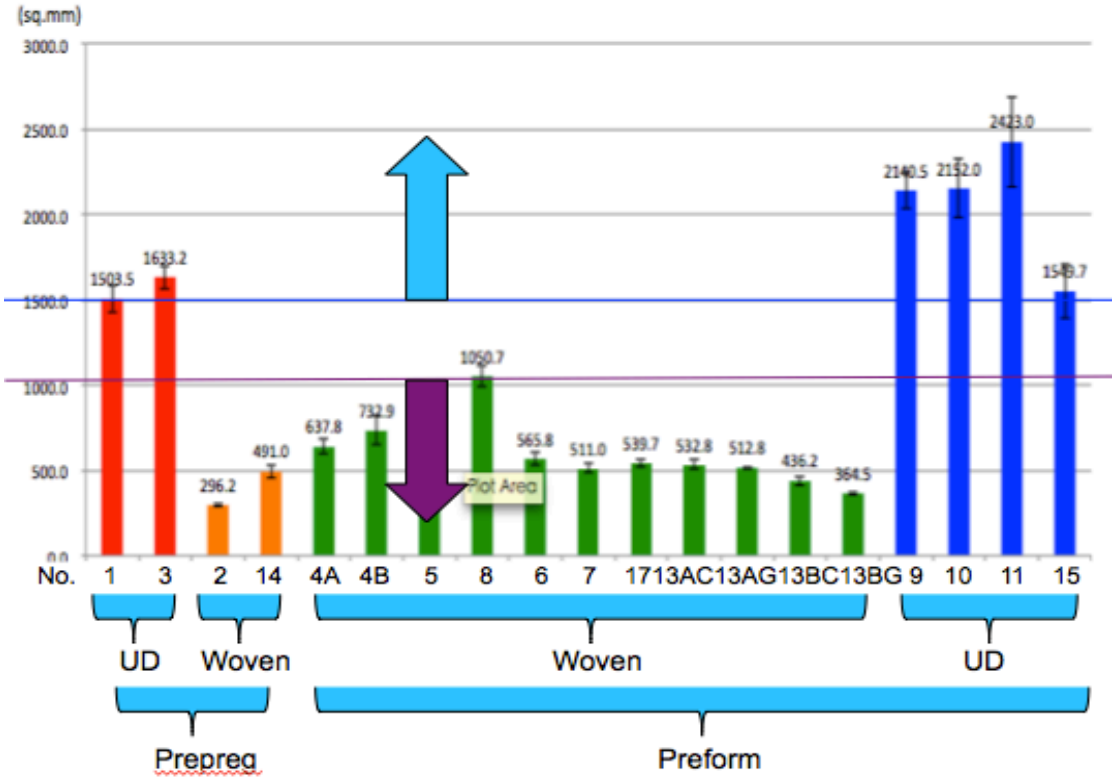

Figure 56 Damage areas with standard deviation (mm^2)

C-scanning inspection of the impacted specimens exposed very different types of impact in both kinds of fabrics. As shown in Figure 56, after identical level energies (the energy to thickness ratio was constant) of impact, the greatest damage was generated within the uniweave panel while the least damage was within the woven prepreg panel. This was important whilst considering the relative damage resistances of the different materials. Furthermore, without exception, all the specimens could be divided into two groups regarding inside damage area. Group one consisted of the panels manufactured using unidirectional fibres (UD, NCF or uniweave fabrics), and group two included all the panels made from woven fabric.

Within group one, all the damage areas were over 1600 mm^2, and the majority of interior damage of this group was delamination between layers. The Uniweave panel

was the worst affected, containing 2423 mm^2 inside damage which was 16% of the total specimen's projected area. The greater the damage inside, the more it was accompanied by standard deviation of damage area.

Within group two, all the damage areas were less than 1050 mm^2. Most of them approximated to 500 mm^2. The lowest damage area for the Prepreg panels was observed in No.2 (Woven Prepreg). Relatively, the No.13BG panel (woven fibre) reinforced by tufting with glass tread showed the biggest decrease in damage area. Compared to camp one, the standard deviations of damage area of camp two are quite small.

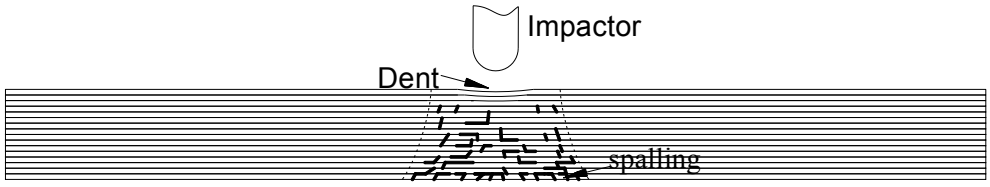

a) illustration of the cross-section of impacted woven fibre panel

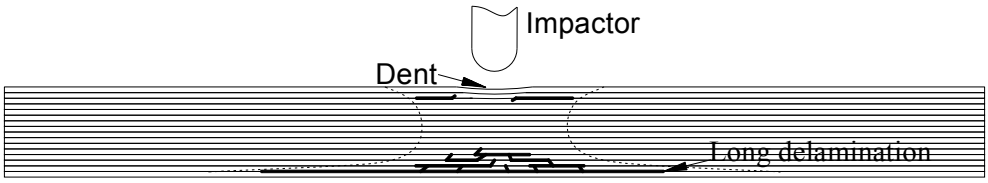

b) illustration of the cross-section of impacted unidirectional fibre panel

Figure 57 Illustrations of two typical cross-sections

Figure 57 reveals two typical longitudinal cross-sections of impacted specimens detailed in **Figure 110** and **Figure 111** in Appendix C. Massive fibre fractures combined with complex, multi-layer delaminations were actually found in relatively high concentrations inside of the woven fibre panel. All the damage was restricted to a conical damage zone. Dissimilarly, the delamination within the unidirectional panel was observed in the top three layers and bottom four layers. Around the impact-induced dent within the top layers, the delaminations were small and typically ended with fibre fracture. The delaminations within the bottom layers extended widely and significantly affected the CAI response. Therefore, we have reason to believe that the bottom de-bonded layers have negligible residual compression

strength after the impact.

Comparing the cross-sections of tested specimens, it was clear to see that the woven fibre plies in some interlocking points were more compact than unidirectional fibre plies. All of the tight connections had the chance to act as obstacles during the delamination expansion. As shown in Figure 59, the delamination propagation stopped at an adhesive point and formed a fibre fracture.

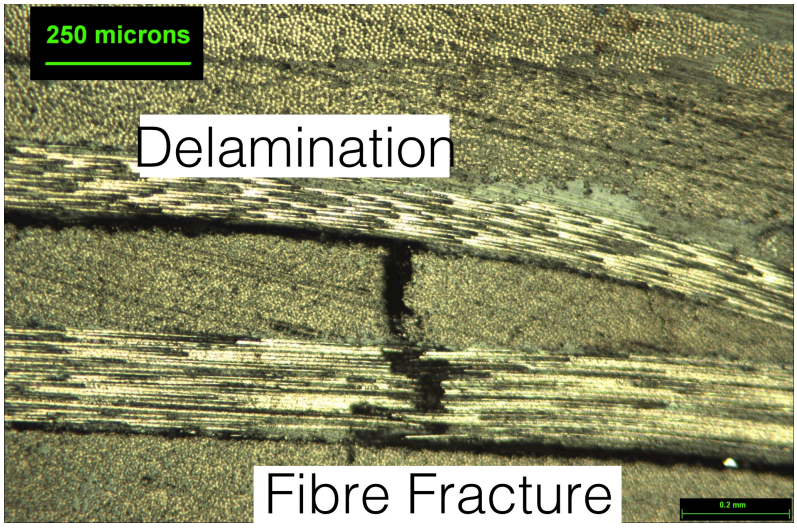

Figure 58 the delamination propagation stopped at an adhesive point

Many evidences of the critical role of tufts in preventing, even eliminating, delamination have been investigated recently [1][37]. It was observed from the micrograph of the cross-section through the impact centre that the tufts acted as bridges improving the delamination resistance of the composite material. The delamination propagation stopped or changed to through thickness direction and formed fibre fractures when spreading near to a tufted thread.

7.2 Compression Procedure

As described earlier, it was quiet during the loading procedure before the failure period, and the compressive load increased linearly against displacement. It was suggested that impact-induced delamination did not progressively propagate before

the failure period. We also have reason to believe that, within the failure period, erratic blips indicated delamination abruptly growing inside. Figure 59 represents the load versus displacement of the control in compression, where local bulking of the separated bottom layers was apparent (bottom feature in **Figure 59**). Finally, sudden extension of the transverse crack toward the edges of the specimen happened as the final failure. This is consistent with the earlier observations [32].

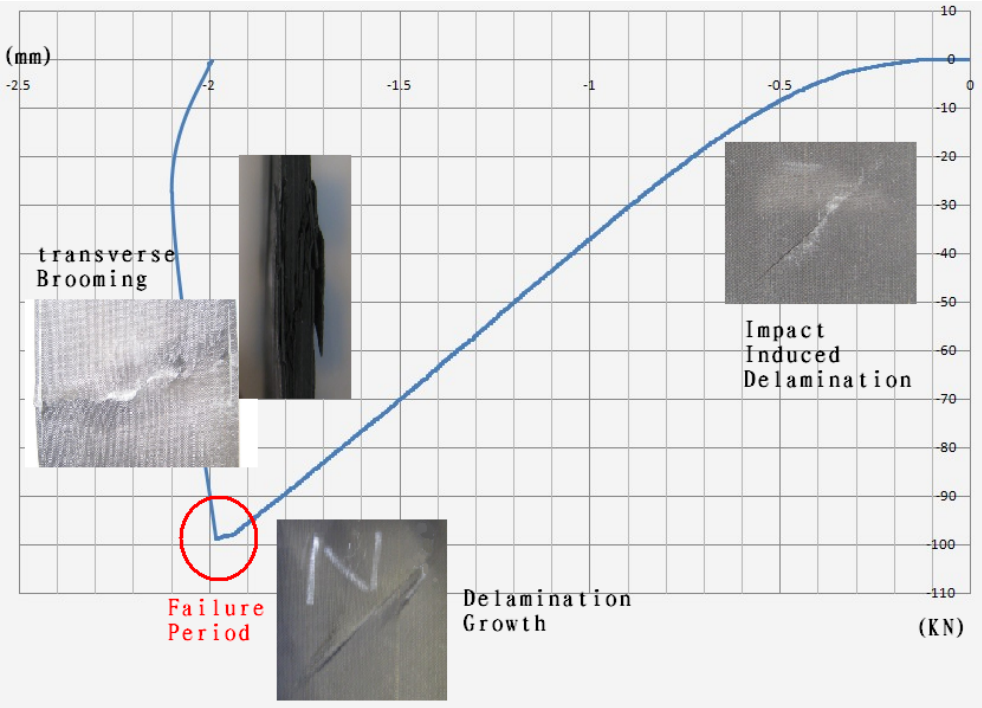

Figure 59 Diagram showing compressive load vs. displacement curve of the control

7.3 CAI Strength

Because the thicknesses of different panels varied between 3.49mm and 5.00mm due to different areal weights of the material, it was reasonable to carry out the comparison using nominal CAI strengths, which came from the CAI strengths corrected for cross-section area. The nominal compression strengths with standard deviation are shown in Table 20, and Figure 60 shows the distinct comparison chart. The huge differences between the strengths of different panels provided a strong comparison regarding different fabrics and different TTRs.

Table 20 The individual CAI strength (mPa)

No.	1st	2nd	3rd	4th	5th	Strength-Mean	STD DEV
1	250.3	278.5	253.5	283.0	275.5	268.2	15.1
2	218.3	219.8	217.5	215.2	221.2	218.4	2.3
3	218.9	245.6	256.1	245.1	261.3	245.4	16.4
4-A	210.6	222.0	211.5	211.9	218.2	214.8	5.0
4-B	242.6	240.7	231.4	234.3	230.8	236.0	5.4
5	227.4	210.3	222.9	220.4	222.7	220.8	6.4
6	251.7	260.0	251.2	252.6	262.5	255.6	5.2
7	281.6	287.5	281.4	284.1	---	283.6	2.9
8	199.1	205.4	198.9	198.9	198.9	200.3	2.9
9	208.6	193.2	209.2	197.0	198.8	201.4	7.2
10	195.3	201.3	171.8	211.5	178.0	191.6	16.4
11	177.9	199.8	---	183.3	205.0	191.5	12.9
13-AC	318.4	319.3	336.0	---	---	324.6	9.9
13-AG	296.2	292.1	306.1	---	---	298.1	7.2
13-BC	304.6	304.8	321.1	---	---	310.2	9.5
13-BG	316.0	322.2	318.7	---	---	319.0	3.1
14	212.7	209.2	211.9	---	---	211.3	1.9
15	196.2	200.4	224.8	191.0	181.8	198.8	16.1
17	245.9	256.5	258.0	256.3	246.8	252.7	5.9

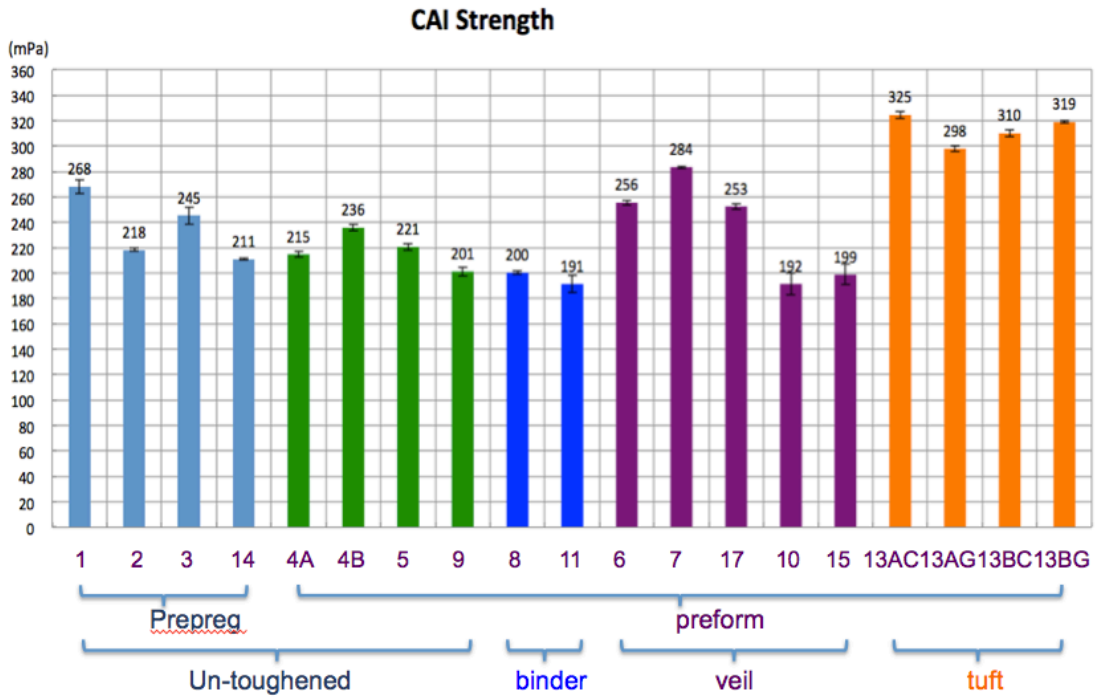

Figure 60 CAI strength of all materials with standard deviation (mPa)

Compared to CAI loads, the differences between each panel in absolute CAI performance were slightly diminished when normalized compressive strength in stresses were considered as shown in Figure 60. It is also worth noting that the woven prepreg panel (No.2) had the lowest CAI strength due to its lowest thickness, but the CAI strength level was slightly higher than that of another woven prepreg panel (No.14).

No.1, No.3, No.2 and No.14 were chosen to study the influence of fibre and fabric types of prepreg. High CAI strength was observed in unidirectional fibre panels, compared to woven fibre panels, even though huge damage areas, more than four times greater, were discovered in the interior of unidirectional panels. The two woven prepreg panels (No.2, No.14) approximately duplicated each other's CAI strength. The details are shown in Figure 61.

No.4A was compared with No.9, No.10, No.11 and No.15 with the purpose of researching the CAI performance of preform panels using woven or unidirectional fibre. The projected damage area of the 5HS woven preform panel was 637 mm^2,

which contrasts with unidirectional fibre preform panels that contained over 2000mm^2 inside damage. What was surprising was that the CAI strength of the woven preform panel was slightly higher than that of unidirectional preform one. The details are shown in Figure 61.

It is noticeable in Figure 61 that the CAI strengths of 4 unidirectional fibre panels (No.9, No.10, No.11, No.15) were in close proximity to each other rather than the saw-toothed view of the strengths in Figure 51. In other words, the fabric of unidirectional fibre, i.e. UD tape, NCF, Uniweave, had no affect on the CAI performance of QI layup preform panels.

No	Description	Stress-Mean	STDEV	Damage	Price
1	T800/M21 UD Prepreg	268.2	15.1	0.0	
3	T700/M21 UD Prepreg	245.4	16.4	1633.2	
2	T800/M21 Woven Prepreg	218.4	2.3	296.2	
14	T300/914 Woven Prepreg	211.3	1.9	491.0	
4-A	5HS woven preform/LY564	214.8	5.0	637.8	
9	NCF preform/LY564	201.4	7.2	2140.5	
10	UD preform/LY564/veil	191.6	16.4	2152.0	
11	uniweave preform/binder/LY564	191.5	12.9	2423.0	
15	UD preform/LY564/veil/binder	198.8	16.1	0.0	

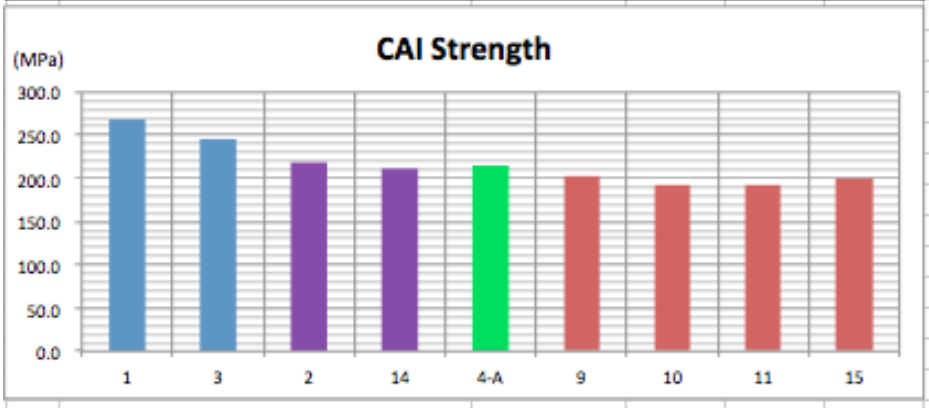

Figure 61 non-reinforced panels comparison

Most worth mentioning is the CAI strengths of prepreg laminates were higher than that of preform laminates, even through the unidirectional prepreg laminates contained far more internal damage, as shown in Figure 61. The possible reason suggested was the higher compression strength of unidirectional fibre than the woven one. The woven prepreg laminates were slightly better than the woven preform laminates possibly due to the slightly higher FVF. The most interesting is the woven

preform laminates performed greater than the unidirectional preform laminates. One possible explanation is the combination of the huge internal damage and low FVF of the unidirectional preform laminates.

No	Description	Stress-Mean	STDEV	↑	Price
4-A	5HS woven preform/LY564	214.8	5.0	---	
5	5HS woven preform/3508	220.8	6.4	2.8%	
4-B	5HS woven preform/RTM6	236.0	5.4	9.8%	

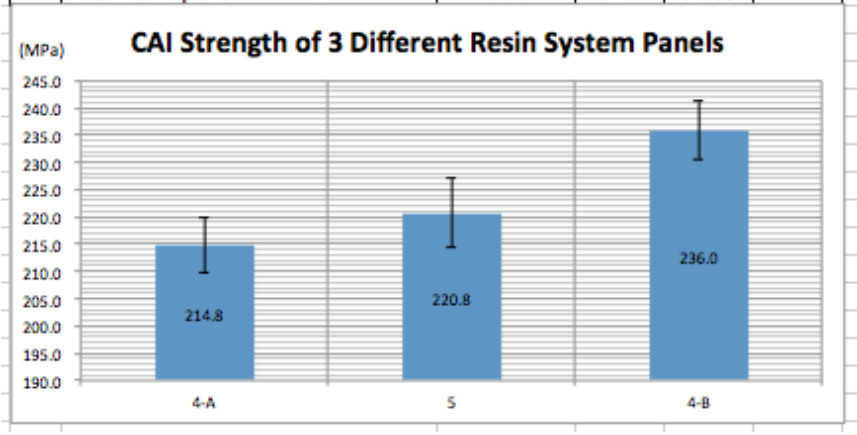

Figure 62 Resin effect on CAI performance

Table 21 The raw material costs

	Preform	Resin	FWF	Panel	Curing Procedure
LY564	£79/KG	£9/KG	65.4%	£54.8/KG	On hot plate, 80°C
3508	£79/KG	£7/KG	65.3%	£54.0/KG	On hot plate, 80°C
RTM6	£79/KG	£50/KG	65.7%	£69.1/KG	In oven, 160°C
Reference	Table 1	Table 1	Table 14		

In order to investigate the effect on CAI performance of different matrices, No.4A, No.4B and No.5, which used the same preform, were selected. Compared to the control (No.4A, using LY564 resin), the CAI strength of the FLAVIIR tougher 3508 resin panel had only risen by 2.8% under the condition of a 15% larger projected damage area, which was beyond expectation. And as shown in Table 21, the cost of the 3508 resin system panel was £54.0/KG, which was slightly cheaper than the control (LY564, £54.8/KG). Comparing RTM6 with LY564 resin, it was exciting that the results proved to be 12.3% higher in CAI strength than expected meanwhile 15%

larger in projected damage area were detected. On the other hand, the cost of RTM6 panel was £69.1/KG, which is 26% higher than the cost of the control (LY564, £54.8/KG).

The whole No.13 set of panels was tufted, using carbon thread and glass thread respectively. Overall, as displacement of loading plate increased, the CAI load growth rate of tufted panels was nearly the same as the baseline due to the same specimen sizes, the same thickness, the same carbon fibre and same matrix. It meant that the elastic modulus wasn't affected by the tufting procedure. Another issue was the ridge in the tufted zone, which was only formed of resin and flattened tuft loops. The ridge complicated the CAI tests however it did not affect the CAI strength.

Interestingly, carbon thread worked better in LY564 matrix than glass thread, preventing damage initiation and propagation. By contrast, glass thread performed better with damage resistance in the RTM6 resin system. In detail, the CAI strength of LY564 resin panel had been improved dramatically by tufting, 51% regarding carbon tufts and 39% regarding glass tufts, respectively. Likewise, the CAI strength of the RTM6 resin panel was significantly upgraded by tufting as well, 31% regarding carbon tufts, 35% regarding glass tufts. The comparative relationship is displayed in Figure 63.

No	Description	F-Mean	STDEV	↑	Price
4-A	5HS woven preform/LY564	214.8	5.0	---	
13-A	5HS woven preform/LY564/C-tuft	324.6	9.9	51.1%	
13-A	5HS woven preform/LY564/G-tuft	298.1	7.2	38.8%	
4-B	5HS woven preform/RTM6	236.0	5.4	---	
13-B	5HS woven preform/RTM6/C-tuft	310.2	9.5	31.5%	
13-B	5HS woven preform/RTM6/G-tuft	319.0	3.1	35.2%	

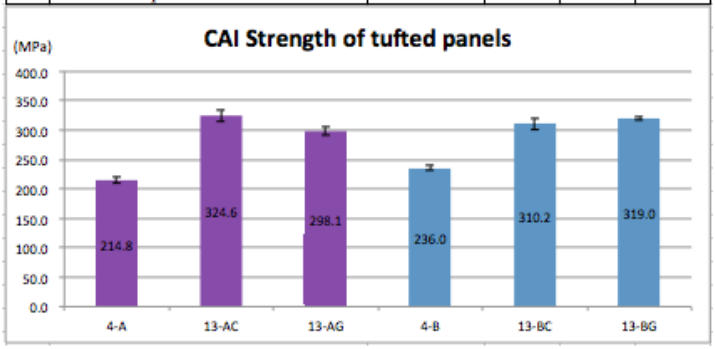

Figure 63 Tufting effect on CAI performance

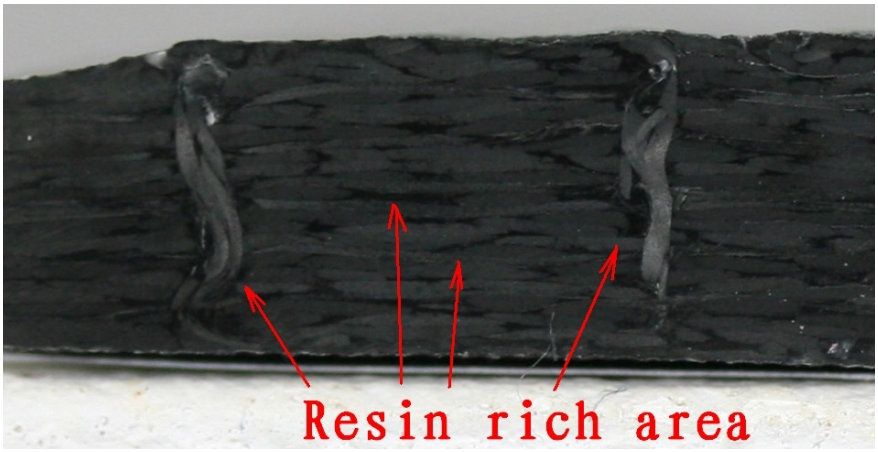

Figure 64 High resolution photograph of the cross-section of tufted panel

As shown in the cross-section of the tufted panel, a number of resin rich areas were formed in the tufted zone, especially near to tufts. It was probably because of the localised fibre crimping and breakage due to the forcible penetration of tufting threads. Another possible reason was the insufficient squeezing action due to the low atmospheric pressure on the confined combination of the tufts and preform. This is why none of the tufts was straight inside the cured panel.

The main impact damage modes of tufted panel were delamination and resin cracking; no serious fibre fracture was revealed in the micrograph. Figure 65 explicitly indicated that the delamination stopped propagating at the tufted point and the resin crack was restricted to a small area.

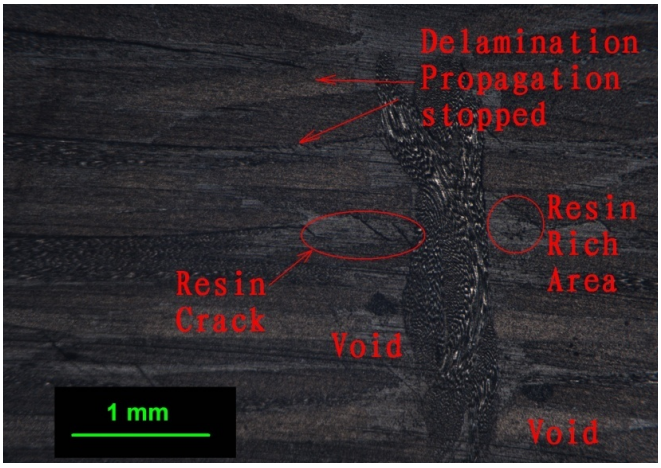

Figure 65 Cross-section micrograph of tufted panel through impact centre

The different performance of the carbon tufts and glass tufts in these two kinds of matrix could be explained referencing Jones' finding [34]. In the brittle LY564 resin system, the carbon tufts acted like a "screw" due to a higher number of twists per metre while the glass tufts behaved like a "nail" due to fewer twists per metre. The lightly twisted and more straight glass thread may be pulled out with minimal resin fracture, one the other hand, more resin fracture and possible thread damage are required to pull the highly twisted carbon thread out. Therefore, the CAI performance of the carbon-tufted panel was better than the glass tufted one. But in the tougher matrix system (RTM6), it is possible to hypothesise that the toughness of tufts dominated the damage resistance. Consequently, the glass tufted panel sustained slightly higher residual compression strength than the carbon-tufted panel.

Three kinds of low cost veil were applied in No.6, No.17 and No.7 separately, to the order of 3gsm, 6gsm and 20gsm respectively. As in the case of the tufted panels, compared to the baseline (No.4), dramatic improvement was achieved in CAI performance with the application of veils. 18%, 19% and 32% increase in CAI strength were quantified respectively in ascending order of veil areal weight. Hence, this technology demonstrated a dramatic improvement, the disadvantage being a small increase in thickness. It is particularly worth mentioning is, as shown in Table 1, the cost of the veils was only £6 per kilogram laminates which was roughly 10% of the cost of the veiled panel.

No	Description	F-Mean	STDEV	↑	Price
4-A	5HS woven preform/LY564	214.8	5.0	---	
6	5HS woven preform/LY564/veil	255.6	5.2	19.0%	
17	5HS woven preform/LY564/veil	252.7	5.9	17.6%	
7	5HS woven preform/LY564/veil	283.6	2.9	32.0%	

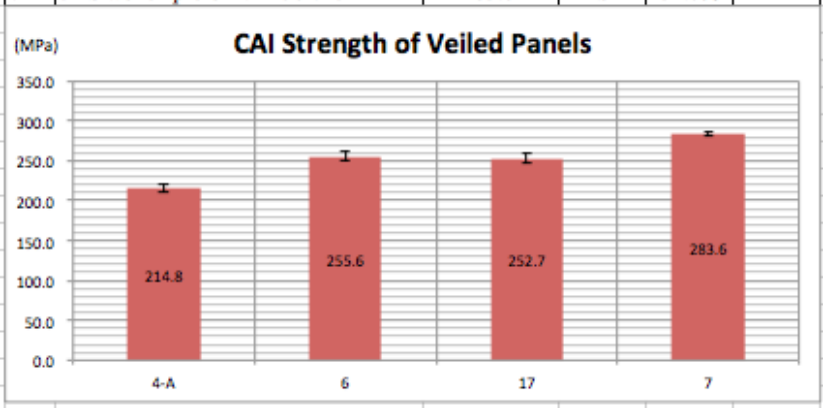

Figure 66 Veiled effect on CAI performance

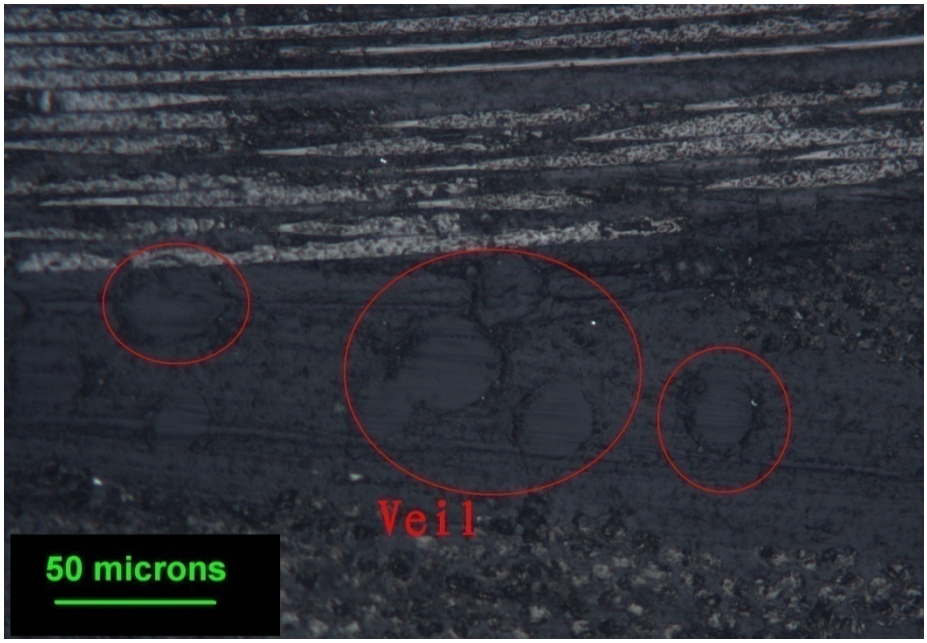

Figure 67 Micrograph of veiled woven panel

Comparing the micrographs of a veiled panel with an unveiled one, it indicates that there were many separate or connected cross-sections, which were the cross-section of veil filaments, inside of the resin zone between each layer, as shown in Figure 67. In other words, the whole veil worked in the resin like a barrier layer. It was surprising that the cross-section of the veil filament remained round even though the preform hot compaction procedure was carried out for 30 minutes before infusion. It appears that

the veils were surrounded by the matrix rather than closely concatenated with the fibre tows as expected. One possible mechanism for reducing or arresting the delamination propagation is the barrier layer.

Finally, It should be noted that the deviations of both CAI strengths and projected damage areas of unidirectional panels were quite high relative to that of woven panels.

7.4 Strength Reduction Due To Impact

As mentioned in chapter 3.3, only 4 local regions rather than whole preform were tufted considering the material costs and labour time. The penalties for this were a 1mm thick thickness step in each specimen and fibre local crimping at the edge of tufted zones. These are totally different from panels manufactured using Resin Transfer Moulding. During the CAI tests, the thickness step and the fibre local crimping were not critical defects because the impact region was the inevitable weak point. But the edge of the tufted zone became the weakest zone during plain compression tests. The load-transferring path had no choice but to change along the kinked fibre direction, and the stress concentration was unavoidable due to the abrupt change in thickness. As a result of these, the failure happened at the edge of the tufted zone in the plain compression test which could not reveal the true compression strength of a real whole-tufted panel. Therefore, the testing data was classified as misleading and hasn't been considered in the strength reduction comparison.

No plain compression testing data was collected for No.2 (T800 woven/M21 prepreg), No.8 (woven/binder/LY564 preform) and No.14 (T300 woven/913 prepreg) because of the specimen quantity limitation.

The useable plain compression strengths associated with CAI strengths are shown in Figure 68. The blue bar (left) indicates the plain compression strength and the red bar (right) expresses the CAI strength. All the strengths and deviation are measured in mPa units. Figure 69 reveals the compression strength reduction due to impact.

ID	Description	PCS_S	DEV	CAI_S	DEV	Reduction
1	No.1:T800/M21 UD Prepreg	431.6	14.6	268.2	15.1	38%
3	No.3:T700/M21 UD Prepreg	416.7	23.0	245.4	16.4	41%
4-A	No.4A:5HS woven preform/LY564	398.6	13.9	214.8	5.0	46%
4-B	No.4B:5HS woven preform/RTM6	412.6	13.9	236.0	5.4	43%
5	No.5:5HS woven preform/3508	397.6	32.1	220.8	6.4	44%
6	No.6:5HS woven preform/LY564/veil	380.3	14.5	255.6	5.2	33%
17	No.17:5HS woven preform/LY564/veil	372.6	26.4	252.7	5.9	32%
7	No.7:5HS woven preform/LY564/veil	403.7	10.0	283.6	2.9	30%
9	No.9:NCF preform/LY564	382.1	26.1	201.4	7.2	47%
10	No.10:UD preform/LY564/veil	338.3	22.0	191.6	16.4	43%
11	No.11:uniweave preform/binder/LY564	298.8	6.8	191.5	12.9	36%
15	No.15:UD preform/LY564/veil/binder	314.4	0.4	198.8	16.1	37%

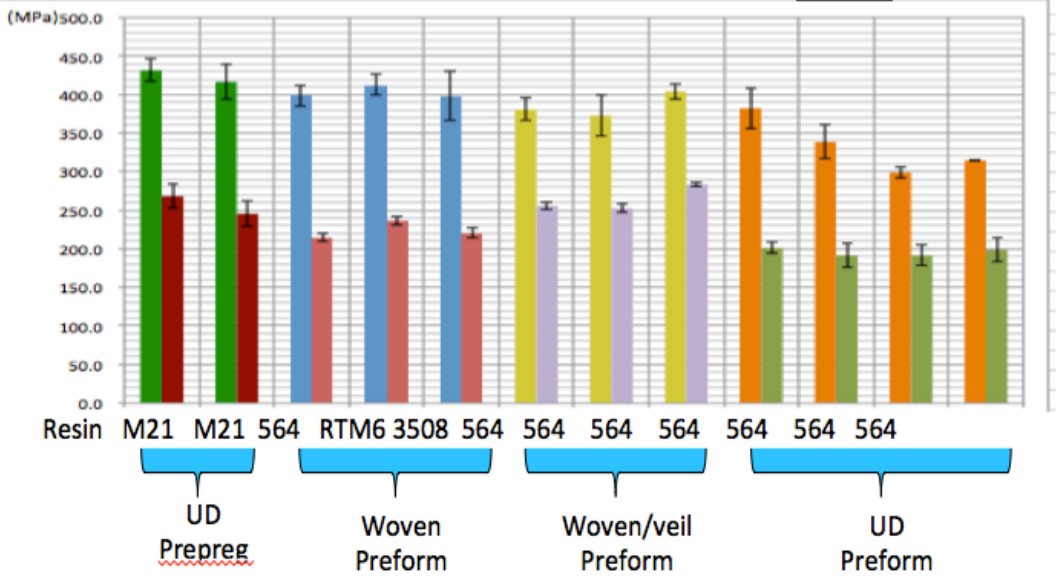

Figure 68 CAI strengths VS. PCS strengths

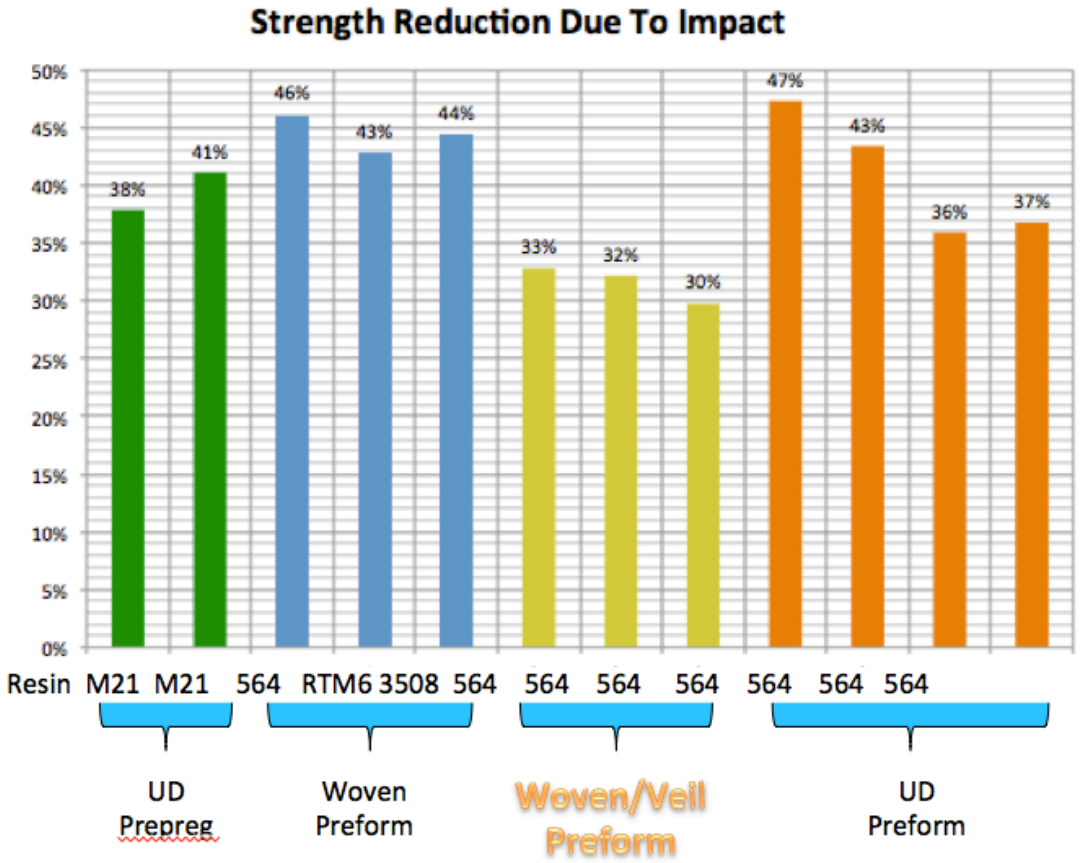

Figure 69 Strength reduction due to impact

Comparing No.1 and No.3, each comprised the same layup panels using UD tape prepreg with the same M21 resin. However, the T800 carbon fibre used in No1 was the intermediate modulus fibre but the T700 carbon fibre for No.3 was the standard modulus fibre. It is easy to understand why the damage inside No.1 was smaller than in No.3. The compression results indicate and support the reasonably expected fact that the compression strength of the high modulus panel was reduced further due to impact than the intermediate modulus panel, as the former was stiffer than the latter.

Differing from the residual compression strength, the strength reductions due to impact of No.4A, No.4B and No.5 were more or less the same, between 43%~46%. It seems that the fibre and the damage area dominated the residual compression strength after this energy level impact, but the resin matrix had nothing to do with the residual compression strength. These explanations are in keeping with the observed experimental results.

Because the veils not only improved the damage resistance of impact but also enhanced the plain compression strength, the strength reductions due to impact of veiled No.6, No.17 and No.7 were not significantly different. The results revealed a 46% strength reduction of the baseline and more than 13% commutation of the veiled panels. What is worth mentioning is that the reduction percentages decreased gradually as the veil thicknesses were increasing.

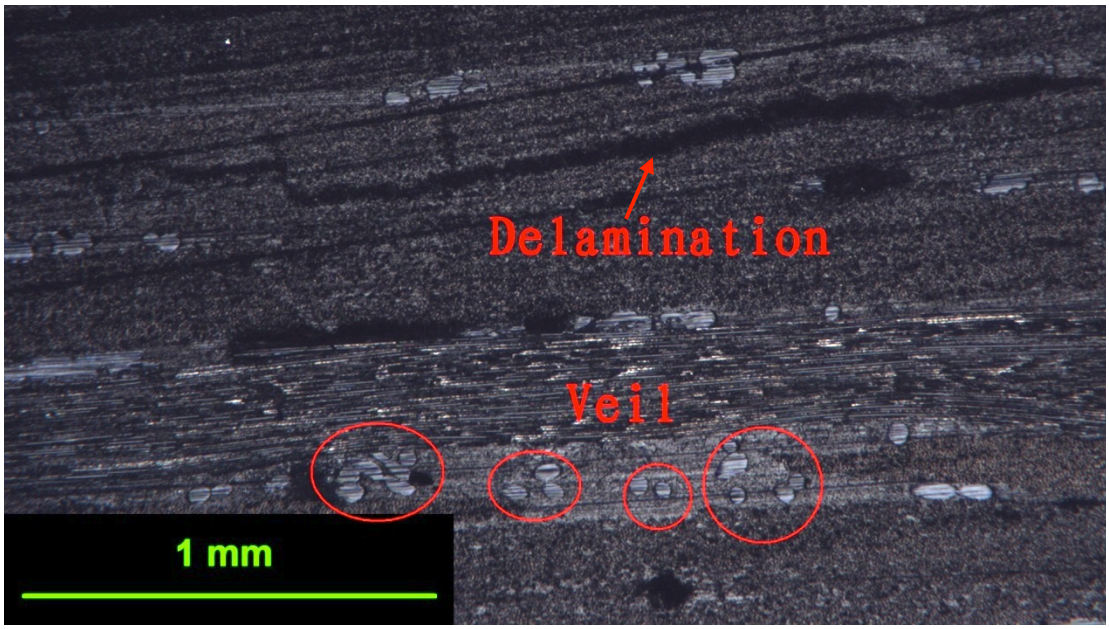

Figure 70 micrograph of veiled unidirectional panel

After careful investigation and comparison of the micrographs, the veiled versus the unveiled and the woven versus the unidirectional, two possible factors may explain the relative correlation between fibre, matrix and veil. One factor is the delamination in woven fibre panel propagated in the resin between layers, but the delamination in UD tape panel spread interior of tape layer as shown in Figure 70.

Another factor, easily and naturally as mentioned before, is that the barrier layer implanted in the resin could slow the delamination propagation down or might arrest it. The combination of these two factors provides some support for the fact that veils improved the CAI performance of the woven fibre panel significantly but had no effect on UD tape panels. These explanations are consistent with the finding of

Pearson in 1992 [35].

Among the unidirectional fibre panels, the NCF panel performed worst in damage resistance and the uniweave one was the best. The compression strength dropped due to the incident impact being at the same energy level, i.e. 47% of the NCF panel and 36% of the uniweave one. The NCF material used in this research consisted of two layers stacked in orthogonal directions held together by a binding yarn system. But the single layer was not gapless because fibre tows were separated from each other, which resulted in resin rich regions in the cured composite between every tow. This is a probable reason why a NCF reinforced brittle matrix was highly sensitive to impact.

The comparison of uniweave fibre panels was expected to exhibit a similar performance in CAI to the NCF panel because of the similar raw material structure, but the white binder, named DX69-2, adsorbed in every fibre tow surface, enhanced the damage resistance of the uniweave fibre panel.

8 Applicability

Because both veils and tufts are new technologies, many issues should be taken into consideration regarding their applicability in aviation.

- Design issues – Based on the results, stiffness remained unaffected by the application of veils or tufts. Furthermore, each of them could be used to locally improve damage resistance of aircraft structures such as leading edges. But the stress concentration at the edge of applied zones due to the changes of thickness needs be controlled or avoided during the design procedure.

- Manufacturing issues – Tufting needs new equipment investment, probably a specialist supplier and professional technicians. The cost of the tufting machine is £50000, the tufting speed usually is 1 meter per 3 minutes and the labour cost including overheads is £30 per hour. Veils are very easy to apply but specific and critical hot preform compaction is required

- Qualification issues – Both veils and tufts are new. Application in aviation requires large databases generated from substantial testing of different fabrics, all with added tufts or veils. Finished parts with added tufts or veils may need to be certified separately.

9 Conclusions

- A wide range of materials was manufactured, tested and compared. The material list consisted of well-established aviation materials and existing improved materials in different fabrics; some novel technologies like tufting and veils were also employed.

- In total, 19 different panels using 9 different fabrics were manufactured. More than 160 specimens were impacted, C-scanned and compressively loaded in the testing sequence. All the contrasting conclusions and analyses were supported by micrographs and high-resolution pictures of cross-sections.

- Compared to the control (LY564 resin), slightly cheaper FLAVIIR tougher (3508) resin increased the CAI strength by 2.8%, but the experimental results revealed a 12.3% growth in CAI strength of RTM6 panel, which cost 26% more.

- Unidirectional fibre fabric is lower cost but is more sensitive to impact than woven fabric, especially in uniweave type fabric. The internal damage to laminates revealed by C-scanning pictures showed that the unidirectional fibre laminates were far more susceptible to impact compared to woven fibre laminates.

- The CAI strengths of prepreg laminates were higher than that of preform laminates, even through the unidirectional prepreg laminates contained far more internal damage. The possible reason suggested was the higher compression strength of unidirectional fibre than the woven fibre. The woven prepreg laminates were slightly better than the woven preform laminates possibly due to the slightly higher FVF. The woven preform laminates performed better than the unidirectional preform laminates. One possible explanation is the combination of the huge internal damage and low fibre

volume fraction of the unidirectional preform laminates.

- Tufting significantly improved the post-impact residual compression strength. A 51.1% improvement in the CAI strength of the LY564 resin system was achieved due to the carbon tufting threads, and a 35.2% increase in the CAI strength of the RTM6 system was observed for the glass tufting. The highly twisted carbon thread worked like a “screw” but the glass thread with fewer twists worked as a “nail”. The carbon thread performed better than the glass thread in the brittle LY564 system but similarly in the tougher matrix system (RTM6). Tufting does however result in a laminate thickness change of around 20-25% which complicates CAI strength calculation. The additional resin weight and the thickness change step may cause structure design issues.

- The major finding was that veils were a very simple and cost effective method of enhancing the damage resistance of a woven fabric laminates. The thicker veils were more effective than the thinner. The veils acted like a barrier layer which prevented or even eliminated delamination between layers. A 32% CAI strength increase was achieved using six gsm veils that increased the materials cost by roughly 10%. However the veils were not effective for unidirectional fabrics because the delamination occurred within the fabric layers.

10 Future Work

- Since this thesis has investigated the performance of a wide range of materials, it would be useful to study those materials with the most beneficial properties in greater detail, particularly veils and tufting.

- This thesis investigated the performance of glass thread and carbon thread using in one specific density. It is suggested to research tufting parameters in more details, e.g. thread twist, thread diameter, tufts density and thread loop depth. Double Cantilever Beam (DCB) tests are also suggested to investigate the performance of highly twisted thread and lightly twisted thread.

- More research on this topic need to be undertaken before the association between CAI performance and FVF is clearly understood. Furthermore, the effects on the CAI performance of fibre areal weight, fibre weight fraction and laminate thickness are suggested.

- Damage initiation is another significant issue for damage resistance investigation. Further research should be carried out to investigate the Barely Visible Impact Damage (BVID) performance of different laminates.

- All the results employed in this thesis were the experimental outcomes. However, finite element modeling is suggested to predict the PCS and CAI strength. Estimations using empirical formulae for damage area and compression strength are also recommended.

- Detailed micrographs and high-resolution pictures of the cross-section through the impacted point were ultilised in this research to investigate the fracture mechanism and the delamination characters. Further investigation into damage patterns will be necessary to understand the damage development mechanisms.

REFERENCES

1: Andrew.R.Mills, J.Jones, “Investigation, manufacture and testing of damage resistant unmanned aircraft wing structures using low cost carbon fibre composite materials and manufacturing technology”, Proceedings of the Institution of Mechanical Engineers, Part G: Journal of Aerospace Engineering, Volume 224, Number 4 / 2010

2: J.F.M. Wiggenraad, E.S. Greenhalg and R. Olsson, “Design and analysis of stiffness composite panels for damage resistance and tolerance”, National Aerospace Laboratory NLR, NLR-TP-2002-193

3: L.Tong, A.P. Mouritz, and M.k. Bannister, “3D Fibre Reinforced Polymer Composites”, ISBN 13: 978-0-08-043938-9, Imprint: ELSEVIER, Published: NOV-2002

4: http://en.wikipedia.org/wiki/Fracture_toughness

5: D.J. Wilkins, “A preliminary damage tolerance methodology for composite structures”, Workshop on failure analysis and mechanisms of failure of fibrous composites NASA, Langley (March, 1982)

6: Kimberley Dransfield, Caroline Baillie & Yiu-Wing Mai, “Improving the Delamination Resistance of CFRP by Stitching--A Review”, Composites Science and Technology 50 (1994) 305-317

7: Joon-Hyung Byun, Sung-Wook Song, Chang-Hoon Lee, Moon-Kwang Um, Byung-Sun Hwang, “Impact properties of laminated composites with stitching fibres”, Composite Structures 76 (2006) 21–27

8: http://en.wikipedia.org/wiki/Tufting_(composites)

9: Denis D.R. Cartié, Giuseppe Dell’Anno, Emilie Poulin and Ivana K. Partridge, “3D reinforcement of stiffener-to-skin T-joints by Z-pinning and tufting”, Engineering Fracture Mechanics Volume 73, Issue 16, November 2006, Pages 2532-2540

10: Akinori Yoshimura, Tomoaki Nakao, Shigeki Yashiro, Nobuo Takeda, “Improvement on out-of-plane impact resistance of CFRP laminates due to through-the-thickness stitching”, Composites Part A: Applied Science and

Manufacturing Volume 39, Issue 9, September 2008, Pages 1370-1379

11: Zhang, Man, “A Review of the Epoxy Resin Toughening”, Department of Chemical Engineering and Materials Science of Syracuse University, April 29, 2003

12: Ivana K. Partridge, Tony Bonnington, and Denis D. R. Cartie, "Manufacture and performance of Z-pinned composites", Advanced polymeric materials: structure property relationships, ISBN: 978-1-58716-047-9, Chapter 3

13: Ivana K. Partridge, Denis D.R. Cartie, "Delamination resistant laminates by Z-Fibre pinning", Composites: Part A 36 (2005) 55–64

14: A.P. Mouritz, “Review of z-pinned composite laminates”, Composites: Part A 38 (2007) 2383–2397

15: Boyce JS, Freitas GA, Magee CL, Fusco TM, Harris JJ, Kunkle E, “Ultrasonic fastening system and method”, Patent WO1998/029243 1998

16: Frietas G, Magee C, Boyce J, Bott R, “Service tough composite structures using z-fibre process”, Proceedings of the 9th DoD/NASA/FAA conference on fibrous composites, Lake Tahoe, Nevada; 1991.

17: Partridge IK, Cartie DDR, Bonnington T, “Manufacture and performance of z-pinned composites”, Advanced polymeric materials: structure property relationships, ISBN: 978-1-58716-047-9, Chapter 3

18: A.P. Mouritz, B.N. Cox, “A mechanistic interpretation of the comparative in-plane mechanical properties of 3D woven, stitched and pinned composites”, Composites: Part A 41 (2010) 709–728

19: A.P. Mouritz, B.N. Cox, “A mechanistic approach to the properties of stitched laminate”, Composites: Part A 31 (2000) 1–27

20: Min-Seok Sohn and XiaoZhi Hu, “Processing of carbon-fibre/epoxy composites with cost-effective interlaminar reinforcement” Composites Science and Technology 58 (1998) 211-220

21: http://en.wikipedia.org/wiki/Composite_material

22: http://www.torayca.com/techref/en/images/off02.html

23: Stephen R. Swanson and Yibo Qian, “Multiaxial characterization of T800/3900-2 carbon/epoxy composites”, Composites Science and Technology 43 (1992) 197-203

24: Jin Zhang and Bronwyn L. Fox, “Manufacturing Influence on the Delamination Fracture Behavior of the T800H/3900-2 Carbon Fibre Reinforced Polymer Composites”, Materials and Manufacturing Processes, 22: 768–772, 2007

25: Hiroshi Saito, Isao Kimpara, “Evaluation of impact damage mechanism of multi-axial stitched CFRP laminate” Composites: Part A 37 (2006) 2226–2235

26: S. Guinarda, O. Allixb, D. Guedra Degeorgesa, A. Vineta, “A 3D damage analysis of low-velocity impacts on laminated composites”, Composites Science and Technology 62 (2002) 585–589

27: Tien-Wei Shyr, Yu-Hao Pan, “Impact resistance and damage characteristics of composite laminates” Composite Structures 62 (2003) 193–203

28: R.W.Hillermeier, J.C.Seferis, “Interlayer toughening of resin transfer moulding composites” Composites: Part A 32 (2001) 721-729

29: J.M.Hodgkinson, “Mechanical testing of advanced fibre composites”, ISBN13: 978 1 85573 312 1

30: Andrew.R.Mills, J.Jones, “Investigation, manufacture and testing of damage resistant unmanned aircraft wing structures using low cost carbon fibre composite materials and manufacturing technology”, Proceedings of the Institution of Mechanical Engineers, Part G: Journal of Aerospace Engineering, Volume 224, Number 4 / 2010

31: ASM Handbook Volume 21 Composites

32: Hao Yan, Caglar Oskay, Arun Krishnan and Luoyu Roy Xu, “Compression-after-impact response of woven fibre-reinforced composites” Composites Science and Technology 70 (2010) 2128–2136

33: E.M. Odom and D.F. Adams, “Failure modes of unidirectional carbon/epoxy composite compression specimens”, Composites Volume 21, Issue 4, July 1990, Pages 289-296

34: John Arthur, Jones Vinchery, Reinforcement of composite aircraft structures using tufting, School of Applied Sciences, Advanced Materials, Cranfield University, September, 2007

35: Raymond A. Pearson and Albert F. Yee, “Toughening mechanisms in

thermoplastic-modified epoxies: 1. Modification using poly (phenylene oxide)" Polymer Volume 34, Issue 17, September 1993, Pages 3658-3670

36: MIL-HDBK-17, Composite Materials Handbook Volume 3. Polymer Matrix Composite Materials Usage, Design, And Analysis, Chapter 8 Supportability

37: Giuseppe Dell'Anno, Denis D. Cartie, Ivana K. Partridge, Amir Rezai, "Exploring mechanical property balance in tufted carbon fabric/epoxy composites" Composites: Part A 38 (2007) 2366–2373

38: Shen Zhen, "Design allowable of composite aircraft structures and their determination principles" Acta Aeronautica Et Astronautica Sinica Vol 19 No.4 July 1998

39: Engineered materials handbook Vol 1 Composite OHID USA: ASM International, 1988